

Bhuvaneshwari Koneru, Inorganic nanoparticles for applications in biomedical sciences Doctor of Philosophy (Biomedical Sciences), November, 2016, 112 pp., 7 tables, 29 figures, bibliography, 225 titles

Nanomedicine is one of the fastest emerging fields in recent times. Small size, tunable surface properties and efficient drug loading capacity are some of the properties that make them a promising option for various applications in biological sciences. Using nanocarriers for drug delivery offers several advantages like delivery of poorly soluble drugs, better bioavailability, targeted delivery and extended release of drugs. In this work, we demonstrated the formulation and methods of use for three different nanocarriers.

1) *<sup>166</sup>Ho iron garnet nanoparticle-containing bandages for treatment of squamous cell carcinoma of skin:*

Squamous cell carcinoma (SCC) of skin is a type of non-melanoma skin cancer (NMSC) which constitutes 20% of all NMSCs. While surgery is the primary treatment option for SCC, radiation therapy also plays an irreplaceable role in the treatment of SCC. Our lab has previously reported an electrospun nanofibrous polyacrylonitrile (PAN) bandage containing holmium-165 iron garnet (<sup>165</sup>HoIG) nanoparticles, which can be neutron activated to <sup>166</sup>Ho and used for radiotherapy of SCC. The synthesis, characterization and stability of the bandage were also reported. Here, we tested the *in vivo* efficacy of the <sup>166</sup>HoIG-PAN bandage for the treatment of SCC. When treated with the radioactive bandage, tumor progression was significantly low in mice compared to those with non-

radioactive bandage. The dose used was clinically relevant. Histological evaluation showed no damage to surrounding organelles.

2) *Targeted chemotherapy for non-small cell lung cancer using antibody-coated gold nanoparticles:*

Non-small cell lung cancer (NSCLC) is a type of lung cancer which constitutes nearly 80% of all lung cancers. Being detected at later stages limits its treatment, thus resulting in a lower five year survival rates. Though limited by their dose related side effects, platinum drugs are the first line of treatment for NSCLC. Several Pt(IV) complexes, which are the prodrugs of Pt(II) compounds are shown to have potent anti-cancer activity and are capable of overcoming the limitations of Pt(II) compounds. Not many targeted therapies are available for NSCLC because of its complex molecular pathology. CD22 is an adhesion molecule that is shown to be broadly expressed on NSCLC cell lines. Hence, in this project, we developed CD22 targeted gold nanoparticles to deliver Pt(IV) complex for the treatment of NSCLC. Synthesis and characterization of polyethylene glycol (PEG) coated gold nanoparticles conjugated with Pt(IV) complex and an antibody against CD22 is reported. The expression of CD22 on various NSCLC and normal cell lines and the uptake of the synthesized nanoparticles in these cell lines was studied.

3) *Tetracycline-Containing MCM-41 Mesoporous Silica Nanoparticles for the Treatment of Escherichia Coli:*

Tetracycline (TC) is a very well-known antibiotic whose use has been limited due to drug resistance. Nanoparticle formulations, can help overcome the resistance mechanisms to certain extent. Mesoporous silica nanomaterials (MSNs) are widely studied for drug delivery applications; Mobile Crystalline Material-41 (MCM-41), a type of MSN, that has a mesoporous structure with

pores forming channels in a hexagonal fashion. We used MCM-41 mesoporous silica nanoparticles for the delivery of TC and tested its efficacy in *E. coli*. The TC containing nanoparticles showed a burst release of drug in PBS and in LB broth medium and most of the drug was released within 1 h. The TC loaded MSNs showed enhanced inhibition of *E. coli* compared to free TC and unloaded MSNs at a concentration of 0.5 $\mu$ g/mL and 1 $\mu$ g/mL. Further, the TC containing MSNs uptake by *E. coli* was demonstrated using transmission electron microscopy.

INORGANIC NANOPARTICLES FOR APPLICATION IN BIOMEDICAL SCIENCES

BHUVANESWARI KONERU, MS

APPROVED:

---

Dr. Anthony Di Pasqua, Major Professor

---

Dr. Riyaz Basha, Major Professor/Committee Member

---

Dr. Ignacy Grysczynski, Committee Member

---

Dr. Lisa Hodge, Committee Member

---

Dr. Kenneth J Balkus, Jr., Committee Member

---

Dr. Yi Qiang Cheng, Committee Member

---

Dr. Caroline Rickards, University Member

---

Dean, Graduate School of Biomedical Sciences

INORGANIC NANOPARTICLES FOR APPLICATION IN BIOMEDICAL SCIENCES

PhD THESIS

Presented to the Graduate Council of the  
Graduate School of Biomedical Sciences

University of North Texas Health Science Center at Fort Worth

in Partial Fulfillment of the Requirements

For the Degree of

DOCTOR OF PHILOSOPHY

By

BHUVANESWARI KONERU, MS

Fort Worth, Texas

November 10, 2016

*Dedicated to my mother,  
who courageously fought  
and won the battle against cancer and  
to my father who helped her fight through it...*

## ACKNOWLEDGEMENTS

I first want to thank God for always landing me among the right people with the right resources at the right time, which made working through my PhD a delightful journey. I would like to thank my mentor and guide, Dr. Anthony J. Di Pasqua, for his unconditional support, constant motivation and patience throughout the last three and half years. It was a great privilege for me to work under his mentorship. It is because of joining his group that I met Dr. Yi Shi, without whose help this work would not have been completed. I can't thank her enough for the kind of help she provided. I would also like to thank Drs. Riyaz Basha, Lisa Hodge, Ignacy Grysczynski, Yi Qiang Cheng, Kenneth J. Balkus, Jr. and Caroline Rickards for taking time to serve on my advisory committee and for their valuable suggestions. I would also like to thank Dr. Yu-Cheih Wang and his lab members, Ashwini Zolekar and Victor Lin, for their immense help in conducting experiments and beneficial discussions. I would also like to thank Drs. Di Pasqua, Balkus, Munaweera and Shi for initiating the radiotherapeutic bandage project. I would further like to thank Sigma Xi and the Department of Pharmaceutical Sciences in the UNT System College of Pharmacy (SCP) for funding these projects. I also want to thank Dr. Myron Jacobson, Dean, UNT SCP and Dr. Iok-Hou Pang, Chair, Department of Pharmaceutical Sciences, UNT SCP, for their support whenever needed. Further I would like to thank my mentor during my Masters, Dr. Steve Mifflin, Director and Professor, Institute of Cardiovascular and Metabolic Diseases, UNTHSC, without whose motivation I would not have pursued a PhD. I would also like to thank Dr. Humam Kadara, Asst. Professor, Department of Biochemistry and Molecular Genetics, American University of Beirut, Beirut, Lebanon, for providing us with the Colo-16 cells and Dr. Mary White-Carter, Assistant Director ARC Diagnostic Lab, UT Southwestern Medical Center for helping us with histological analysis.

Lastly, I would like to thank my beloved husband, Vamsi Krishna, who has been my greatest support system throughout; my parents, without whom I am nobody; my brother Goutham, who has taken care of me like a father since the day I entered the USA; my uncle Dr. Ratna Vadlamudi who was my inspiration to get into research; and my friends Dr. Dinesh Jasti, Vishwanath Edara, Rutika Kokate and Soumya Kavuluri; my brother-in-law, Bharat Raj; and sister-in-law, Varsha. I'm truly grateful to have you all in my life; you have been with me through thick and thin no matter how far we are physically.

## LIST OF PUBLICATIONS

1. **Koneru, B.**, Shi, Y., Munaweera I., Carter, M.W., Kadara, H., Hong, Y., Di Pasqua, A.J., & Balkus, K.J., Jr. Radiotherapeutic bandage for the treatment of squamous cell carcinoma of the skin. *Nuclear Medicine and Biology* 43, 333-338 (2016).
2. **Koneru, B.**, Shi, Y., Wang, Y.C., Chavala, S.H., Miller, M.L., Holbert, B., Conson, M., Ni, A., & Di Pasqua, A.J. Tetracycline-containing MCM-41 mesoporous silica nanoparticles for the treatment of *Escherichia coli*. *Molecules* 20, 19690-19698 (2015).
3. Munaweera, I., Shi, Y., **Koneru, B.**, Patel, A., Dang, M.H., Di Pasqua, A.J., & Balkus, K.J., Jr. Nitric oxide-and cisplatin-releasing silica nanoparticles for use against non-small cell lung cancer. *Journal of Inorganic Biochemistry* 153, 23-31 (2015).
4. Munaweera, I., Shi, Y., **Koneru, B.**, Di Pasqua, A.J., & Balkus, K.J., Jr. Chemoradiotherapeutic magnetic nanoparticles for targeted treatment of non-small cell lung cancer. *Molecular Pharmaceutics* 12, 3588-3596 (2015).
5. Shi, Y., **Koneru, B.**, Redfearn, W., Miller, M.L., Myers, L. & Di Pasqua, A.J. Platinum (IV) cisplatin derivative trans, cis, cis-bis (heptanoato) amine (cyclohexylamine) dichloridoplatinum (IV) has an enhanced therapeutic index compared to cisplatin for the treatment of non-small cell lung cancer. *Inorganica Chimica Acta* 423, 215-219 (2014).
6. Munaweera, I., **Koneru, B.**, Shi, Y., Di Pasqua, A.J. & Balkus Jr, K.J. Chemoradiotherapeutic wrinkled mesoporous silica nanoparticles for use in cancer therapy. *APL Materials* 2, 113315 (2014).
7. **Koneru, B.**, Bathina, C.S., Cherry, B.H. & Mifflin, S.W. Mineralocorticoid receptor in the NTS stimulates saline intake during fourth ventricular infusions of aldosterone. *American Journal of Physiology-Regulatory, Integrative and Comparative Physiology* 306, R61-R66 (2014).

8. Rahaman, S.A., Prasad, Y.R., **Koneru, B.**, Kumar, P. Synthesis and antihistaminic activity of novel pyrazoline derivatives. *International Journal of ChemTech Research* 2, 16-20 (2010).

## TABLE OF CONTENTS

<b>ACKNOWLEDGEMENTS.....</b>	<b>ii</b>
<b>LIST OF PUBLICATIONS.....</b>	<b>iv</b>
<b>TABLE OF CONTENTS.....</b>	<b>vi</b>
<b>ABBREVIATIONS.....</b>	<b>ix</b>
<b>LIST OF TABLES.....</b>	<b>xi</b>
<b>LIST OF FIGURES.....</b>	<b>xii</b>
<b>CHAPTER</b>	
<b>I. AN INTRODUCTION TO NANOPARTICLES IN BIOMEDICAL SCIENCES.....</b>	<b>1</b>
USES OF NANOCARRIER FORMULATIONS FOR DRUG DELIVERY.....	1
TYPES OF NANOPARTICLES SYSTEMS USED IN BIOMEDICAL SCIENCES .....	4
INORGANIC NANOPARTICLES.....	6
NANOPARTICLES IN CANCER DIAGNOSIS AND THERAPY.....	7
NANOPARTICLES FOR VACCINE DELIVERY .....	12
NANOPARTICLES FOR ANTIMICROBIAL THERAPY .....	14
OBJECTIVE .....	17
<b>II. <sup>166</sup>Ho IRON GARNET NANOPARTICLE-CONTAINING BANDAGES FOR TREATMENT OF SQUAMOUS CELL CARCINOMA OF SKIN .....</b>	<b>18</b>

ABSTRACT.....	18
INTRODUCTION.....	20
MATERIALS AND METHODS.....	26
RESULTS & DISCUSSION.....	30
CONCLUSIONS.....	36
<b>III. TARGETED CHEMOTHERAPY FOR NON-SMALL CELL LUNG CANCER USING ANTIBODY-COATED GOLD NANOPARTICLES.....</b>	<b>38</b>
ABSTRACT.....	38
INTRODUCTION.....	40
MATERIALS AND METHODS.....	46
RESULTS & DISCUSSION.....	52
CONCLUSIONS.....	62
<b>IV. TETRACYCLINE-CONTAINING MCM-41 MESOPOROUS SILICA NANOPARTICLES FOR THE TREATMENT OF <i>ESCHERICHIA COLI</i>.....</b>	<b>63</b>
ABSTRACT.....	63
INTRODUCTION.....	65
MATERIALS AND METHODS.....	69
RESULTS & DISCUSSION.....	74
CONCLUSIONS.....	81

<b>V. SUMMARY AND FUTURE PERSPECTIVES.....</b>	<b>82</b>
<b>REFERENCES.....</b>	<b>85</b>
<b>APPENDIX.....</b>	<b>114</b>

## ABBREVIATIONS

NP- Nanoparticle

SCC – Squamous Cell Carcinoma

NSCLC – Non-Small Cell Lung Cancer

NMSC – Non-Melanoma Skin Cancer

<sup>166</sup>Ho – Holmium-166

PAN - Poly Acrylo Nitrile

HoIG – Holmium Iron Garnet

AuNP- Gold nanoparticle

AuNP-PEG-NH<sub>2</sub> – PEGylated gold nanoparticles

mAb – monoclonal antibody

Pt – Platinum

AuNP-PEG-Pt – Platinum conjugated PEGylated gold nanoparticles

AuNP-PEG-Pt-mAb – Platinum and monoclonal antibody conjugated PEGylated gold nanoparticles

CD22 – Cluster Differentiation 22

PEG – Poly Ethylene Glycol

EPR- Enhanced Permeability and Retention

PLGA- Poly (lactic-co-glycolic acid)

PBS- Phosphate Buffered Saline

TEM- Transmission Electron Microscopy

SEM- Scanning Electron Microscopy

DLS – Dynamic Light Scattering

TC – Tetracycline

MSNs – Mesoporous silica nanoparticles

MCM41 – Mobile Crystalline Material 41

FDA – Food and Drug Administration

EGFR – Endothelial Growth Factor Receptor

VEGFR – Vascular Endothelial Growth Factor Receptor

HPV – Human Papilloma virus

NO – Nitric Oxide

## LIST OF TABLES

### CHAPTER I

Table 1: List of nanomedicines for cancer therapy which are FDA approved/under clinical trial.....	13
Table 2: List of FDA approved nanomedicines.....	16

### CHAPTER II

Table 3: Electrospinning parameters.....	27
--	----

### CHAPTER III

Table 4: Size, PDI and zeta potential of AuNP.....	53
Table 5: Particle size of –COOH and –OH capped AuNP in PBS and various culture mediums.....	54
Table 6: Characterization data of AuNP-PEG-NH <sub>2</sub> , AuNP-PEG-Pt and AuNP -PEG-Pt-mAb.....	55
Table 7: Percent of Alexaflour-488 positive cells in each cell line.....	58

## LIST OF FIGURES

### CHAPTER I

Figure 1: Major size-dependent biological barriers regulating the bio-distribution of blood-circulating nanoparticles.....9

### CHAPTER II

Figure 2: Digital image of 33% (w/w)  $^{165}\text{HoIG}$ -containing PAN bandages and SEM and TEM images.....23

Figure 3: 33% (w/w) HoIG-containing PAN bandages before and after neutron-activation.....24

Figure 4: SEM images and fiber diameter distributions of 33% (w/w) HoIG-containing PAN bandages before and after neutron-activation.....25

Figure 5: Diagram showing homogeneity of radiotherapeutic bandage.....26

Figure 6:  $^{165}\text{HoIG}$ -containing PAN non-radioactive bandage. ....30

Figure 7: Mouse with  $^{165}\text{HoIG}$ -containing PAN attached on the tumor.....32

Figure 8: TVR plotted against the number of days after treatment .....33

Figure 9: Tumor burden on mice.....34

Figure 10: Representative histological evaluation of skin surrounding the tumor .....35

Figure 11: Representative histological evaluation of tissues.....35

### CHAPTER III

Figure 12: Examples of Pt(II) anti-cancer agents .....41

Figure 13: Examples of Pt(IV) anti-cancer agents .....42

Figure 14: Schematic of the synthesis of oxoplatin and its carboxyl derivative.....48

Figure 15: TEM image of AuNP.....53

Figure 16: TEM images of AuNP-PEG-NH <sub>2</sub> , AuNP-PEG-Pt, AuNP-PEG-Pt-mAb.....	55
Figure 17: NMR spectra of the Pt(IV) complex .....	56
Figure 18: Expression of CD22 on various lung cancer and normal cell lines .....	58
Figure 19: Antibody conjugation efficiency.....	60
Figure 20: Uptake of AuNP-PEG-NH <sub>2</sub> , AuNP-PEG-Pt and AuNP-PEG-Pt-mAb by different cell lines .....	61
<b>CHAPTER IV</b>	
Figure 21: Structure of tetracycline.....	65
Figure 22: Schematic representation of MCM-41 nanoparticle synthesis and structure..	71
Figure 23: TEM images of tetracycline-containing MCM-41 nanoparticles .....	75
Figure 24: UV-vis spectra of tetracycline at 0 and 24 h .....	75
Figure 25: Adsorption of TC by MSNs.....	76
Figure 26: <i>In vitro</i> release of tetracycline from MSNs in PBS.....	77
Figure 27: <i>In vitro</i> release of TC from MSNs in LB broth medium.....	78
Figure 28: Survival (%) of <i>E. coli</i> when treated by TC containing MSNs.....	79
Figure 29: Uptake of TC from TC-MCM-41A by <i>E. coli</i> determined using TEM .....	81
<b>APPENDIX</b>	
Figure A1: Peak shift in fluorescence intensity AuNP-PEG-Pt-mAb.....	110
Figure A2: Peak shift in fluorescence intensity of Ramos and Jurkat.....	111
Figure A3: Peak shift in fluorescence intensity in A549(1).....	111
Figure A4: Peak shift in fluorescence intensity in A549(2).....	112
Figure A5: Peak shift in fluorescence intensity in H596, BEAS-2B, WI-38.....	112

## **Chapter 1**

### **An Introduction To Nanoparticles In Biomedical Sciences**

Merging the fields of material sciences and biomedical sciences, “nanomedicine” is emerging as a promising technology for many biological applications. A variety of inorganic and organic nanoparticles are being tested and a great deal of research is being conducted on their applications. The size of the nanoparticles can be tuned from as small as 1 nm to several hundred nm depending on the core material used and surface modifications used in the nanoparticle formulation. Their small size, unique optical, magnetic, structural and electronic properties are the key factors in nanoparticles being highly valuable for biological applications. The goal of nanomedicine is to develop efficient, targeted, biocompatible formulations for therapies and diagnosis of several complex and challenging diseases.

#### **Uses of nanocarrier formulations for drug delivery:**

Research relating to biomedical applications of nanoparticles has increased greatly in the past decade. There are several advantages of using nanocarrier systems for drug delivery.<sup>1-3</sup> Delivery of poorly soluble drugs, can be made easy with nanocarriers. Poor water solubility of drug

is always a major limitation for several pharmaceutical formulations.<sup>4,5</sup> For example, encapsulating the poorly water soluble drug in the hydrophobic cores of polymeric micelles, help in better dispersion of the drug in water.<sup>6,7</sup> Yu et al. formulated polymeric micelles loaded with amphotericin which is a broad spectrum antifungal agent and is quiet water insoluble.<sup>8</sup> They showed that using micelles of poly(ethylene oxide)-block-poly( $\beta$  benzyl-L-aspartate) (PEO-PBLA), not only made amphotericin soluble, but also reduced its toxic side effects.<sup>8</sup> Nanocrystal drug formulations are another type of nanocarrier formulations that have been shown to be useful in delivering poorly water soluble drugs.<sup>6,9</sup> Tricor™, a nanocrystalline formulation of fenofibrate, is currently being used for treatment of hypercholesterolemia.<sup>9,10</sup> Wortmannin is a potent PI3K inhibitor, but a poorly water soluble drug, which limited its use. Karve et al. developed a poly ethylene glycol (PEG) coated lipid nanoparticle formulating for wortmannin which improved the solubility and toxicity of the drug.<sup>11</sup>

Using nanoparticles for drug delivery, the enzymatic degradation of drugs can be prevented, thereby increasing the bioavailability of the drug. This can be achieved by coupling the nanoparticles with biocompatible polymers like polyethylene glycol (PEG; a process usually termed as PEGylation) or by delivering polymeric drug conjugates.<sup>12</sup> Further PEG can also be used as a linker, through which drug and other biomolecules can be attached to the nanoparticles. PEGylation increases the hydrophilicity of the formulation and reduces glomerular filtration thereby increasing the circulation time of the formulation.<sup>13</sup> It further enhances the pharmacokinetic profile by protecting from the reticuloendothelial system, and proteolytic enzymes.<sup>14,15</sup> The anticancer drug doxorubicin encapsulated in a liposome coated with PEG

(Doxil®) is currently being used in cancer therapy.<sup>16,17</sup> Using a PEGylated formulation showed to increase the circulation time and bioavailability of the drug.<sup>18</sup>

Another advantage of nanoparticle drug delivery is better targeting of drugs to the targeted organs; this reduces the uptake by non-targeted organs and increases drug dose delivered to intended sites. Targeted nanoparticle delivery can be dependent on size, charge and surface properties of the nanoparticle. For example, Bourges et al. showed that polylactide nanoparticles are capable of targeting retinal cells.<sup>19</sup> Quantum dots (<10 nm) were shown to be useful in accumulating in lungs and tumor vasculatures.<sup>20</sup> Targeted nanoparticles are also developed by conjugating them with specific biomarkers that are expressed on the target site. For example, Thamake et al. synthesized curcumin and bortezomib containing poly-lactic-co-glycolic acid (PLGA) nanoparticles conjugated with alendronate to target bone metastasis.<sup>21</sup> Their formulations successfully targeted bone, and also showed improved efficacy of the drug combination in an *in vivo* model of bone metastasis of breast cancer.<sup>21</sup>

The major obstacle in delivering drugs to brain, is to cross the blood brain barrier (BBB).<sup>22</sup> Researchers have formulated nanoparticle formulations targeting brain, which successfully accumulated in the brain crossing the BBB.<sup>22</sup> Cheng et al. reported AuNP modified with transactivator of transcription peptide (TAT), which successfully crossed the BBB and delivered drug cargoes (doxorubicin and Gadolinium, Gd<sup>3+</sup> imaging agent) to the intended site.<sup>23</sup> Kong et al. used magnetic nanoparticles to target brain using external magnetic field.<sup>24</sup> Using silica coated

magnetic nanoparticles with fluorophore, they demonstrated the nanoparticles crossing BBB and accumulating in brain in an *in vivo* model.<sup>24</sup>

Nanocarriers can be designed to be triggered release formulations. Triggered release formulations, will release the drug only in the presence of a suitable trigger. The trigger can be external, like a laser or internal like pH change. Sharma et al. developed, vitamin B6 conjugated lipid nanoparticles containing Doxorubicin.<sup>25</sup> The nanoparticles are pH sensitive charge reversing nanoparticles, intended for intracellular release of doxorubicin.<sup>25</sup> In another study, Mesoporous  $\gamma$ -iron oxide nanoparticles containing doxorubicin, which can be triggered by sudden burst of magnetic heating were prepared by Benyettou et al.<sup>26</sup> A triggered release cisplatin formulation was reported by Rocca et al. using polysilsesquioxane nanoparticles.<sup>27</sup> They tested the release of cisplatin from these formulations in the presence and absence of L-cysteine, a model endogenous reducing agent.<sup>27</sup>

### **Types of nanoparticles systems used in biomedical sciences:**

Nanoparticles used in biomedical sciences typically fall into two categories, inorganic nanoparticles (examples: gold, silver, magnetic, silica nanoparticles.) and organic nanoparticles (examples: polymeric, liposomes, micelles.). Polymer nanoparticles are a widely used nanoparticles in biology for the treatment of various diseases. Copaxone® is an example of polymer nanomedicine which is Food and Drug Administration (FDA) approved for treatment of multiple sclerosis.<sup>17,28</sup> Polymers like PEG are also used as conjugates to drug molecules. Neulasta® is a PEGylated granulocyte colony stimulating factor used for treatment of

chemotherapy induced neutropenia.<sup>17,28</sup> Polylactide-glycolic acid (PLGA) nanoparticles are one of the well-studied class of polymeric nanoparticles, which are known to decompose into their monomeric units overtime. ELIgard® is an FDA approved PLGA nanoparticle formulation used for the management of prostate cancer symptoms.<sup>29</sup> Polymeric micelles are another class of nanoparticles used in medicine. These are core-shell structures formed by self-assembly of polymeric amphiphiles. These are suitable for the delivery of hydrophobic drugs by encapsulating them in the inner core. Estrasorb™ is an FDA approved micelle for topical treatment of the symptoms of menopause.<sup>17</sup>

Liposomal formulations are one of the most significant and successful nanoparticle formulations used for drugs with low bioavailability. They are very easy to synthesize and are the first class of nanoparticles that entered the FDA clinical trials. Using liposomes have shown to increase the drug circulation time.<sup>30</sup> Further, PEGylation of liposomes increased the drug circulation time even more. Doxil® is an example of FDA approved liposomal formulation for the treatment of Kaposi's sarcoma, ovarian cancer, multiple myeloma and metastatic breast cancer.<sup>31</sup>

In addition to the nanoparticle formulations, electrospun polymeric nanofibers are being well studied in the field of regenerative medicine. Electrospinning of nanofibers is tested using several different polymers including polyacrylonitrile (PAN), collagen, elastin, and fibrinogen. Bioactive molecules and drugs of interest were shown to be incorporated into these nanofibers successfully. Polycaprolactone (PCL) nanofibers-loaded with curcumin (Cur) and PEG showed enhanced the rate of wound healing.<sup>32</sup> Katti et al. used PLGA nanofibers loaded with cefazolin, a broad spectrum antibiotic for wound treatment.<sup>33</sup> In another study, Shahi et al. demonstrated the potential anti-biofilm activity of TC loaded poly(DL-lactide), poly( $\epsilon$ -caprolactone), and gelatin polymer blend nanofibers.<sup>34</sup> Zhang et al. reported the efficacy of a dual-drug loaded (dichloroacetate and

oxaliplatin) poly-l-lactide nanofiber mats for treating cervical tumors recurring after surgery.<sup>35</sup> The fibers, demonstrated control release of drugs and showed synergistic effect along with reduced toxicity to other surrounding tissue in an *in vivo* model.<sup>35</sup>

### **Inorganic nanoparticles:**

Several different types of inorganic nanoparticles are currently being used for biological applications. The materials used in the synthesis of most of the inorganic nanoparticles are well characterized in their bulk form. Iron garnet, gold, silver are examples of some of the materials used. They exhibit unique properties as they approach nanosize, like tunable surface chemistry, exhibiting local plasmon resonance, surface charge, higher biomolecule conjugation efficiency.<sup>36,37</sup>

Quantum dots (QDs; CdSe, ZnSe, ZnS) which are nanocrystalline semiconductors are mainly used as multimodal contrasting agents for bioimaging.<sup>38</sup> They have intriguing properties different from the bulk material from which they are produced. Quantum dots emitting light at different wavelengths can be produced by just varying the crystal size. Nanoparticles with various metal cores were prepared previously. Plasmonic nanoparticles (mainly gold and silver based) are another group of inorganic nanoparticles, which are more advantageous in biomedical research. They exhibit the local plasmon resonance which can be used for sensing, triggering light activated events.<sup>37</sup> The surface chemistry of these nanoparticles allows for an effective bio conjugation of several molecules. AuNPs are widely studied because of their unique combination of optical, thermal, properties, and surface chemistry.<sup>39</sup>

Silica nanoparticles are another group of inorganic nanoparticles. Though they do not have interesting optical or electronic properties, the structure and composition of these nanoparticles can be modified easily.<sup>40</sup> Mesoporous silica nanoparticles (MSNs) belong to the family of silica nanoparticles, were discovered in 1992 by the Mobile Oil Corporation. They are since being studied for their use in medicine because of their high surface area, large pore volume, tunable pore diameter, and narrow pore size distribution.<sup>41</sup> A solid framework with porous structure and large surface area allows the attachment of different functional group to the mesoporous silica nanoparticles. This helps in developing targeted the formulation to a particular site by attaching targeting moiety.<sup>42,43</sup> MSNs have honeycomb-like structure and active surface which enables the surface functionalization.<sup>44</sup> The loading of the cargo can be achieved at a higher rate because of the higher surface area available for loading. Fan et al. developed MSNs containing doxorubicin for cancer therapy.<sup>45</sup> The drug was attached to the folic acid conjugated MSNs through a linker which can be cleaved under acidic conditions.<sup>45</sup> Iron oxide nanoparticles are another widely investigated group of nanoparticles by researchers, which have undergone clinical trials. Most of the FDA approved iron oxide nanoparticles till date are used as a replacement to iron supplements (Monofer®, Feridex®, DexIron®).<sup>16,17</sup> Supramagnetic iron oxide nanoparticles are being developed for local tissue hyperthermia therapy. Nanotherm™ is one such formulation which is under clinical trial for cancer therapy.<sup>46</sup>

### **Nanoparticles in cancer diagnosis and therapy:**

Cancer is the major cause of death in the United States. It is expected that ~600,000 Americans die of cancer in 2016.<sup>47</sup> In order to successfully eradicate any disease, one should be able to diagnose it early and then treat it in a localized environment. Nanoparticles are proven helpful in

both the above aspects. When circulating in the bloodstream, nanoparticles are subjected to clearance by the mononuclear phagocytic system (MPS). A large fraction of nanoparticles with a hydrodynamic diameter greater than 100 nm can be removed by resident phagocytosing Kupffer cells of the liver vasculature (Figure 1A). Nanoparticles with a hydrodynamic diameter <5.5 nm can cross the glomerular filtration system in the kidneys and be excreted with urine (Figure 1B). Nanoparticles with hydrodynamic diameters between 30–200 nm, can permeate easily through the leaky vasculature of the tumors and retain in tumors for longer period of time, which is usually termed as enhanced permeation and retention effect (EPR effect; Figure 1C). The majority of nanoparticles are internalized by cells through an endocytosis mechanism (Figure 1D).<sup>48</sup>

Many of the currently used cancer drugs face the problem of poor drug solubility, which limits the dose that can be administered to the patients and bioavailability of the drug. Using nanoparticles, the delivery of poorly water soluble anti-cancer drugs can be achieved. For example, a liposomal formulation of docetaxel ATI-1123, where the poorly soluble docetaxel is encapsulated in a liposomal formulation is currently entering phase-2 clinical trials for use in non-small cell lung cancer, gastric cancer, pancreatic cancer and soft-tissue sarcoma.<sup>49</sup>

First generation nanoparticles developed for cancer therapy relied on passive targeting of the nanoparticles to cancer site. For example, the nanoparticles retention in the tumor site due to leaky vasculature of the tumors (EPR effect). Liposomal doxorubicin (Caelyx®) and nab-paclitaxel (Abraxane®) are the examples of passively targeted nanoparticle formulations.<sup>40,50</sup> Passive targeting however is not sufficient to control the side effects of the drug. Therefore, researchers

started focusing on active targeting of nanoparticles. In active targeting, a ligand is attached either to the nanoparticle or to the active agent directly. The ligand of choice usually binds to the receptor selectively on the target site.

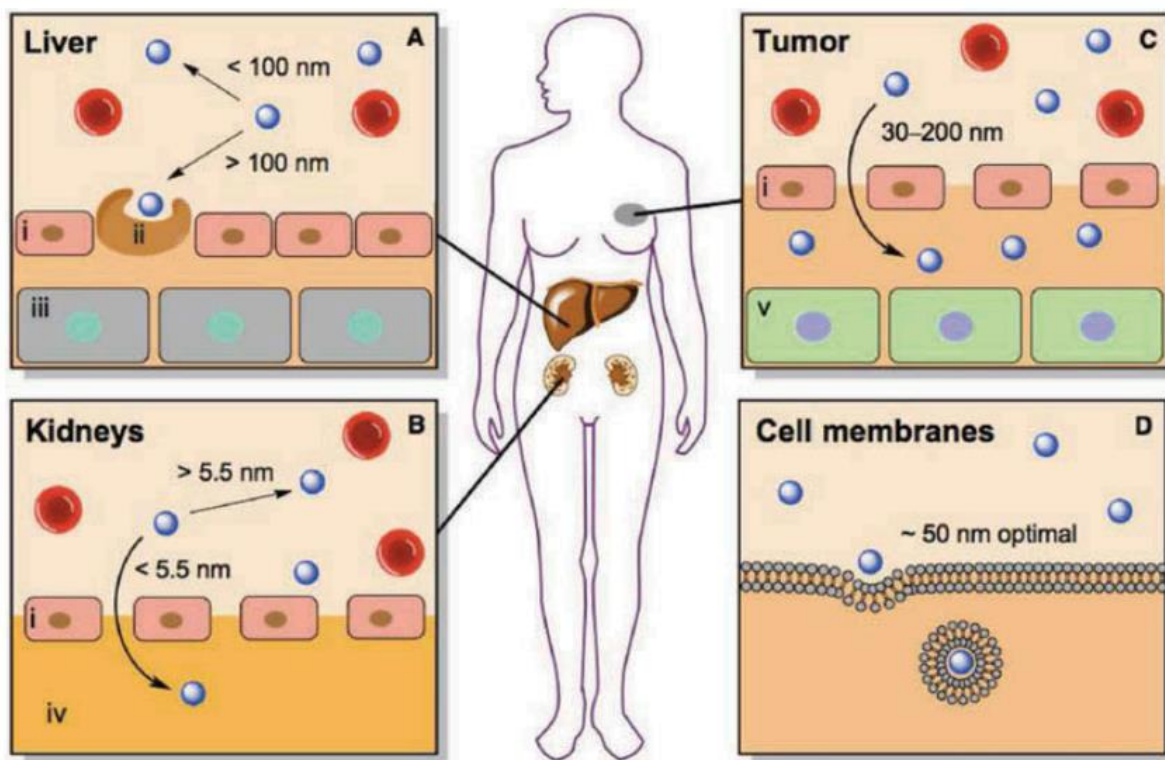


**Figure 1:** Major size-dependent biological barriers regulating the bio-distribution of blood-circulating nanoparticles.<sup>48</sup>

Targeted drug conjugates are the most clinically successful agents used to deliver drugs to the tumor sites. In these formulations usually the active agents are covalently linked to the targeting antibodies, peptides or polymers. Oncaspar® (PEGylated L-asparaginase) used for treatment of acute lymphoblastic leukemia, Neulasta® (PEGylated G-CSF protein) used for treating chemotherapy induced neutropenia are examples of some polymer-protein conjugates currently used in clinic.<sup>17,28</sup> Liposomes coated with antibodies against epidermal growth factor receptor

(EGFR) are currently under clinical investigation for delivery of doxorubicin.<sup>51</sup> Senanayake et al. used cholesteryl-polyvinyl alcohol-floxuridine nanogel to deliver paclitaxel and geldanamycin analog, 17-AAG for combination therapy and tested their efficacy in a breast cancer mouse model.<sup>52</sup>

Liposomes are used in the clinic against cancer. Liposomes can be formulated to target the cancer cells both actively and passively. Passive targeting of liposomes by EPR effect is size dependent. Liposomes should be in the range of 200 - 400 nm in order to be entrapped in the leaky vasculature of the tumors.<sup>53</sup> However, liposomes <200 nm were shown to have more efficient extravasation.<sup>40,53</sup> Ligand targeting of liposomal formulations is also widely reported in the literature. Xiang et al. reported the formulation of folate receptor targeted liposomes for the delivery of doxorubicin.<sup>54</sup> In another study, Malhi et al. dual targeted liposomal formulation by attaching folic acid for cancer cell targeting and triphenylphosphine a cationic lipophilic compound for mitochondrial targeting of doxorubicin.<sup>55</sup> Transferrin receptor targeted liposomes for the delivery of docetaxel were developed by Zhai et al. and showed enhanced cytotoxicity than the non-targeted liposomes *in vitro*.<sup>56</sup> Liposomes targeting the angiogenesis markers were also reported. Wicki et al. reported the formulation of liposomes conjugated with antibodies against vascular endothelial growth factor receptor (VEGFR) to deliver doxorubicin.<sup>57</sup> Their formulation showed superior toxicity to free drug in an *in vivo* model.

Metal nanoparticles are also developing as a promising delivery system for cancer therapy. Iron oxide nanoparticles, one of the extensively studies nanoparticle delivery systems, both as contrast

agents in MRI imaging and as drug carriers. Feridex® is a supramagnetic iron oxide nanoparticle formulation with dextran approved by FDA intended for its use as contrast agent in MRI imaging.<sup>20</sup> Nanotherm™, which consists of aminosilane-coated supramagnetic iron nanoparticles is currently being investigated in later phase clinical trials for tissue hyperthermia (heating the nanoparticles in an external magnetic field).<sup>46</sup> Torres et al. reported the formulation of an oleic acid (OA)-Pluronic-coated iron oxide magnetic nanoparticles which can be efficiently loaded with poorly soluble drugs.<sup>58</sup> Xu et al. used HER-2 conjugated iron oxide nanoparticles for selectively separating cancer cells from blood.<sup>59</sup>

AuNPs with their unique and tunable surface properties are emerging as a promising nanoparticle delivery system for cancer therapy. Patra et al. investigated the use cetuximab coated AuNP for EGFR targeted delivery of gemcitabine for the treatment of pancreatic adenocarcinoma.<sup>60</sup> They demonstrated the efficacy of the formulation in an orthotopic model of pancreatic cancer. They were able to achieve intratumoral gold concentrations of  $4500 \mu\text{g g}^{-1}$  using their formulations with minimal accumulation in the kidney. Hirsch et al. used gold nanoshells and demonstrated their use in photo thermal therapy.<sup>61</sup> When breast cancer cells incubated with gold nanoshells underwent exposure to near IR light (820 nm,  $35 \text{ W/cm}^2$ ), displayed morbidity; cells without nanoshells did not encounter any cytotoxicity due to the light exposure. Further, in an *in vivo* study, the tumor temperature raised to nearly  $37^\circ\text{C}$  when treated with nanoshells while the non-treated group the temperature raise is less than  $10^\circ\text{C}$ . Gold has better mass attenuation at energies greater than 80 keV making it an efficient contrast agent.<sup>62</sup> Aurovist™ has demonstrated superior contrast properties compared to iodine. These 1.9 nm AuNP, when injected *in vivo* in mice, demonstrated superior contrast and longer retention times.<sup>63</sup> In another study Popovtzer et al. developed gold

nanorods conjugated with UM-A9 antibody (antibody against A9 antigen expressed in squamous cell carcinoma of head and neck) and demonstrated its use as a contrast enhancing agent in CT imaging.<sup>64</sup> Aurimmune (CYT-6091) which is a PEGylated, citrate coated AuNP system with tumor necrosis factor alpha (TNF $\alpha$ ) is currently under clinical investigation.<sup>65</sup>

Use of nanoparticles as radiotherapeutic agents was also studied. Di Pasqua et al. were successful in reducing tumor burden in an *in vivo* ovarian cancer model using neutron-activable mesoporous silica nanoparticles containing holmium-166 (<sup>166</sup>Ho) as a radionuclide.<sup>66</sup> AuNP were also reported to be used as radiosensitizers. NBTXR3, is a hafnium oxide nanoparticle formulation is currently in clinical trials for its use as a radioenhancer in soft tissue sarcoma and head and neck cancers.<sup>67</sup> Table 1 gives the details of some FDA approved nanoparticle formulations currently in use for cancer therapy.

### **Nanoparticles for vaccine delivery:**

Use of nanoparticle for vaccine delivery is an emerging field in vaccinology. Nanoparticles can be used as delivery vehicles for vaccines or as adjuvants to enhance immunity.<sup>68</sup> Using nanoparticles provide an efficient delivery method for antigens, which would otherwise degrade upon injection *in vivo*.<sup>69</sup> Moon et al. developed a pathogen-mimicking PLGA nanoparticle coated with a lipid membrane for the delivery of malaria antigen.<sup>70</sup> When injected *in vivo*, these Nanoovaccines promoted germinal center formation and significantly higher titers of antigen specific antibodies.

**Table 1:** List of nanomedicines for cancer therapy which are FDA approved / under clinical trial

Product	Drug	Type of formulation	Use
Doxil ® (Samyang Biopharm)	Doxorubicin	Liposome	Kaposi's sarcoma Ovarian cancer Breast cancer Multiple myeloma
Marqibo® (Talon)	Vincristine	Liposome	Acute lymphoid leukemia
DaunoXome® (Galen)	Daunorubicin	Liposome	Kaposi's sarcoma
Abraxane® (Abraxis/Celgene)	Paclitaxel	Albumin-bound nanoparticle	Breast cancer, pancreatic cancer, non-small-cell lung cancer
Onco-TCS® (Inex)	Vincristine	Liposome	Non-Hodgkin lymphoma (in P I/II clinical trial)
Aroplatin® (Antigenics, Inc.)	Cisplatin analog	Liposome	Colorectal cancer (in P I/II clinical trial)
Onivyde® MM-398 (Merrimack)	Irinotecan	Liposome	Metastatic pancreatic cancer
MEPACT® (Millennium)	Mifamurtide	Liposome	Osteosarcoma
Ontak® (Eisai Inc)	IL-2and diphtheria toxin	Engineered protein	Cutaneous T-cell lymphoma
Feridex® (Amag pharmaceuticals)		Supramagnetic iron nanoparticle coated with dextran	Imaging agent

Gardasil is a vaccine approved by FDA against human papilloma virus (HPV).<sup>71</sup> In this formulations, the HPV antigens are formulated as four different viral like nanoparticles which are combined to form a cocktail of antigen containing nanoparticles.<sup>71</sup> Kim et al. investigated the immune response generated by oral delivery of *H.Pylori* lysate loaded PLGA nanoparticles.<sup>72</sup> When tested *in vivo*, the nanoparticles induced significant *H. pylori*-specific mucosal IgA response as well as serum IgG responses. Nanoparticles are also used for delivering DNA vaccines. Poly-l-lysine coated polystyrene particles when used for delivery of plasmid DNA encoding for chicken

egg ovalbumin, showed enhanced immune response in mice.<sup>73</sup> Further, when the mice were challenged with OVA expressing EG7 tumor cell line, the tumor growth was inhibited. Feng et al. developed a chitosan nanoparticle based DNA vaccine for *Mycobacterium tuberculosis* (*M.tb*). Mice that received these nanoparticles containing Esat-6 three T cell epitopes (Esat-6/3e) and fms-like tyrosine kinase 3 ligand (FL) genes (termed Esat-6/3e-FL), showed enhanced T-cell response and protection when challenged with *M.tb* H37Rv.<sup>73</sup>

### **Nanoparticles for antimicrobial therapy:**

Nanoparticles are emerging as a powerful strategy to deliver antibiotics to resistant bacteria. Using nanoparticles to deliver antibiotics can help address the bacterial resistance mechanisms like regulation of drug permeability, efflux pumps, and antibiotic degradation by enzymes. Metal nanoparticles like silver, gold and zinc oxide (ZnO) nanoparticles are shown to have potent antimicrobial activity.<sup>74-76</sup> AuNP capped with amino-substituted pyrimidines showed antimicrobial activity against multi drug resistant bacteria.<sup>77</sup> They acted by damaging the bacterial cell membrane via sequestering of Mg and Ca ions. Li et al. showed that AuNP with different cationic and hydrophobic surface functionalities, inhibited the growth of 11 multi drug resistant bacteria.<sup>78</sup> Nitric oxide releasing silica nanoparticles were evaluated for their efficacy against various biofilms by Hetrick et al.<sup>79</sup> When treated with nanoparticles,  $\geq 99\%$  of cells from each type of biofilm were killed via NO release. Vancomycin capped AuNP were reported to have enhanced *in vitro* antibacterial activity.<sup>80</sup> Nanoparticles are also useful in hyperthermia induced killing of bacteria. For example, superparamagnetic iron oxide nanoparticles were used by Park et al. to inactivate biofilms of *Pseudomonas aeruginosa*.<sup>81</sup> Other inorganic nanoparticles like magnesium fluoride nanoparticles, iron oxide nanoparticles, and copper oxide nanoparticles were also shown to exert

potent anti-microbial activity.<sup>82-84</sup> Organic nanoparticles like liposomes are explored for their use as delivery of anti-microbial agents. In a study by Muppidi et al., vancomycin encapsulated in PEGylated liposomes, showed enhanced accumulation in lungs and increased the circulation times.<sup>85</sup> A gentamycin liposomal formulation showed an enhanced antimicrobial activity against *Pseudomonas aeruginosa* compared to the free drug.<sup>86</sup> The field of nanoantibiotics is emerging fast and several promising nanocarrier formulation can be produced to combat multi drug resistant bacteria in near future.

Nanoparticles are also used for anti-retroviral drug delivery. For example, Garg et al. developed Stavudine-loaded mannosylated liposomal formulations for targeting HIV-infected cells.<sup>87</sup> These formulations showed enhanced cytotoxicity and reduced side effects compared to free drug. Surface engineered mannosylated liposomes were shown to enhance the targeting of zidovudine to lymphatic system.<sup>88</sup> Dutta et al. developed poly(propyleneimine) dendrimer-based nanocarriers for targeting of efavirenz (EFV) to monocytes/macrophages.<sup>89</sup> The uptake of EFV by cells increased 5.5 times more when delivered through dendrimers compared to free drug.

Apart from being used in medicine, nanoparticles are also useful in bio assays. Zhao et al. reported a bio conjugated nanoparticle based bioassay for *in situ* pathogen quantification down to single bacterium within 20 min.<sup>90</sup> Using this system, they were able to identify a variety of bacterial strains. Silver and AuNP were found to be useful in calorimetric assays.

Nanoparticles thus have evolved as a strong and promising system for biomedical applications. Researchers are continuously investigating to use the unique properties of nanoparticles for

biological applications. Table 2 gives the details of some FDA approved nano formulations for various disorders.

**Table 2:** List of FDA approved nanomedicines

<b>Product</b>	<b>Drug/type of formulation</b>	<b>Use</b>
Copaxone® (Teva)	Random copolymer of L-glutamate, L-alanine, L-lysine and L-tyrosine	Multiple sclerosis
Neulasta® (Amgen)	PEGylated GCSF protein	Chemotherapy induced neutropenia
Cimzia® (UCB)	PEGylated antibody fragment of cetrolizumab	Cohn's disease, rheumatoid arthritis
Macugen® (Hoffman-La Roche)	PEGylated anti-VEGF aptamer	Age related macular degeneration
PegIntron® (Merck)	Pegylated INF-alpha 2a protein	Hepatitis C
DepoCyt®	Liposomal cytarabine	Lymphomatous meningitis
AmBisome(Gilead sciences)	Liposomal Amphotericin B	Fungal/protozoal infections
DexIron® (Sanofi Avertis)	Iron dextran nanoparticles	Iron deficiency in chronic kidney disease
Estrasorb® (Novavax)	Micellar estradiol	Menopausal therapy

**Objective:** The objective of this work is to explore the use of various inorganic nanomaterials for applications in biomedical sciences. Here, we developed three novel nanocarrier formulations for treatment of three different disorders.

- 1)  $^{166}\text{Ho}$  iron garnet nanoparticle-containing bandages for treatment of squamous cell carcinoma of the skin
- 2) Targeted chemotherapy for non-small cell lung cancer using antibody-coated gold nanoparticles
- 3) Tetracycline-containing MCM-41 mesoporous silica nanoparticles for the treatment of *Escherichia coli*

## Chapter 2

# **<sup>166</sup>Ho iron garnet nanoparticle-containing bandages for treatment of squamous cell carcinoma of skin**

### Abstract

#### Introduction

Squamous cell carcinoma (SCC) is the second most common form of skin cancer in the United States. The efficacy of a pharmaceutically elegant radiotherapeutic bandage, previously described by us for application against SCC of the skin, was tested for the first time *in vivo* using a subcutaneous SCC mouse model and a therapeutically relevant radiation dose.

#### Methods

Female athymic nude mice were injected with human Colo-16 SCC cells subcutaneously and after eight days (average tumor volume:  $35 \pm 8.6 \text{ mm}^3$ ) received no treatment, or were exposed to non-radioactive or radioactive ( $2.5 \pm 0.5 \text{ mCi}$ ) bandages for approximately 1 h ( $n = 10$  per group). After treatment, tumors were measured over fifteen days, tumor volume ratios (TVRs) compared and histopathology performed.

## **Results**

Fifteen days after treatment, the TVR of the radioactive bandage treatment group was  $3.3 \pm 4.5$ , while TVRs of the non-radioactive bandage treatment and no treatment control groups were  $33.2 \pm 14.7$  and  $26.9 \pm 12.6$ , respectively. At the time of necropsy, there was mild focal epidermal hyperplasia surrounding a small area of epidermal ulceration in the radioactive bandage group. No other examined tissue (i.e., muscle, liver, kidney, lung, spleen and heart) showed histological abnormalities.

## **Introduction**

It is currently estimated that one in every five Americans will develop skin cancer; most will be diagnosed with non-melanoma skin cancer (NMSC),<sup>91</sup> and the incidence of NMSC may increase by an estimated 50% by 2030.<sup>92</sup> Most NMSCs develop on sun-exposed areas of the body, such as the face and back of the hands. The two major forms of NMSCs are basal cell carcinoma (BCC) and squamous cell carcinoma (SCC). BCC develops in the basal cells of the skin, which are found in the lower epidermis. SCC develops in the squamous cells, which are flat-scale like cells that constitute most of the epidermis.<sup>92</sup> SCC accounts for approximately 20% of all the NMSCs.<sup>92</sup> The incidence of SCCs is often not known much as it is not required to be noted by the cancer registries. A recent study showed that up to approximately 400,000 new cases of SCC were diagnosed among the white population alone in the US in 2012; the incidence data for other racial/ethnic groups was limited.<sup>93</sup>

Treatment options for SCC include surgery, chemotherapy, and radiation therapy. Therapy for SCC are generally selected based on the characteristics of the patients and their neoplasm, such as a patient's age, surgical candidacy, lesion size and location, level of differentiation and depth of invasion.<sup>92</sup> For low risk tumors, the treatment options include, surgical excision, electrodesiccation, and curettage, or cryosurgery.<sup>94</sup> For high risk tumors, the primary line of treatment is surgical excision.<sup>94</sup> When feasible, the treatment of choice is Mohs micrographic surgery (MMS), which allows for excision of a lesion and its histological examination, to achieve complete removal of the cancerous tissue.<sup>95</sup> The key to the surgical removal of SCC is the ability to achieve negative surgical margins,<sup>95,96</sup> i.e., complete removal of cancerous tissue. At first, the targeted lesion and its surgical margins will be microscopically determined by the surgeon and

excision will be carried out. The margins that are remaining will undergo excisions until negative surgical margins are achieved. As the risk level of the tumor increases, the cure rate with surgical excision goes down as it becomes difficult to achieve negative margins. When surgical margins are inherently compromised, radiation therapy is critical for the destruction of SCC.<sup>97</sup> Chemotherapy is usually used in case advanced or metastatic SCC. However, the investigation on systemic/topical chemotherapy for SCC is limited. Cisplatin, 5-fluorouracil, bleomycin are some of the commonly preferred chemotherapeutic agents.<sup>98</sup>

Radiation therapy plays an irreplaceable role in current SCC therapy.<sup>99</sup> Radiation is used as a primary/adjuvant therapy in management of high risk tumors and also to treat recurring lesions after a primary surgical approach.<sup>100</sup> External beam radiation therapy, which is currently used for the treatment of SCC,<sup>100</sup> uses high energy X-rays or particles (photons, protons, electrons) to kill the cancer cells. Radiation kills the cancer cells by either damaging the DNA or producing reactive oxygen species which in turn damage the DNA of cancer cells.<sup>101</sup> Several newer forms of external beam radiation therapy are now being used. Three dimensional conformal radiation therapy, intensity modulated radiation therapy, and stereotactic radiosurgery<sup>101</sup> are some examples. External beam radiation therapy requires specialized equipment, requires multiple in-patient sessions and, furthermore, the safety margin around the tumors is high (~1–1.5 cm) causing more side effects on normal tissue.<sup>102</sup> Another approach of radiotherapy used is brachytherapy, an internal radiation therapy. Radioactive source is placed in the form of an implant and held near the tumor with the help of an applicator.<sup>100</sup> This also requires special equipment for application and, due to the nature of the technique, there is a risk of radiation exposure to medical personnel who perform the therapy. Sometimes, stitches may be required to hold the applicator in position.

Radionuclide therapy is another type of radiation therapy. Here, the radiation source will be radioactive isotope. A radioactive isotope can emit three kinds of radiations, alpha particles ( $\alpha$ ; consist of two protons and two neutrons), beta particles ( $\beta$ ; is a high energy electron or positron) and gamma particles ( $\gamma$ ; electromagnetic radiation)<sup>103</sup>. Among all,  $\alpha$  particles have the highest energy and lower penetration, followed by  $\beta$  and  $\gamma$ . Strontium-89, iodine-131, radium-223, phosphorus-32, are some of the radio isotopes used as radiopharmaceuticals.<sup>103</sup>

A radiotherapeutic patch comprised of  $^{166}\text{Ho}$  particles coated on the surface of a paper and laminated with a polyethylene film has been reported and was used to suppress SCC in animals and in a human trial, albeit with limited numbers of subjects in both studies ( $n = 3$  per group).<sup>104</sup> Although it was mentioned that the particles, which had a wide range of size (1–6  $\mu\text{m}$ ), were uniformly affixed on an adhesive tape, the uniformity of  $^{166}\text{Ho}$  in the construct was not quantitated.<sup>104</sup> Moreover, stability of the patch after neutron-activation was not discussed; it is possible that the radionuclides on the surface could flake off, and therefore affect the efficacy and cause safety hazards. To overcome these limitations, we constructed and previously reported<sup>105</sup> a bandage containing  $^{166}\text{Ho}$ , which can be easily manipulated and applied externally to the skin; it was suggested that this device could be used for selective radiotherapy of skin tumor lesions.<sup>105</sup> As previously reported, the radiotherapeutic bandage used in this study was prepared using uniform non-radioactive holmium-165 ( $^{165}\text{Ho}$ )-containing iron garnet ( $^{165}\text{HoIG}$ ) nanoparticles and polyacrylonitrile (PAN) fibers via electrospinning and achieved good stability and uniformity of  $^{165}\text{Ho}$  distribution<sup>105</sup> (Figure 2).

Electrospinning is the process of producing nanofibers by applying electric potential to polymeric solutions.<sup>106</sup> An electrical potential will be applied to the polymer solution held at the tip of a capillary tube by virtue of its surface tension; thus the solution will be charged. Mutual charge repulsion in the polymer solution induces a force that is directly opposite to the surface tension of the polymer solution.

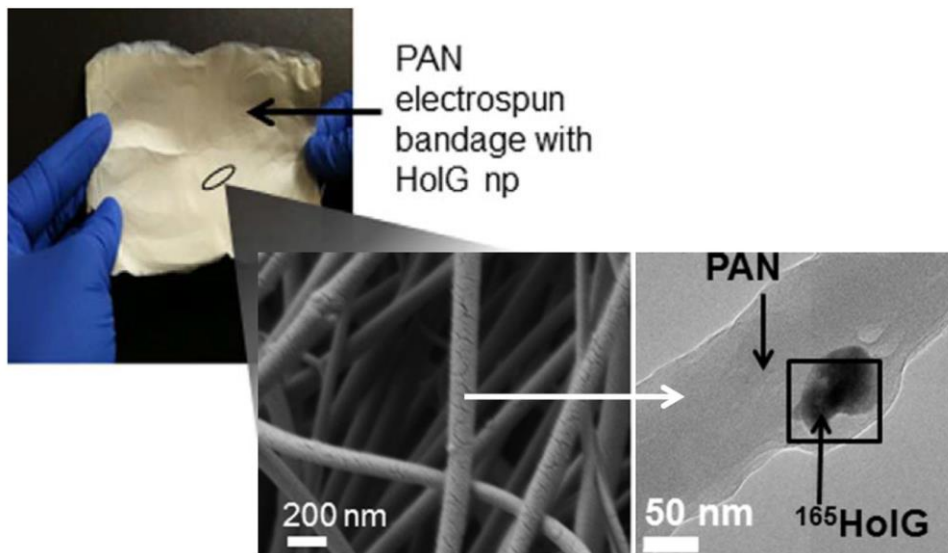


**Figure 2:** Digital image of 33% (w/w)  $^{165}\text{HoIG}$ -containing PAN bandages and SEM and TEM images (left to right).<sup>105</sup>

An increase electric potential (critical value) overcomes the surface tension forces causing the formation of a jet.<sup>107,108</sup> The charged jet will then elongate and solvent evaporation will take place causing instabilities and gradually thinning in air. The randomly oriented fibers thus formed from the charged jet can be collected on a stationary or rotating grounded metallic collector.<sup>108-110</sup> This technique allows us to embed radionuclide containing nanoparticles directly in the fibers of the bandages, which is an improvement over previously reported radioactive bandages/ patches/films based on coatings, as it facilitates uniform distribution throughout the construct<sup>104</sup>. Moreover, the

thickness of the electrospun bandages can be varied by controlling parameters such as spinning duration, polymer concentration, applied voltage, temperature and humidity.<sup>110,111</sup>

The radiotherapeutic bandage was prepared while non-radioactive and made radioactive by neutron-activating  $^{165}\text{Ho}$  to  $^{166}\text{Ho}$  prior to treatment.<sup>105</sup>  $^{166}\text{Ho}$ , which has a short half-life (26.8 h), emits both beta ( $\beta^-$ ) particles and gamma ( $\gamma$ ) photons. Its high-energy  $\beta^-$  particles (1.84 MeV)<sup>112</sup> are sufficient to damage DNA in cancer cells just beneath the outermost layer of the epidermis, while the  $\gamma$  photons (6.6% photon yield)<sup>112</sup> can be used to easily quantify radiation dose of the bandage prior to its application. The bandage will be non-radioactive after approximately ten half-lives, making its storage and disposal easy. Importantly, our previous study showed that the prepared bandages were stable during and after neutron activation;<sup>105</sup> no changes were observed in the bandage after neutron-activation upon visual inspection (Figure 3A-E).<sup>105</sup> SEM shows that fiber diameter determined from there is a slight increase in the diameter after neutron-activation (Figure 4).<sup>105</sup>

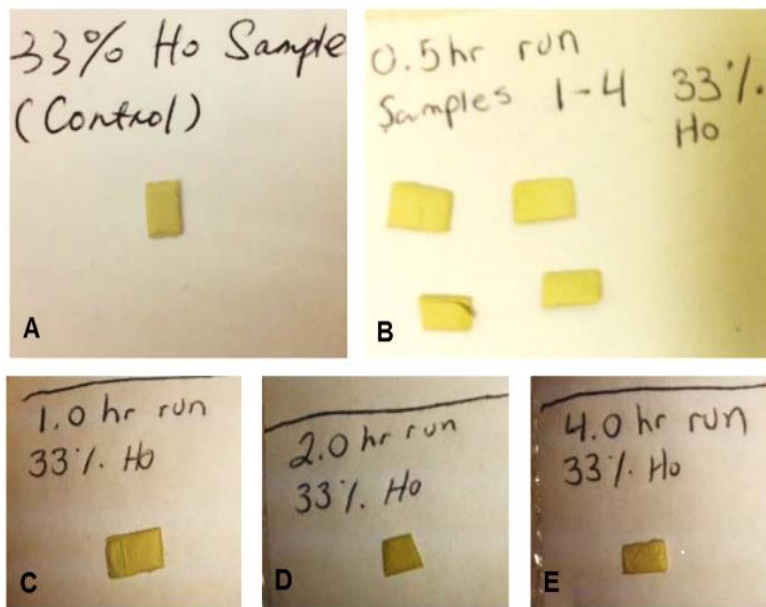


**Figure 3:** 33% (w/w) HoIG-containing PAN bandages before (A) and after neutron-activation for 0.5 h, 1.0 h, 2.0 h and 4.0 h (B-E) in a thermal neutron flux of approximately  $3.5 \times 10^{12} \text{ n/cm}^2 \cdot \text{s}$  in a 1 MW nuclear reactor. All pieces were cut from same fiber mat. No difference was observed between control and treatment groups upon visual inspection.<sup>105</sup>

Since the bandage will be prepared non-radioactive, this helps achieving GMP standards during manufacture, which is very important for future clinical trials. The neutron-activation can be performed off-site and then the material can easily be shipped to a clinic with a precise radiation

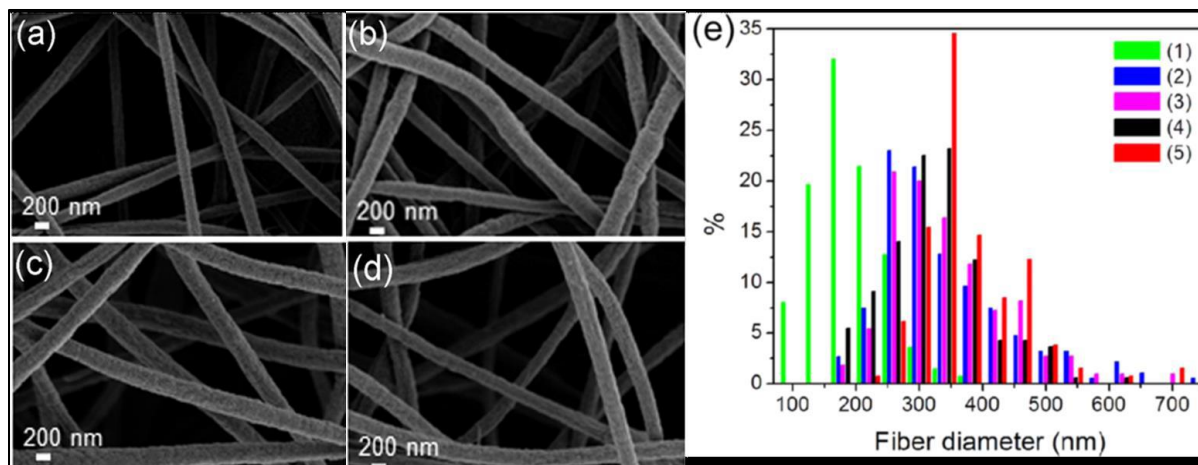


**Figure 4:** SEM images and fiber diameter distributions of 33% (w/w) HoIG-containing PAN bandages before (e-1) and after neutron activated for (a) (e-2), 0.5 h; (b) (e-3), 1.0 h; (c) (e-4), 2.0 h; (d) (e-5), 4.0 h (using 25 images). No significant changes in fiber diameter were observed upon neutron activation.<sup>105</sup>

dose. It is important for a formulation, which is intended to deliver radiation to a topical lesion, that it should emit uniform radiation. We have previously demonstrated that our formulation emits radiation uniformly throughout (Figure 5).<sup>105</sup>

The advantage of this formulation is that the radiation source is embedded into the fiber. Therefore, the chance of particles leaching out is less. This was previously confirmed by soaking the bandages in stimulated body fluids for up to 8 h and examining the fluid (SBF) under transmission electron microscope;<sup>105</sup> no free nanoparticles were observed in the SBF. The application of the bandage during treatment of animals here was as easy as applying a piece of tape onto the skin, which will minimize the risk of radiation exposure of medical personnel if moved to the clinic.

In the present study, the efficacy of the radiotherapeutic bandage was tested in an *in vivo* model of SCC.

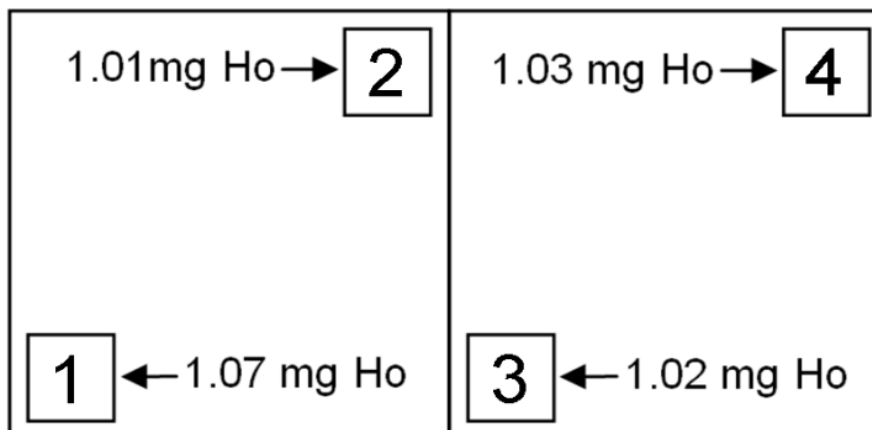


**Figure 5:** Diagram showing homogeneity of 33% (w/w)  $^{166}\text{HoIG}$  containing PAN bandage. Four pieces of bandage were cut from corners of same bandage and were neutron activated. The amount of Ho was then calculated from the emitted radiation. As represented in the figure, the amount of Ho was homogenous throughout the bandage.<sup>105</sup>

## Materials and Methods:

### Preparation of $^{165}\text{HoIG}$ -PAN bandage:

The  $^{165}\text{HoIG}$ -containing PAN bandages were synthesized as described previously.<sup>105</sup> Briefly, Stoichiometric mixtures (5:3) of 1 M iron (III) nitrate (5 mL) and 1 M holmium (III) nitrate (3 mL) were mixed with ethylene glycol (21 mL) at room temperature with stirring. Then 6 M NaOH (10 mL) was added dropwise to form the  $^{165}\text{HoIG}$  nanoparticle precipitate. The product was centrifuged and washed with deionized water, then dried at 100 °C overnight. The  $^{165}\text{HoIG}$  was annealed in air at 900 °C for 3 h.

Polyacrylonitrile (PAN) (1.0 g) was dispersed in dimethylformamide (DMF) (5 mL), with gentle heating and stirring.  $^{165}\text{HoIG}$  nanoparticles were dispersed in DMF (5 mL) and mixed with the PAN solution at room temperature to prepare 33 w/w dispersions. The PAN solutions containing  $^{165}\text{HoIG}$  nanoparticles were drawn into a 12 mL syringe equipped with a 20-gauge needle and electrospun on an aluminum foil substrate wrapped around a rotating drum. The condition used for electrospinning are shown in table 3.

**Neutron-activation of  $^{165}\text{HoIG}$ -PAN bandage:**

$^{165}\text{HoIG}$ -PAN bandages were then cut into small squares (average weight:  $10.3 \pm 0.3$  mg and size:  $6-7 \times 6-7$  mm) and neutron-activated in a 1 MW TRIGA® reactor at the Texas A&M nuclear

**Table 3:** Electrospinning parameters.<sup>105</sup>

<b>Sample</b>	<b>PAN (g)</b>	<b><math>^{165}\text{HoIG}</math> nanoparticles (g)</b>	<b>volume of DMF (mL)</b>	<b>rate (mL/h)</b>	<b>voltage (kV)</b>	<b>electrode separation distance (cm)</b>
$^{165}\text{HoIG}$ 33% (w/w)	1	0.5	10	0.05	14	6

science center. Neutron-activation was carried out at a neutron flux of  $1.8 \times 10^{13}$  neutrons/cm<sup>2</sup> · s for 1.33 h. Radioactivity from the bandages was quantified before application using a 2470 Wizard2 automatic gamma counter (Perkin Elmer, Shelton, CT).

**Cell culture and animals:**

Human SCC Colo-16 cells were from the laboratory of Dr. Reuben Lotan (University of Texas MD Anderson Cancer Center, Houston, TX)<sup>113</sup> and authenticated via short tandem repeat (STR) DNA fingerprinting using the PowerPlex 16 HS System (Promega, Madison, WI) on March 2014. The cells were grown in Keratinocyte-SFM medium (Gibco® by Life Technologies, Grand Island, NY) supplemented with 3% fetal bovine serum and cultured under standard conditions in a humidified, 37 °C, 5% CO<sub>2</sub> atmosphere incubator. Female Hsd:Athymic Nude-Foxn1nu mice (5 to 6 weeks, ~20 g) were obtained from Harlan Laboratories (Indianapolis, IN). All animal procedures were performed following a protocol approved by the University of North Texas Health Science Center Institutional Animal Care and Use Committee in accordance with the NIH Guidelines.

**Animal studies**

The efficacy of the radiotherapeutic bandages was tested in a xenograft mouse model for SCC. One million Colo-16 cells were resuspended in a total volume of 100 µL of PBS and Matrigel (Corning™, Bedford, MA; 1:1) and then injected into the flank of the left hind leg of each mouse. Matrigel is often used to establish xenograft tumors in mice; however, care must be taken to avoid gelation during the procedure. Eight days after injection, when the tumors were palpable (average tumor volume:  $35 \pm 8.6 \text{ mm}^3$ ), the mice were assigned to one of the three following groups (n = 10 per group): group A, no treatment control; group B, non-radioactive bandage treatment control; and group C, radioactive bandage treatment. The mice in group B and group C were anesthetized

via isoflurane inhalation for 3 min and either non-radioactive bandage (group B) or radioactive bandage (group C) was attached onto the tumor using NipEAZE™ tape (Owensboro, KY).

An average radiation dose of  $2.5 \pm 0.5$  mCi per mouse was delivered through the bandages in group C. The bandages were removed after approximately 1 h and the tumor volume was then monitored. The tumor size was measured using a Vernier caliper and the tumor volume (V) was calculated using the following equation:

$$V = (L \times W^2)/2$$

where L is the length (large diameter) and W is the width of the tumor (small diameter), both in millimeters. Tumor volume ratios (TVRs) were calculated using tumor volume on the day of measurement divided by tumor volume on the day of treatment (Day 0)<sup>114</sup>. Twelve days after treatment, two mice from group B and one mouse from group A were sacrificed as their cumulative tumor scores were high. Fifteen days after treatment, when all mice in the control groups reached high cumulative tumor scores, all mice were euthanized via CO<sub>2</sub> inhalation followed by cervical dislocation. The efficacy of the bandages was determined by comparing the TVRs after treatment among the groups.

The tumor along with the adjacent skin and muscle and heart, kidneys, lung, liver and spleen were collected in 10% neutral buffered formalin for histopathologic examination. The tissues were embedded in paraffin and stained with hematoxylin and eosin, and were then examined for signs of radiation toxicity.

### **Statistical analysis:**

Statistical analysis was performed using SigmaPlot™ (Version 11.0; Systat Software Inc., San Jose, CA). All the data were analyzed using two-way repeated measured ANOVA followed by

Bonferroni t-test for post hoc analysis to compare the difference among groups on each day. It was determined as a significant difference between values of different groups when  $p \leq 0.05$ .

## Results and Discussion:

The incidence of NMSCs is increasing rapidly.<sup>93</sup> SCC, a form of NMSC, is being diagnosed widely, but very little is being done to improve its therapy. Radiation therapy is used as primary and/or adjuvant therapy for the treatment of SCC. External beam therapy, which is often used, requires cumbersome equipment and can cause damage to surrounding healthy tissues. We previously reported a radiotherapeutic bandage that may be useful for the treatment of SCC in clinic.<sup>105</sup> The bandage consists of  $^{166}\text{Ho}$  as a source of radiation, which is both a  $\beta^-$  and  $\gamma$  emitter and has a short half-life. These bandages were shown to be stable and emit uniform radiation throughout.<sup>105</sup> The shape of the radiotherapeutic bandage can be manipulated as per the tumor size and therefore helps in reducing the healthy tissue damage. The bandages are prepared while non-radioactive and are made radioactive by neutron-activation.

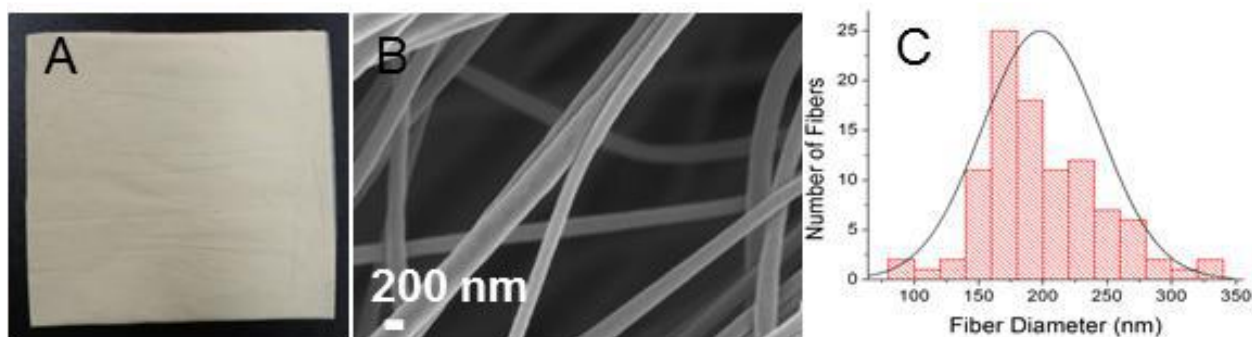


**Figure 6:** A (A) digital image, (B) SEM image and (C) fiber diameter distribution of the  $^{165}\text{HoIG}$ -containing PAN non-radioactive bandage. The approximately 5 cm  $\times$  5 cm piece of bandage was placed on weighing paper and the picture taken on a black background.

In this study polyacrylonitrile (PAN) (Molecular weight: 150,000 mol/g) solution containing  $^{165}\text{HoIG}$  nanoparticles (33% w/w) were electrospun to produce a flexible bandage (Figure 6 A), as described previously.<sup>105</sup> SEM image of the electrospun fiber mat is shown in Figure 6 B. As shown in the histogram, the average diameter of nanofibers is  $198 \pm 45$  nm (Figure 6 C).

In order to test the efficacy of the bandage (Figure 6 A), an *in vivo* efficacy study was carried out in a xenograft mouse model. Female athymic nude mice were injected with one million human SCC cells (Colo-16) subcutaneously into their left flank. The mice were then divided into three groups (n = 10 per group) and received either no treatment (Group A), or non-radioactive (Group B) or radioactive bandage treatment (Group C). The  $\beta^-$  particles emitted from  $^{166}\text{Ho}$ , have a range of maximum 8.7 mm (average 2.1 mm) in human tissues.<sup>104,115</sup> Therefore, the energy from the bandages should be enough to damage the subcutaneous tumor in the mouse model. Each mouse in Group C received an average dose of  $2.5 \pm 0.5$  mCi for approximately 1 h. According to a dosimetry estimation by Lee et al.<sup>104</sup> on a  $^{166}\text{Ho}$  skin patch and by Mowlavi et al.<sup>116</sup> on a similar configuration, exposure to 2.5 mCi  $^{166}\text{Ho}$  for 1 h could result in 31 Gy of radiation at 1.5 mm below the skin and 14 Gy at 2.5 mm, but dramatically reduced to only 1.9 Gy at 4.5 mm depth. Thus, this dose is therapeutically relevant<sup>102</sup>. The Ho content in the bandages was  $20.7 \pm 4.4\%$  w/w, calculated based on the radioactivity of each piece of bandage measured using a gamma counter, which is similar to that of the previously reported radiotherapeutic bandages. Figure 7 shows the mice with bandage attached to it.

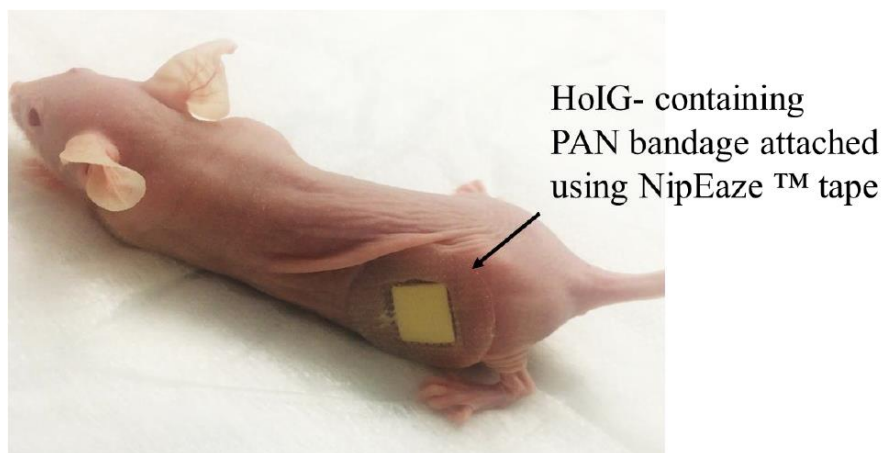


**Figure 7:** Mouse with  $^{165}\text{HoIG}$ -containing PAN attached on the tumor 8 days after injecting with Colo-16 cells.

To evaluate the efficacy of the radiotherapeutic bandage (Group C), TVRs were calculated and compared among the radioactive treatment group and the other two control groups (Groups A and B). In Figure 8, the comparison of TVRs among Groups A, B and C on 1, 2, 3, 5, 7, 9, 12 and 15 days after treatment is shown. On Day 2, the TVR of Group C ( $1.0 \pm 0.4$ ) was significantly lower than that of Group A ( $1.9 \pm 0.8$ ). From Day 3 up to sacrifice on Day 15, the TVR of Group C was significantly lower than that of both Groups A and B. The overall tumor growth rate was lower in Group C compared to Groups A and B as indicated by the increase in TVRs with time (Figure 8). TVRs were also compared within the group, no significant increase in tumor volume was observed in group C. In groups A and B, the TVR was significantly increased from Day 1 to Day 15. Figure 9 shows the tumor burden of the mice on the day they were euthanized. When high cumulative tumor scores were reached (rapid weight loss, signs of impaired mobility and/or ulcerated tumor), one mouse (A10) from Group A and two (B9 and B10) from Group B were euthanized on Day 12.

All the mice (A 1-9, B1-8 and C1-10) were sacrificed on Day 15 after treatment, as the mice in Groups A and B reached high cumulative tumor scores (impaired mobility, weight loss and/or

ulcerated tumors). It is obvious that the tumor burden of Groups A and B was higher compared to that of Group C. On Day 15, three (C1, 2 and 4) out of ten mice in the radioactive bandage treatment group had complete tumor elimination with another one having a very small tumor (C3); the other six in the same group had significantly smaller volume compared to the control groups; the TVR of Group C was only  $3.3 \pm 4.5$ , while TVRs of Groups A and B were  $26.9 \pm 12.6$  and  $33.2 \pm 14.7$ , respectively.

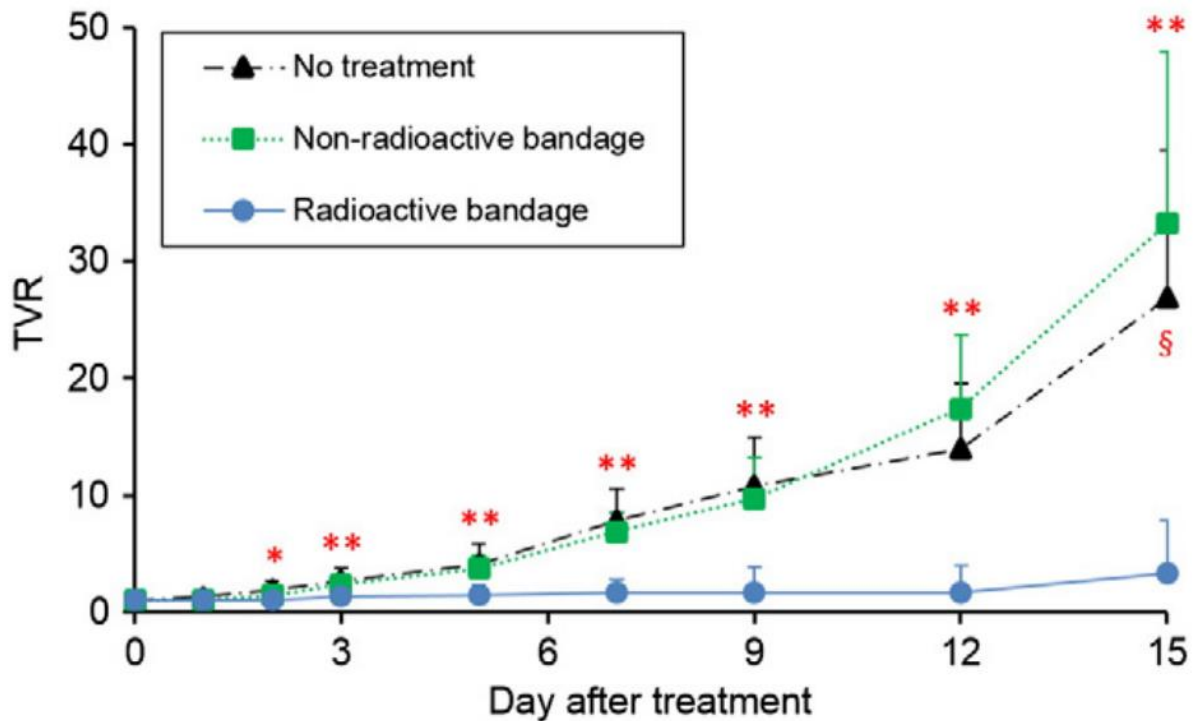


**Figure 8:** TVR plotted against the number of days after treatment. §Three mice (one from Group A and two Group B) were euthanized and tumors were harvested due to high cumulative tumor score 12 days after treatment. \*The average of TVR of Group C was significantly different from Group A ( $p < 0.05$ ). \*\*The average of TVR of Group C was significantly different from both Groups A and B ( $p < 0.05$ ).

The non-radioactive bandage (Group B) showed no significant effect on the tumor growth (Figure 8, 9) compared to the no treatment group (Group A) and there were no gross or histologic abnormalities of the skin due to the non-radioactive bandage (Figure 10). The radioactive bandage (Group C) showed slight skin damage, which started on Day 5, but the damage was recovering

without any intervention. At the time of necropsy, there was mild focal epidermal hyperplasia surrounding a small area of epidermal ulceration (Figure 11). All other tissues in the control group, non-radioactive bandage group and radioactive bandage group showed no significant lesions (Figure 10). Similar skin damage was also observed by Lee et al.<sup>104</sup> and Jeong et al.,<sup>117</sup> when their

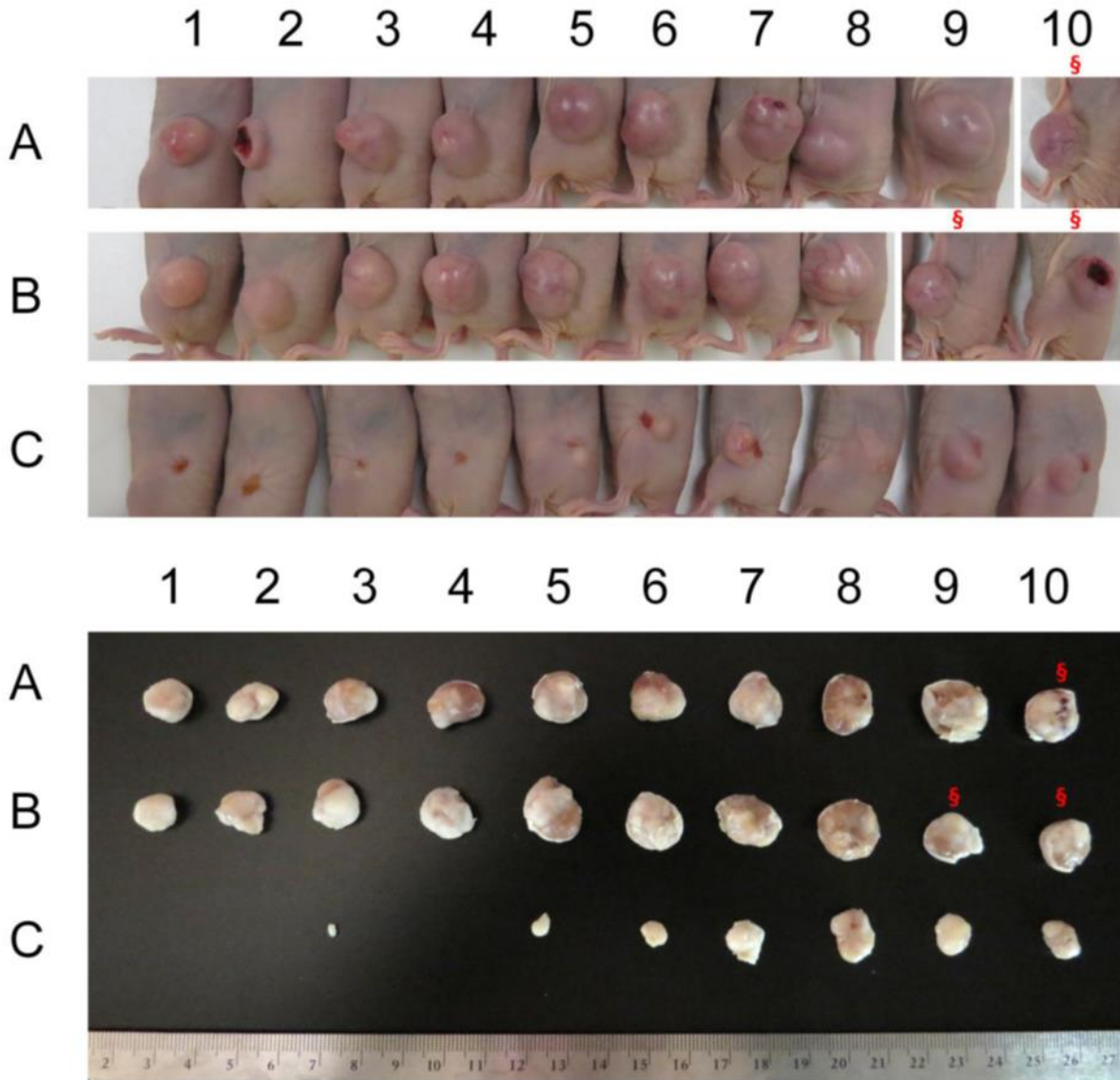


**Figure 9:** Top: Tumor-bearing mice in (A) no treatment, (B) non-radioactive bandage and (C) radioactive bandage treatment groups 15 days after treatment. Bottom: Tumors harvested from mice in (A) no treatment, (B) non-radioactive bandage and (C) radioactive bandage treatment groups 15 days after treatment. § Three mice (one from group A and two from group B) were euthanized and tumors were harvested due to high cumulative tumor score 12 days after treatment.

$^{166}\text{Ho}$  patch and rhenium-188 ( $^{188}\text{Re}$ ) paper were used, respectively. Their mice recovered from skin damage in 7 days.<sup>104,117</sup>

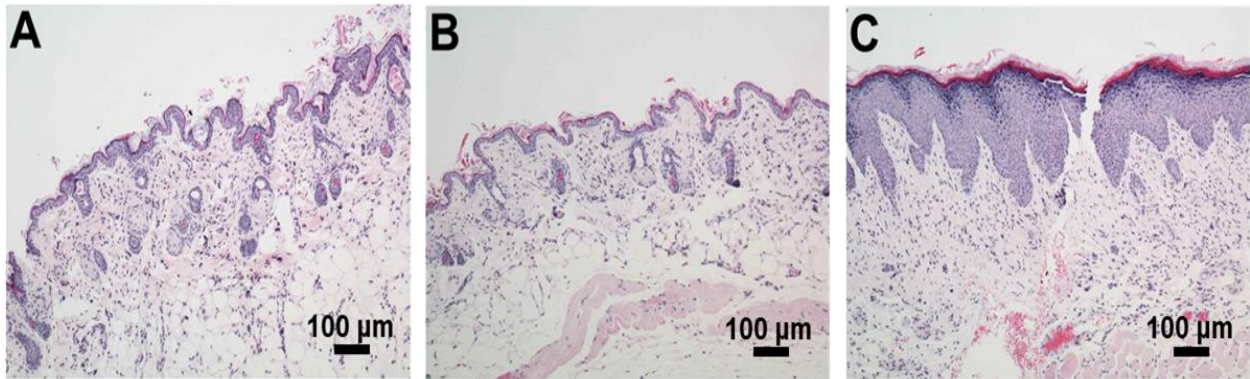


**Figure 10:** Representative histological evaluation of skin surrounding the tumor in mice from (A) no treatment, (B) nonradioactive bandage and (C) radioactive bandage groups. Epidermal thickening and increased infiltration of immune cells was observed when treated with radioactive bandage (C).

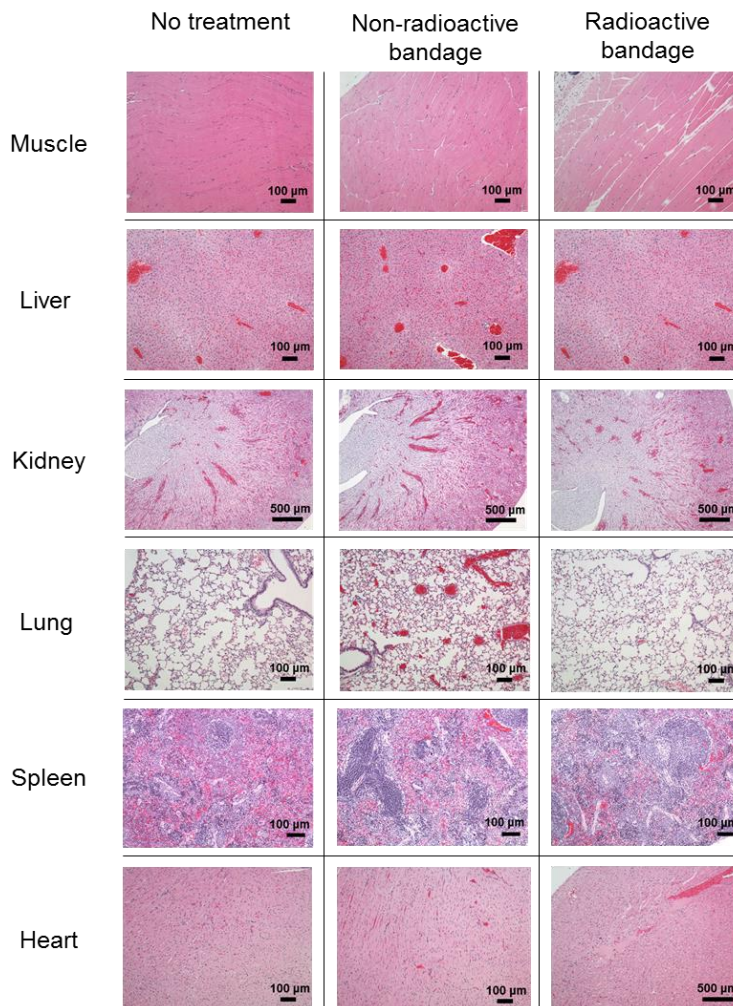


**Figure 11:** Representative histological evaluation of tissues from the no treatment, non-radioactive bandage and radioactive bandage groups.

Lee and co-workers prepared a  $^{166}\text{Ho}$  skin patch, which was successfully used to treat chemically induced SCC in mice, and three SCC patients.<sup>104</sup> As stated earlier, our bandage represents a more stable radiotherapeutic and fully characterized construct<sup>105</sup> that is suitable for transition to the clinic. In another aforementioned study, Jeong and co-workers prepared  $^{188}\text{Re}$  labelled nitrocellulose paper and tested its efficacy in a syngeneic mouse model for SCC<sup>117</sup>. Rhenium can produce two radioactive daughters,  $^{186}\text{Re}$  and  $^{188}\text{Re}$ , when neutron-activated, which makes dosimetry difficult.<sup>117,118</sup> Though  $^{188}\text{Re}$ , which is suitable for therapeutic purposes, can be produced from tungsten-186 ( $^{186}\text{W}$ ), it requires a generator unique for this reaction ( $^{188}\text{W}/^{188}\text{Re}$  reactor),<sup>118</sup> and it is difficult to produce therapeutically relevant radioactivities. Only one non-radioactive isotope of holmium exists,  $^{165}\text{Ho}$ , so only  $^{166}\text{Ho}$  is produced via simple neutron-activation. Furthermore, while the  $^{188}\text{Re}$  paper was prepared using generator-eluted  $^{188}\text{Re}$ , which might complicate GMP, our bandage is prepared when non-radioactive and then made radioactive just before therapy.

**Conclusions:** The efficacy of a “radiotherapeutic bandage” containing  $^{166}\text{HoIG}$  nanoparticles, when used in therapeutically relevant doses for the treatment of cutaneous SCC was demonstrated in an *in vivo* model. The mice treated with the radioactive bandage showed significant reduction in tumor volume compared to no treatment and non-radioactive bandage group. No significant side effects were observed except for epidermal ulceration, which started to heal without any intervention. Current standard of care radiation requires the use of cumbersome equipment, specialized instrumentation and facilities, whereas the bandages described here could potentially be applied with nothing more than a lead band to cover it, while the patient sits in an office room. These bandages can be individually tailored for easy application on tumor lesions of all shapes and

sizes, and manufactured on a large scale, making them an especially attractive material. The radiotherapeutic bandage is an innovative approach to reduce the tumor burden aggressively in the clinic.

## Chapter 3

# Targeted chemotherapy for non-small cell lung cancer using antibody-coated gold nanoparticles

### Abstract

#### Introduction:

Lung cancer is the leading cause of cancer-related death in the United States among both men and women, accounting for about 27% of all cancer related deaths. Approximately 85 to 90% of all lung cancers are non-small cell lung cancer (NSCLC). NSCLC is extremely difficult to treat and the five-year survival rate is less than 20%. Treatment options for NSCLC include a combination of surgery, radiotherapy and/or chemotherapy. Pt drugs are the first line of choice for treatment of NSCLC. Pt(IV) complexes are prodrugs of Pt(II) compounds which were shown to have anti-cancer activity and fewer side effects than Pt(II) compounds. Here, we developed a gold nanoparticle (AuNP) formulation, conjugated with Pt(IV) complex and a monoclonal antibody (mAb) against CD22 (an adhesion molecule shown to be widely expressed on NSCLC cells) as a targeted therapy for NSCLC.

#### Methods:

PEGylated AuNP conjugated with Pt(IV) complex and a mAb against CD22 were synthesized according to previously described procedure and characterized. The amount of Pt attached to AuNP-PEG-Pt and AuNP-PEG-Pt-mAb was measured using inductively coupled plasma mass

spectrometry (ICP-MS). Flow cytometry was used to measure the CD22 expression on various NSCLC and normal cell lines and to estimate the mAb conjugation efficiency. The uptake of the nanoparticles was then measured in various CD22 positive and negative cell lines.

### **Results:**

The particle size of AuNP-PEG-NH<sub>2</sub>, AuNP-PEG-Pt and AuNP-PEG-Pt-mAb were all ~166-216 nm. AuNP-PEG-Pt and AuNP-PEG-Pt-mAb had 0.5% w/w Pt/Au and 0.75% w/w Pt/Au as measured by ICP-MS. The efficiency of mAb conjugation was 35.4% (truly positive % of alexaflour-488 positive nanoparticles) based on flow cytometry. The expression of CD22 was higher in the normal cell line WI-38, followed by H596, A549 and then BEAS-2B. The uptake of the nanoparticles however did not follow the status of CD22 expression.

## **Introduction:**

Lung cancer is one of the foremost causes of death in the United States.<sup>119</sup> About 27% of all cancer related deaths are due to lung cancer.<sup>119</sup> According to the American Cancer Society, it is estimated that nearly 220,000 new lung cancer cases will be diagnosed in the USA in 2016.<sup>119</sup> There are two major types of lung cancers 1) small cell lung cancer (SCLC) and 2) non-small cell lung cancer (NSCLC) depending on the cellular morphology. About 85-90% of lung cancers are classified to be NSCLC<sup>119,120</sup>. Unfortunately, NSCLC is mostly diagnosed in later stages and is extremely difficult to treat. The five-year survival rate is less than 20%.<sup>119</sup> Current treatment strategies are strongly dependent on the type of malignancy and stage at the time of diagnosis but often involve a combination of surgery, chemotherapy, and/or radiation therapy. As most patients are being diagnosed at later stages when tumor is spread all through the lung, it is difficult to combat NSCLC with surgery. Hence, chemo and/or radiotherapy are most sought after strategies.

## **Chemotherapy for NSCLC:**

The standard first line of therapy for NSCLC is with platinum (Pt) based drugs like cisplatin, carboplatin, and oxaliplatin.<sup>120</sup> Depending on the stage of diagnosis and metastasis, a combination of Pt drugs and taxens (paclitaxel, or docetaxel) and gemcitabine are also used.<sup>121</sup> Several combinations of therapies to improve NSCLC treatment are currently under clinical trials.<sup>122</sup> A combination of nab-paclitaxel and carboplatin for elderly patients having stage IV NSCLC is currently under phase IV clinical trial.<sup>123</sup> Another phase III clinical trial investigating the combination of Atezolizumab with paclitaxel and carboplatin with or without bevacizumab is currently under progress.<sup>124</sup>

Cisplatin was the first drug in the class of Pt compounds approved by FDA for treatment of cancer.<sup>125</sup> It is currently used for the treatment of several different types of cancers like NSCLC, bladder, head and neck cancers.<sup>126</sup> Cisplatin is a Pt(II) compound (where the oxidation state of Pt is +2). It acts by forming DNA adducts once it enters the cell and thereby causing cellular apoptosis.<sup>127-129</sup> Several other Pt(II) compounds were developed after cisplatin (example: carboplatin and oxaliplatin). Figure 12 shows the structures of some Pt(II) anti-cancer agents.<sup>127</sup>

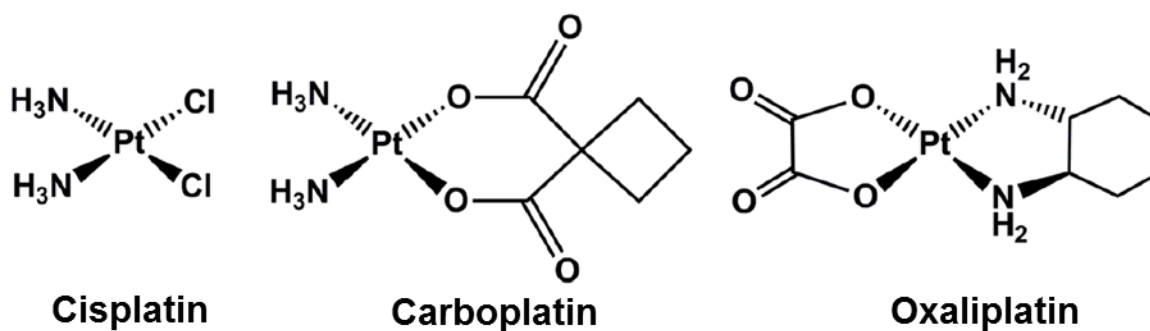


**Figure 12:** Examples of Pt(II) anti-cancer agents.<sup>127</sup>

Though cisplatin and other derivatives are still being used for cancer therapy, they cause certain severe dose related side effects like neurotoxicity and nephrotoxicity.<sup>130</sup> Several other Pt derivatives were explored thereafter to overcome the limitations of Pt(II) compounds.<sup>127,131</sup> In this quest, scientists developed another class of Pt compounds which contained a Pt(IV) central molecule.<sup>132</sup> Pt(IV) complexes are the pro drugs of Pt(II) anti-cancer agents. Pt(IV) complexes will be biologically reduced into their Pt(II) pro drugs *in vivo* by ascorbic acid (AsA) or glutathione (GSH).<sup>133-135</sup> Studies showed that AsA reduced Pt(IV) drugs like iproplatin into a Pt(II) complex.<sup>133</sup> However, reduction by GSH was not clearly demonstrated. It was shown that when reduced by GSH, a Pt(IV) complex was not necessarily being reduced into its prodrug form and thus, their capacity to form intrastrand crosslinks with DNA is under inquiry.<sup>136-138</sup>

Pt(IV) complexes have several advantages over their Pt(II) precursor, like enhanced stability *in vivo*, kinetic inertness by resisting premature aquation, and reduced side effects.<sup>139</sup> Tetraplatin, satraplatin and iproplatin are the examples of Pt(IV) complexes that have entered clinical trials.<sup>140-</sup>

142

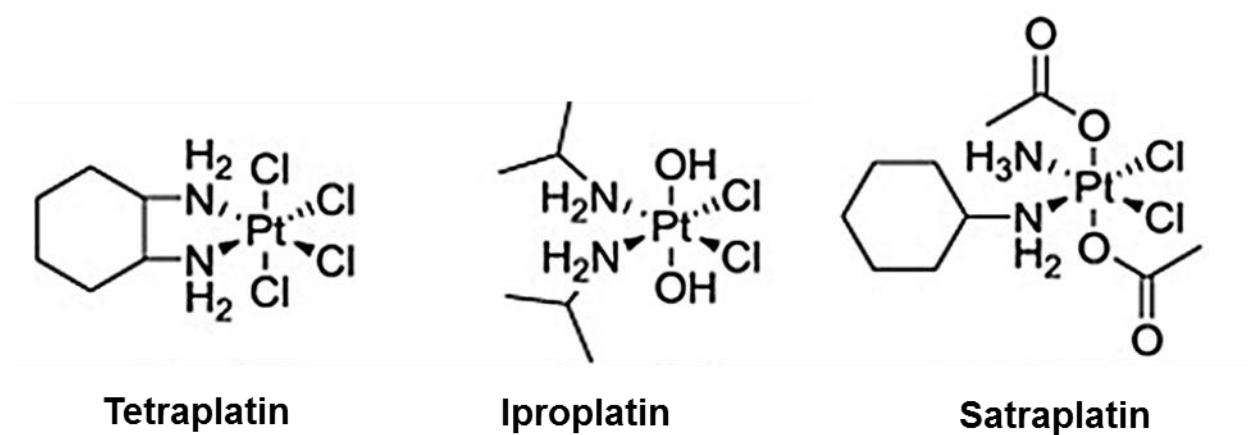


**Figure 13:** Examples of Pt(IV) anti-cancer agents.<sup>142</sup>

Prodrugs of cisplatin like oxoplatin,  $c,t,c$ -[PtCl<sub>2</sub>(OH)(O<sub>2</sub>CCH<sub>2</sub>CH<sub>2</sub>CO<sub>2</sub>H)(NH<sub>3</sub>)<sub>2</sub>] (which is a carboxylic derivative Oxoplatin) and  $trans, cis, cis$ -bis(heptanoato)amine(cyclohexylamine)dichloridoplatinum(IV) are some examples of the Pt(IV) complexes were shown to have anti-cancer activity.<sup>143-145</sup> Pt(IV) prodrugs are also suitable for delivery through nanocarrier. Dhar et al. used PSMA-specific aptamer targeted PEG functionalized PLGA nanoparticles to deliver a Pt(IV) complex ( $c,t,c$  [Pt(NH<sub>3</sub>)<sub>2</sub>(O<sub>2</sub>CCH<sub>2</sub>CH<sub>2</sub>CH<sub>2</sub>CH<sub>2</sub>CH<sub>3</sub>)<sub>2</sub>Cl<sub>2</sub>]) for prostate cancer therapy.<sup>146</sup> They conjugated the same complex on polyvalent oligonucleotide AuNP and demonstrated the cytotoxicity of the formulation in A549 cells *in vitro*.<sup>147</sup> Shi et al. used the same Pt(IV) complex to attach on to cyclodextrin capped AuNP and demonstrated their cytotoxicity in neuroblastoma cells.<sup>148</sup> Therefore in this study we used  $c,t,c$ -[PtCl<sub>2</sub>(OH)(O<sub>2</sub>CCH<sub>2</sub>CH<sub>2</sub>CO<sub>2</sub>H)(NH<sub>3</sub>)<sub>2</sub>], which has been

shown to exhibit potent anti-cancer activity as a chemotherapeutic agent in our targeted chemotherapeutic formulation for NSCLC.

### **Nanomedicine for NSCLC Therapy:**

Dose related toxicities of Pt compounds like nephrotoxicity, neurotoxicity, myelosuppression is a major limitation in achieving better response in patients as it is inhibiting the delivery of a higher dose.<sup>149</sup> Another common problem in treating NSCLC patients with platinum compounds is drug resistance. Using nanocarrier based drug delivery systems can help minimize the toxic side effects, improve drug efficacy and avoid the development of drug resistance to certain extent. The nanocarrier systems may be composed of polymeric, lipid, or inorganic materials. To these systems, the drug of interest and a targeting moiety are attached usually via chemical modifications and/or conjugations to the surface of the formulation.<sup>131</sup> Several groups of researchers have developed various nanoparticles formulations and demonstrated their successful use in reducing the tumor burden both *in vitro* and *in vivo*.

Koshkina et al. developed a lipid aerosol formulation composed of dilauroylphosphatidylcholine (DLPC) lipids to deliver paclitaxel.<sup>150</sup> It was shown to prolong survival rate by 25% in a murine metastatic lung cancer model. Poly (lactic acid-co-glycolic acid) (PLGA) nanoparticles with cetuximab as a targeting agent were used to deliver paclitaxel showed significantly higher reduction of tumor volume in an *in vivo* lung cancer model.<sup>151</sup> Lipoplatin is a liposomal formulation for cisplatin, is under clinical investigation for treatment of NSCLC.<sup>152</sup> Drug-polymer conjugates are also being investigated in clinical trials for NSCLC. The drug of interest is usually

conjugated to a bio compatible polymer like PEG or N-(2-Hydroxypropyl) methacrylamide (HPMA). For example, HPMA conjugated doxorubicin showed promising results for patients with NSCLC in phase II clinical trials.<sup>153</sup> Inorganic nanoparticles are also shown to be useful in treatment of NSCLC. Munaweera et al. developed a chemoradiotherapeutic formulation using iron garnet nanoparticles, where cisplatin is used as a radiosensitizer and <sup>166</sup>Ho as a source of radiation.<sup>154</sup> They successfully demonstrated the efficacy of the formulation in an *in vivo* NSCLC model. Supramagnetic iron nanoparticles for magnetic hyperthermia treatment, reduced the tumor burden *in vivo*.<sup>155</sup>

Gold nanoparticles are excellent candidates for both drug delivery and imaging. Due to their large surface area to volume ratio, Au nanoparticles can be easily functionalized with various functional groups, which makes it an ideal candidate for conjugation of biomolecules like antibodies, peptides, and DNA.<sup>39</sup> AuNPs are being used as contrast agents in imaging by attaching various antibodies to target cancer cells.<sup>156</sup> AuNP conjugated with antibodies, were used to detect proteins in saline, serum, and whole blood using near infrared spectroscopy<sup>157,158</sup>. Au nanoparticles can also be useful as theronostic.<sup>156</sup> Au nanoparticles conjugated with dithiolated diethylenetriamine pentaacetic acid (DTDTPA) increased radiosensitivity of prostate tumors and also enhanced the CT-image contrast simultaneously.<sup>159</sup> Antibody conjugated AuNP have been shown to be effective in reducing the tumor burden in several cancers. In the present study, we used PEGylated AuNP as nanocarrier platform to selectively deliver Pt(IV) anti-cancer agent to NSCLC tumor sites.

## Targeted therapy for NSCLC

NSCLC has no single molecular pathology making it difficult to develop standard targeted therapy.<sup>160,161</sup> Most of the currently available targeted therapies for NSCLC are targeting the mutations in epidermal growth factor receptor (EGFR).<sup>162,163</sup> EGFR and its downstream pathways are so far best studied in NSCLC which helped develop some of the currently available targeted therapies.<sup>163,164</sup> Gefitinib and erlotinib are the tyrosine kinase inhibitors of EGFR used for targeted therapy of NSCLC.<sup>165,166</sup> Bevacizumab is another targeted therapy used in advanced NSCLC.<sup>167</sup> It targets the vascular endothelial growth factor (VEGF), and stops the growth of new blood vessels.<sup>167</sup> Crizotinib is an oral small molecule which targets the anaplastic lymphoma kinase (ALK) gene mutations.<sup>168</sup> A major limitation to these targeted therapies is patients developing resistance to the therapy<sup>169</sup>. These are also available only to certain patients that exhibit these mutations. For example, only 7-8% of NSCLC patients have ALK gene mutations.<sup>170</sup>

Cluster Differentiation-22 (CD22) is a cell adhesion protein known to influence B-cell survival<sup>171</sup>. Tuscano et al.<sup>172</sup> showed that CD22 is broadly expressed in human lung cancer cells; it was reported that a murine anti-human CD22 mAb HB22.7, had significant preclinical efficacy against CD22-positive human lung cancer cells and tumor xenografts.<sup>172</sup> However, in another study reported contradicting findings to Tuscano et al.<sup>173</sup> Therefore, in this study, we verified the expression of CD22 on lung cancer cells and its feasibility to be used as a targeting agent to deliver platinum drugs for NSCLC.

The goal of this project is to develop a targeted chemo therapeutic AuNP formulation with an anti CD22 mAb as a targeting agent to deliver cisplatin prodrug (Pt IV complex) to improve therapeutic outcomes for patients with NSCLC, who are typically treated with cisplatin and other platinum drugs.

## **Materials and Methods:**

### **Synthesis of –COOH and –OH capped gold nanoparticles (AuNP):**

Chloroauric acid ( $\text{HAuCl}_4 \cdot 3\text{H}_2\text{O}$ ), 11-mercapto-1-undecanol, 16-mercaptohexadecanoic acid, and sodium borohydride were purchased from Sigma Aldrich (St.Louis, MO).

The Au nanoparticles, functionalized with 11-mercapto-1-undecanol and 16-mercaptohexadecanoic acid, were synthesized using a method reported by Di Pasqua et al.<sup>174</sup> Briefly, To a solution containing  $\text{HAuCl}_4 \cdot 3\text{H}_2\text{O}$  (386.6 mg) in water (5.65 mL) was added 188 mL of an ethanol solution containing 2.54 mmol 11-mercapto-1-undecanol and 0.28 mmol 16-mercaptohexadecanoic acid. After cooling down the solution for  $0^\circ\text{C}$ , freshly prepared solution of  $\text{NaBH}_4$  (358.5 mg) in water (18.8 mL) was added drop wise and stirred vigorously for 3 h. The resulting AuNP with pendant –COOH and –OH groups were washed twice with 80% ethanol followed by centrifugation and decantation and the material was finally washed with 100 mL of ethanol containing  $\sim 50 \mu\text{L}$  of 1 M HCl solution. The final material was dried *in vacuo* overnight. The dried nanoparticles were then suspended in water (1 mg/mL) and sonicated on water bath (Branson ultrasonic bath, Branson ultra-sonics, Danbury, CT) at room temperature (RT) for 1 h and the particle size and zeta potential was measured using Delsa™ Nano Submicron Particle Size and Zeta Potential (Beckman coulter Inc., Fullerton CA). For Transmission Electron Microscopy

(TEM), the AuNP were dispersed in water and sonicated using probe (Qsonica, Newtown, CT) for 1 h before imaging using TEM (Zeiss EM 910 Transmission Electron Microscope).

**Synthesis of oxoplatin and its carboxyl derivative *c,t,c-*  
[PtCl<sub>2</sub>(OH)(O<sub>2</sub>CCH<sub>2</sub>CH<sub>2</sub>CO<sub>2</sub>H)(NH<sub>3</sub>)<sub>2</sub>] (Pt(IV) complex):**

Oxoplatin was synthesized in a manner similar as previously reported by Shi et al.<sup>143</sup> Briefly, A suspension of cisplatin, (0.4 g, 1.33 mmol; Sigma Aldrich, St. Louis, MO) in H<sub>2</sub>O (12 mL) was stirred at RT for 3 h and hydrogen peroxide (30 wt.%, 20 mL; Sigma Aldrich, St. Louis, MO) was added dropwise to the suspension at 60 °C. After 4 h stirring at 60 °C, the bright yellow solution was cooled at room temperature overnight to afford yellow crystals. The crystals were collected by vacuum filtration and washed with ice cold water.

The synthesis of the Pt(IV) complex was then carried out in a manner previous described (ref). Succinic anhydride (0.06 g, 0.6 mmol) was added to a suspension of oxoplatin (0.2 g, 0.6 mmol) in DMSO (16 mL) and the mixture stirred overnight at RT to afford a bright yellow solution. The volume of the solution was reduced in vacuo to ~ 0.5 mL, followed by an addition of ~ 10 mL of ice cold acetone to cause the precipitation of a pale yellow solid, which was collected via filtration, washed with acetone and dried in vacuo. <sup>1</sup>H NMR (300 MHz, DMSO-d<sub>6</sub>), δ (ppm) = 5.92 m, 6H (NH<sub>3</sub>); 2.39 m, 4H (CH<sub>2</sub>). Figure 14 shows the schematic of the synthesis.

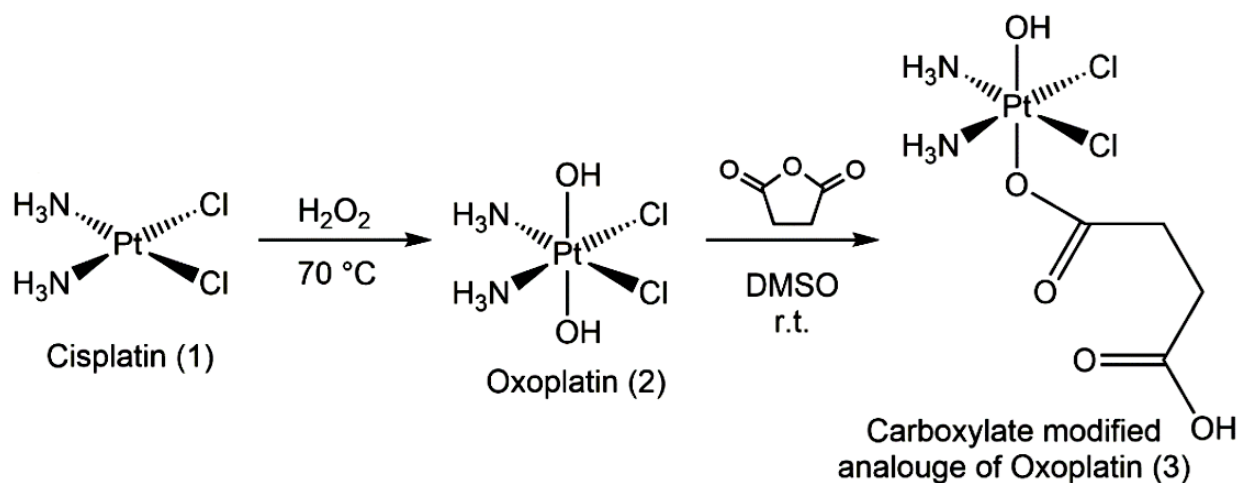


**Figure 14:** Schematic of the synthesis of oxoplatin and its carboxyl derivative.

#### Synthesis of PEGylated AuNP (AuNP-PEG-NH<sub>2</sub>):

AuNP-PEG-NH<sub>2</sub> was synthesized in procedure similar to AuNP with slight modifications. The stabilizing agents, 11-mercapto-1-undecanol and 16-mercaptohexadecanoic acid were replaced with thiol-PEG-amine (HS-PEG-NH<sub>2</sub>; MW: 3400 KD; Creative PEGworks, Chapel Hill, NC). Briefly, to an aqueous solution of H<sub>2</sub>AuCl<sub>4</sub>•3H<sub>2</sub>O (57.3 mg in 0.806 mL H<sub>2</sub>O), was added a solution of HS-PEG-NH<sub>2</sub> in ethanol (195.52 mg in 27.935 mL) slowly and stirred vigorously. To this, freshly prepared solution of NaBH<sub>4</sub> in water (26.5 mg in 1.38 mL) was added slowly and stirred for 1 h at RT. The resulting nanoparticles were collected by centrifuging the solution at 100,000 x g in an ultracentrifuge (Beckman coulter, Fullerton, CA) for 10 h at 4 °C. The AuNP-PEG-NH<sub>2</sub> were then washed with 80% ethanol twice by centrifuging as above. The AuNP-PEG-NH<sub>2</sub> were then suspended in 3 mL PBS. For particle size and zeta potential measurement, the nanoparticles were diluted 300 x times with PBS.

### **Attachment of Pt(IV) complex to AuNP-PEG-NH<sub>2</sub>:**

To the synthesized AuNP-PEG-NH<sub>2</sub>, Pt(IV) complex was attached via 1-ethyl-3-(3-dimethylaminopropyl) carbodiimide hydrochloride (EDC; Thermo Fisher Scientific, Waltham, MA) / N-hydroxysuccinimide (NHS; Sigma Aldrich, St. Louis, MO) coupling. To the suspension of AuNP-PEG-NH<sub>2</sub> in PBS (2 mL), were added solutions of EDC (~3 mg in 114.5  $\mu$ L of PBS) and NHS (~3 mg in 114.5  $\mu$ L of PBS). To this solution of Pt(IV) complex (3 mg in 771 (~3 mg in 114.5  $\mu$ L of PBS) was added while stirring at RT. Stirring was continued for 1 h at RT. The resulting AuNP-PEG-Pt were then collected and washed twice with PBS by centrifuging the solution at 100,000 x g in an ultracentrifuge for 10 h at 4 °C. The nanoparticles were then suspended in 1 mL PBS. For particle size and zeta potential measurement, the nanoparticles were diluted 150 x times with PBS.

### **Attachment of monoclonal antibody against (mAb) CD22 to AuNP-PEG-Pt:**

To the synthesized AuNP-PEG-Pt, mAb (HB22.7; kindly gifted by Dr. Tuscano, UC Davis) was attached via EDC/NHS coupling. To the suspension of AuNP-PEG-Pt in PBS (0.5 mL), was added of EDC (~1.5 mg in 0.174  $\mu$ L) and NHS (~1.5 mg in 0.174  $\mu$ L) were added. To this, mAb (1.5 mg in 0.652  $\mu$ L) was added while stirring. The solution was then stirred for 1 h at RT. The resulting AuNP-PEG-Pt-mAb were then collected by centrifuging the solution at 100,000 x g in an ultracentrifuge for 10 h at 4 °C and washed twice with PBS by centrifuging the solution at 100,000 x g in an ultracentrifuge for 10 h at 4 °C. The nanoparticles were then suspended in 1 mL PBS. For particle size and zeta potential measurement, the nanoparticles were further diluted with PBS.

**Pt and Au content determination using ICP-MS:** To prepare samples for ICP-MS analysis, 10  $\mu\text{L}$  of AuNP-PEG-NH<sub>2</sub>, AuNP-PEG-Pt and AuNP-PEG-mAb were dried and 200  $\mu\text{L}$  of aquaregia was added. After evaporating aquaregia at 70 °C, 200  $\mu\text{L}$  of 70 % HNO<sub>3</sub> was added and heated over night at 70 °C. The acid was then evaporated and the dry film was resuspended in 200  $\mu\text{L}$  of aquaregia. All the samples were then diluted with 2% nitric acid (final concentration of nitric acid was ~2%) and analyzed using inductively coupled plasma mass spectrometry (ICP-MS; NexION 300D ICP-MS, Perkin Elmer, CT) for measuring the Pt and Au content. For the standard curve, a stock solution of 1000 ppm gold (1000  $\mu\text{g}/\text{mL}$  Gold in 2% HCl - ISO Guide 34 Certified Reference Material, High purity standards, Charleston, SC) and 1000 ppm Platinum (1000  $\mu\text{g}/\text{mL}$  Platinum in 5% HCl - ISO Guide 34 Certified Reference Material, High purity standards, Charleston, SC) was used and further diluted to various concentrations with 2% nitric acid spiked with internal standards. A total of 10 points were used for the construction of the calibration curve and R<sup>2</sup> ~ 0.999. Bismuth (ICP-MS internal standard-1 High Purity standards, Charleston, SC) at a concentration of 20 ppb was used as internal standard. Isotopes of elements with minimal interferences were chosen for ICP-MS analysis.

### **Cell Culture:**

All the cell lines were purchased from ATCC (Manassas, VA). Cells were grown in a humidified, 37 °C, 5% CO<sub>2</sub> (standard conditions) atmosphere incubator. The culture medium used for the WI-38 cells was minimum essential medium (MEM) containing 100  $\mu\text{g}/\text{mL}$  streptomycin, 10% fetal bovine serum (FBS), 2.0 mM l-glutamine and 100 IU/mL penicillin. The culture medium used for the BEAS-2B cells was bronchial epithelial basal medium (BEBM) with 10% FBS and

supplements. The culture medium used for H596, A549, Jurkat and Ramos cells was Roswell Park Memorial Institute (RPMI) medium containing 100 µg/mL streptomycin, 100 IU/mL penicillin, 10% FBS and 2.0 mM l-glutamine.

### **Flow cytometry:**

To assess the expression of CD22 on various NSCLC (A549 and H596) normal cell lines (BEAS-2B and WI-38), flow cytometry was used. Ramos and Jurkat cell lines were used as positive and negative controls. Cells were grown in t-25 culture flasks in their respective medium. At about 80% confluency, adherent cells were detached from surface using EDTA (1 mM; Thermo Fischer Scientific, Waltham, MA). Cell pellets were then washed twice with PBS by centrifuging at 1000 × g at 4°C. Cells were then incubated in primary antibody against CD22 (HB22.7; 25 µg/mL) for 30 min at 4°C followed by 3 washes with ice-cold PBS. Cells were incubated with Alexaflour-488 conjugated donkey anti-mouse IgG secondary antibody, Alexa flour 488 (Thermo Fisher Scientific, Waltham, MA) for 30 min at 4°C followed by two washes with ice cold PBS. For each cell line, a corresponding negative control was used, which was processed same as above, but was not incubated with the primary antibody. These were used to normalize the false positive data for each cell line. The samples were then analyzed using a BD LSR II Flow Cytometer System. A minimum of 10,000 events were analyzed per sample.

### **Antibody conjugation efficiency:**

To quantify the antibody conjugation efficiency on AuNP-PEG-Pt-mAb flow cytometry was used. AuNP-PEG-NH<sub>2</sub> and AuNP-PEG-Pt-mAb were processes same as detailed above along with

corresponding negative controls. All the samples were then analyzed using a BD LSR II Flow Cytometer System. A minimum of 10,000 events were analyzed per sample.

### **Uptake study:**

The uptake of AuNP-PEG-NH<sub>2</sub>, AuNP-PEG-Pt and AuNP-PEG-Pt-mAb in A549, H596, BEAS-2B, WI38, Jurkat and Ramos cell lines was carried out. Cells were grown in 6 well plates (300,000 cells / well) in their respective medium. Twenty-four hours after seeding the cells, the cells received either AuNP-PEG-NH<sub>2</sub>, AuNP-PEG-Pt or AuNP-PEG-Pt-mAb. Each well received 10µg of Au. 5 h after treatment, cell pellets were collected and protein analysis (Pierce BCA protein assay kit) was performed. Content of Au and Pt up taken by cells was then measured using ICP-MS and the Au uptake reported was normalized with protein content.

### **Statistical Analysis:**

One-way ANOVA followed by Bonferroni t-test for posthoc analysis was used for analyzing Au uptake, student's t-test (unpaired t-test) was used to compare the Pt uptake among different treatments. A p value of  $\leq 0.05$  was considered as statistically significant.

### **Results and discussion:**

In this project, our aim is to develop a novel targeted chemotherapeutic formulation for the treatment of NSCLC. We chose AuNP as our nanocarrier platform because of the unique properties like Plasmon resonance, tunable surface chemistry<sup>39,175</sup> to name some. As they can be used for

both drug delivery and an imaging agent,<sup>156</sup> there is a larger scope for developing it into a theranostic in the future. At first, AuNP capped with –COOH and –OH groups were prepared following a method previously described by Di Pasqua, et al.<sup>174</sup> The –COOH groups can be used for antibody and drug conjugation via EDC/NHS coupling while the –OH groups act as spacers. The size of AuNP thus prepared was measured using dynamic light scattering (DLS), after suspending in water and sonicating in a water bath for 1 h at room temperature. The size of AuNP was 95.2 nm with a zeta potential of -39.3 (Table 4). Transmission electron microscopy (TEM) showed that the size of the gold core was  $10.8 \pm 2$  nm. Figure 15 shows the TEM image of AuNP dispersed in water after 1 h probe sonication on ice.

**Table 4.** Size, PDI and zeta potential of AuNP.

Sample	Size (nm)	PDI	Zeta potential (mV)
AuNP	95.2	0.3	-39.3

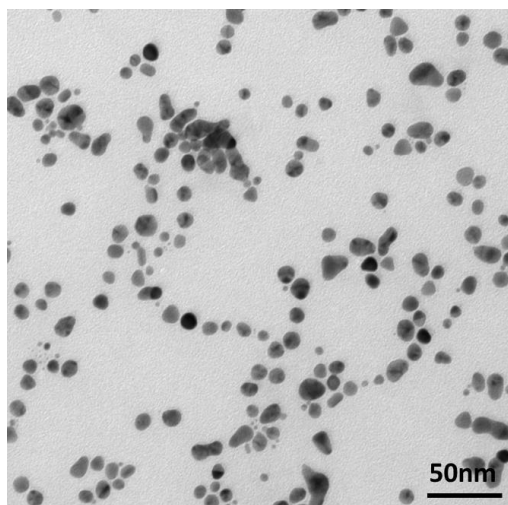


**Figure 15:** TEM image of AuNP in water. Au core size was  $10.8 \pm 2$  nm.

For a formulation aimed for *in vivo* application, it is important that it is stable and has uniform dispersion characteristics in buffers and relevant biological fluids. Therefore, we tested the particle

size of AuNP in PBS and culture medium. Aggregation of AuNP was observed when added to PBS and culture medium. When dispersed in PBS, the relatively high ionic strength of the buffer, which can alter the dispersion properties of the nanoparticles can cause aggregation of the nanoparticles.<sup>176,177</sup> Surface interactions between AuNP and the salts present in PBS and culture media with fetal bovine serum (FBS) and growth factors can also cause nanoparticle aggregation.<sup>177</sup> Table 5 shows the particle size of nanoparticles in PBS, and various culture mediums.

**Table 5:** Particle size of –COOH and –OH capped AuNP in PBS and various culture mediums.

Solvent	Size (nm)	PDI
PBS	779.4	0.2
RPMI	749.3	0.2
BEBM	901.2	0.2

In order to improve the dispersion of AuNP in PBS and other biologically relevant solvents, the nanoparticles were modified by replacing 16-mercaptohexadecanoic acid (source of –COOH functional group on AuNP) and 11-mercapto-1-undecanol (source of –OH functional group on AuNP) groups with poly ethylene glycol (PEG), a process usually termed as PEGylation. Here we used a thiol-PEG-amine (HS-PEG-NH<sub>2</sub>). It has been shown that PEGylation of nanoparticles increase the circulation time of nanoparticles *in vivo* by reducing their uptake by the reticuloendothelial system.<sup>178</sup> The dispersion of nanoparticles in buffer and serum increases due to the hydrophilic ethylene glycol repeats formed by PEGylation. PEGylation further increases the

steric hindrance between the nanoparticles due to the long PEG chains on the surface of the nanoparticles and thereby reduces the nanoparticle aggregation.<sup>178</sup> The PEGylated gold nanoparticles (AuNP-PEG-NH<sub>2</sub>) were synthesized using HS-PEG-NH<sub>2</sub> (MW 3400 KD) by reduction of HAuCl<sub>4</sub> with NaBH<sub>4</sub> and further analyzed for particle size and zeta potential by

**Table 6:** Characterization data of AuNP-PEG-NH<sub>2</sub>, AuNP-PEG-Pt and AuNP - PEG-Pt-mAb.

Sample	Size (nm)	Zeta potential (mV)	PDI
AuNP-PEG-NH <sub>2</sub>	174.3	-10.62	0.181
AuNP-PEG-Pt	172.6	15.34	0.220
AuNP-PEG-Pt-mAb	165.5	-16.66	0.232

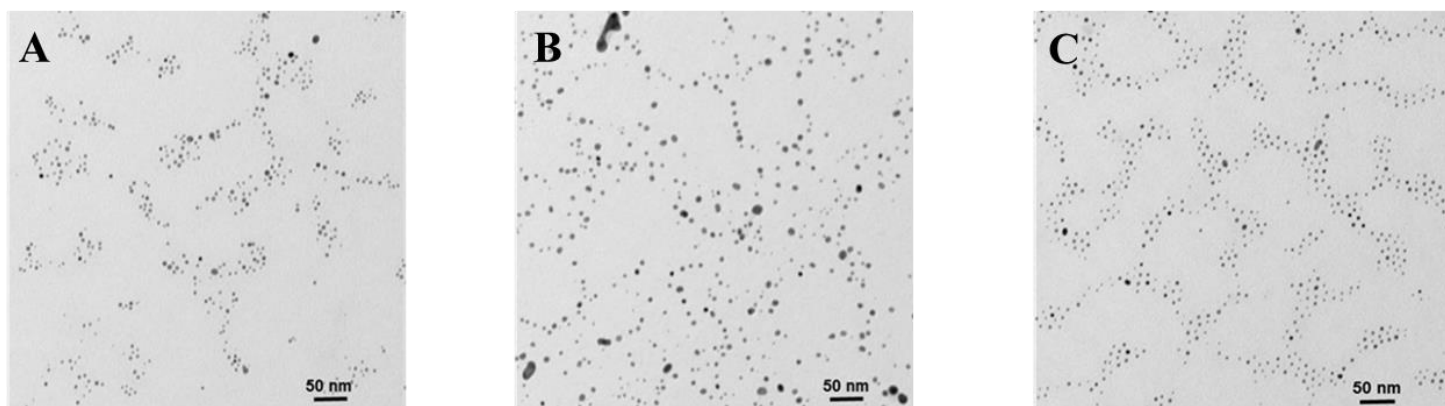


**Figure 16:** TEM images of A) AuNP-PEG-NH<sub>2</sub>, B) AuNP-PEG-Pt, C) AuNP-PEG-Pt-mAb.

dispersing in PBS followed by 0.5 h bath sonication at RT. The particle size of AuNP-PEG-NH<sub>2</sub> was 174.3 nm (Table 6), with a  $4.3 \pm 1.3$  nm gold core when measured from TEM (Figure 16A), and the zeta potential was -10 mV in PBS. Thus, PEGylation reduced the aggregation of nanoparticles in PBS.

The synthesized AuNP-PEG-NH<sub>2</sub> has free pendant -NH<sub>2</sub> groups. This can be used to conjugate drug molecules, and targeting agents like antibodies, proteins and DNA on the nanoparticles. Here, we used a cisplatin prodrug, a Pt(IV) complex (c,t,c [PtC<sub>12</sub>(OH)(O<sub>2</sub>CCH<sub>2</sub>CH<sub>2</sub>CO<sub>2</sub>H)(NH<sub>3</sub>)<sub>2</sub>) as the therapeutic agent to be attached on the AuNP-PEG-NH<sub>2</sub>. The Pt(IV) complex, which is a carboxyl derivative of oxoplatin was shown to be a potential anti-cancer agent.<sup>143</sup> Dhar et al. successfully conjugated this Pt(IV) complex on to polyvalent oligonucleotide capped gold nanoparticles via EDC/NHS coupling.<sup>147</sup> The Pt(IV) complex was synthesized as previously described by Shi et

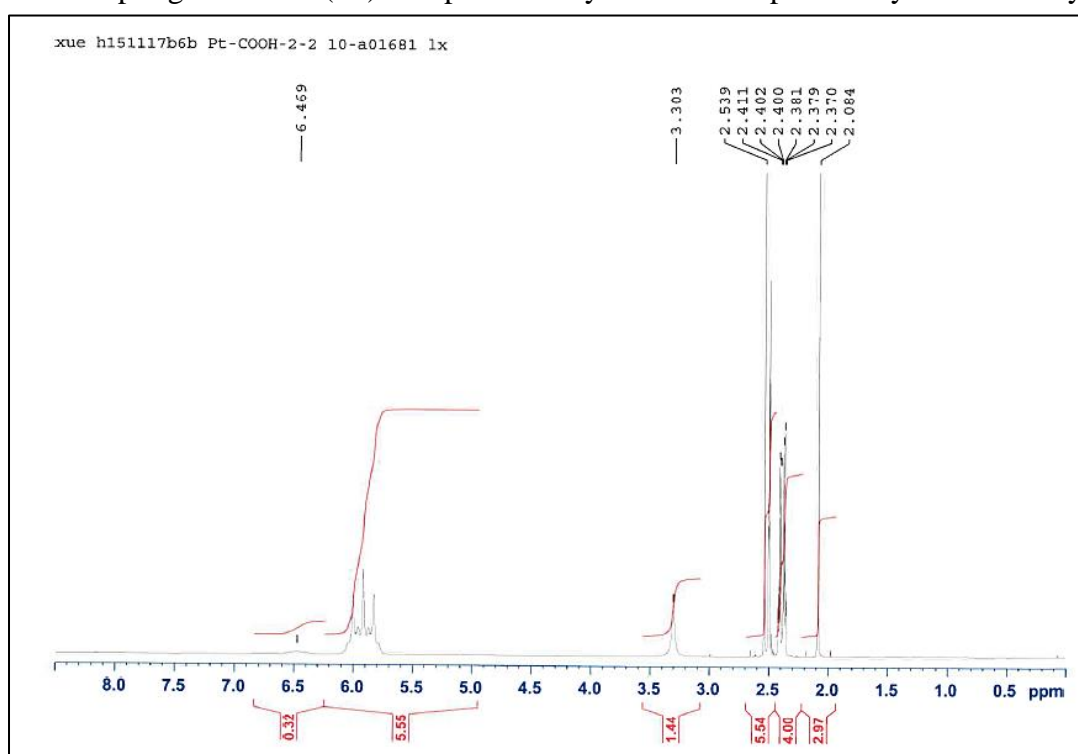


**Figure 17:** NMR spectra of the Pt(IV) complex.

al.<sup>143</sup> and characterized using NMR spectroscopy. <sup>1</sup>H NMR (300 MHz, DMSO-d<sub>6</sub>), δ (ppm) = 5.92 m, 6H (NH<sub>3</sub>); 2.39 m, 4H (CH<sub>2</sub>). Figure 17 shows the NMR spectra of the Pt(IV) complex.

The Pt(IV) complex was then attached to AuNP-PEG-NH<sub>2</sub> via EDC/ NHS coupling. Particle size and zeta potential of AuNP-PEG-Pt were measured. Addition of Pt(IV) complex did not change the particle size of the nanoparticles significantly, (172.6 nm diameter and 6.3 ± 2.4 nm gold core,

Table 6 and Figure 16B, respectively), but the zeta potential shifted to +15 mV. Pt and gold (Au) content was measured using inductively coupled plasma mass spectrometry (ICP-MS) Pt content was 0.5% w/w Pt/Au.

The AuNP-PEG-Pt were further modified by adding human anti-CD22 mAb as a targeting moiety (AuNP-PEG-Pt-mAb). CD22 is an adhesion molecule expressed on the surface of mature B cells.<sup>171</sup> In 2012, Tuscano et al. reported that CD22 is widely expressed on various lung cancer cell lines and demonstrated the efficacy of mAb against CD22 in reducing the tumor volume in an *in vivo* model for NSCLC.<sup>172</sup> Later in 2014, Pop et al. reported contradicting findings in regards to the expression of CD22 on lung cancer cells<sup>173</sup>. In their study, no measurable expression of CD22 was observed on the surface of lung cancer cells. In the event of these contradicting findings, we measured the expression of CD22 on NSCLC and normal cell lines using flow cytometry. Figure 18 shows the bar graph comparing the mean fluorescence intensity (MFI) among various cell lines. Ramos and Jurkat cell lines were used as positive and negative controls for CD22 expression. The expression of CD22 was higher in Ramos and lowest in Jurkat. This confirms that the mAb (HB22.7) used is specific for CD22. Among the various NSCLC and normal cell lines tested for CD22 expression, WI-38 a normal lung fibroblast cell line showed highest expression of CD22. While A549 and H596, both NSCLC cell lines showed similar level of expression but the expression is lower compared to WI-38. The total percentage of Alexa flour-488 positive cells were calculated for each cell line and represented in Table 7.

Our results therefore corroborate with the findings of Tuscano et al.,<sup>172</sup> as we can observe measurable levels of CD22 on NSCLC cell lines. However, the expression of CD22 is also observed in the normal lung fibroblasts (Figure 18, Table 4). It was reported that a <sup>64</sup>Cu-DOTA-

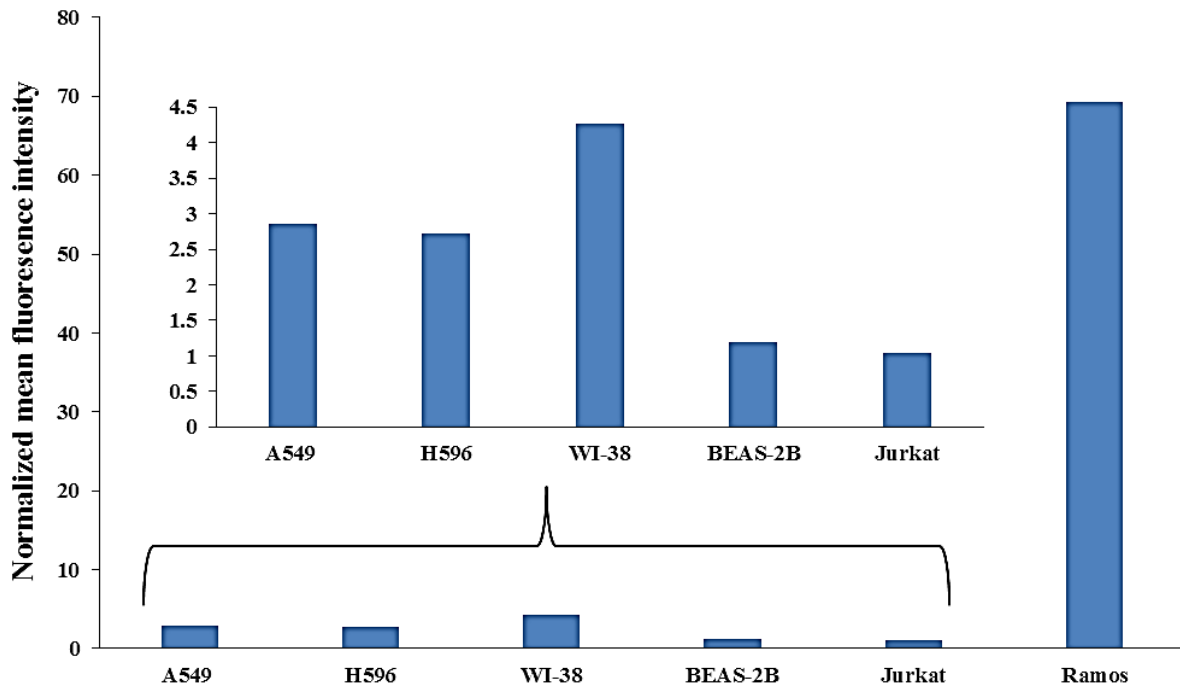


**Figure 18:** Expression of CD22 on various lung cancer and normal cell lines determined using flow cytometry. Mean fluorescence intensity was measured for each cell line and normalized with its negative control of the respective cell line.

**Table 7:** Percent of Alexaflour-488 positive cells in each cell line.

Sample	Total % Alex.488 + cells
A549	48.4
H596	35
WI-38	53.5
BEAS-2B	8
Jurkat	0.23
Ramos	95.62

HB22.7 antibody when injected *in vivo*, and monitored through anti-CD22 i-PET methodology, a selective accumulation of the antibody was observed in the lung cancer tumor xenograft.<sup>172</sup> Since antibody targeting was reported to work *in vivo*, we attached mAb onto AuNP-PEG-Pt via EDC/NHS coupling and tested its uptake of AuNP-PEG-Pt-mAb in cell lines expressing different levels of CD22 (uptake results discussed later).

The hydrodynamic diameter of the nanoparticles did not change significantly (165.5 nm, with a  $4.3 \pm 1.9$  nm gold core; Table 2 and Figure 16C) upon the addition of mAb, but the zeta potential shifted to -16 mV. The Pt content was 0.4% w/w Pt/Au. Figure 2C shows the TEM image of AuNP-PEG-Pt-mAb. The dispersion of all three formulations, AuNP-PEG-NH<sub>2</sub>, AuNP-PEG-Pt and AuNP-PEG-Pt-mAb in PBS is improved compared to AuNP due to PEGylation. We then reproduced our preparation; the second preparation yielded nanoparticles with similar sizes and Pt content. The size of AuNP-PEG-NH<sub>2</sub>, AuNP-PEG-Pt and AuNP-PEG-Pt-mAb were 189.3 nm, 193.1 nm and 216.2 nm, respectively. The Pt content measured by ICP-MS showed 0.8% w/w Pt/Au (0.36 % w Pt/w nanoparticles) in AuNP-PEG-Pt, and 0.71% w/w Pt/Au (0.45 % w Pt/w nanoparticles) in AuNP-Pt-mAb. The antibody conjugation efficiency was determined for this preparation using flow cytometry. The antibody conjugation was found to be 35.4% (truly positive % of alexaflour-488 positive nanoparticles) based on flow cytometry. Figure 19 shows the peak shift data from flow cytometry confirming the attachment of antibody on the nanoparticle.

The uptake of AuNP-PEG-NH<sub>2</sub>, AuNP-PEG-Pt and AuNP-PEG-Pt-mAb were studied in all the cell lines tested for CD-22 (A549, H596, WI38, BEAS-2B, Ramos (positive control) and Jurkat

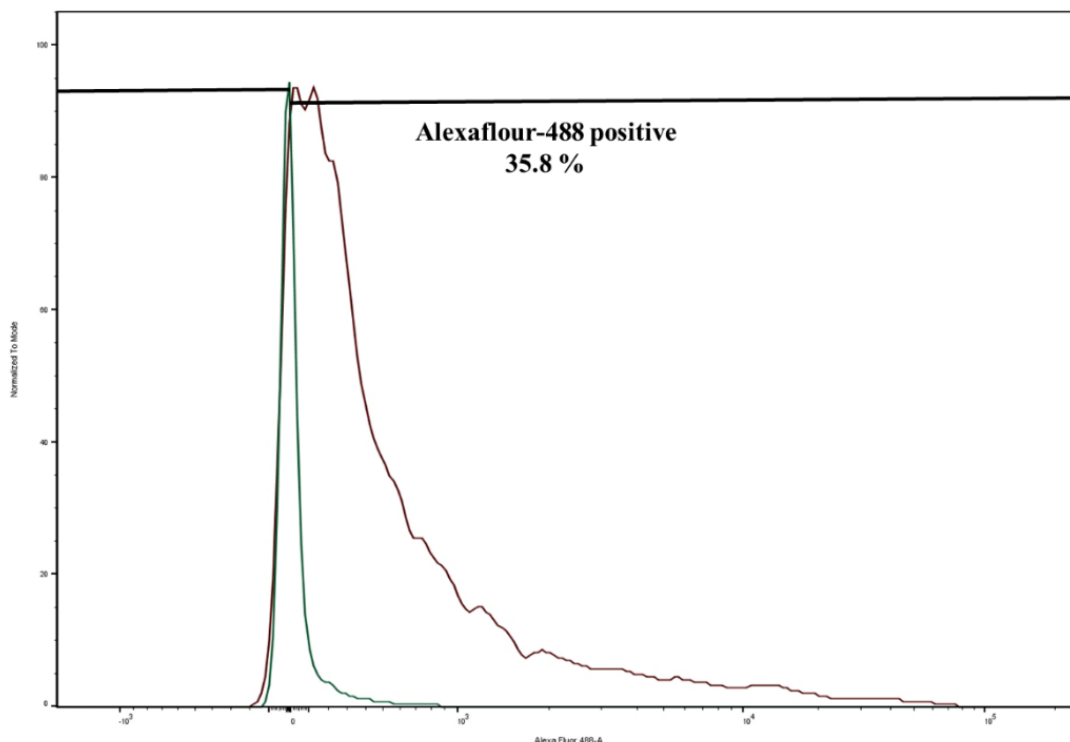


**Figure 19:** Image showing the peak shift in fluorescence intensity for AuNP-Pt-mAb (red line) compared to AuNP-PEG-NH<sub>2</sub> (green line). (The gates were drawn manually for the purpose of easy understanding after normalizing with the negative control. The original image with gates drawn using Flow Jo software is provided in the appendix).

(negative control). The uptake of Au and Pt was measured using ICP-MS after treating the cells for 5 h with their respective treatments. For cell lines A549, H596, BEAS-2B and WI-38, the first preparations of AuNP-PEG-NH<sub>2</sub>, AuNP-PEG-Pt and AuNP-PEG-Pt-mAb were used. For the positive and negative controls for CD22 (Ramos and Jurkat), the second preparations of AuNP-PEG-NH<sub>2</sub>, AuNP-PEG-Pt and AuNP-PEG-Pt-mAb were used. All the cells were seeded in a six well plate and treated with 10 µg of Au per well for five hours. Cells were collected after treatment, lysed and the Au and Pt contents analyzed using ICP-MS. Figure 20 shows the comparison of the uptake of Au and Pt among all the cell lines. The uptake of Au in cells treated with AuNP-PEG-Pt is similar to that of cells treated with AuNP-PEG-Pt-mAb in most cell lines. This increased uptake of AuNP-PEG-Pt may be due to its surface charge. Higher levels of Au were detected in

WI-38 cells treated with AuNP-PEG-Pt-mAb than those treated with any of its precursors. Higher Pt levels were observed in WI-38, Ramos (+ CD-22 control) and Jurkat (- CD-22 control) when treated with AuNP-PEG-Pt-mAb, compared to AuNP-PEG-Pt. Thus, in our formulation, increased Pt uptake does not correlate with CD-22 status.

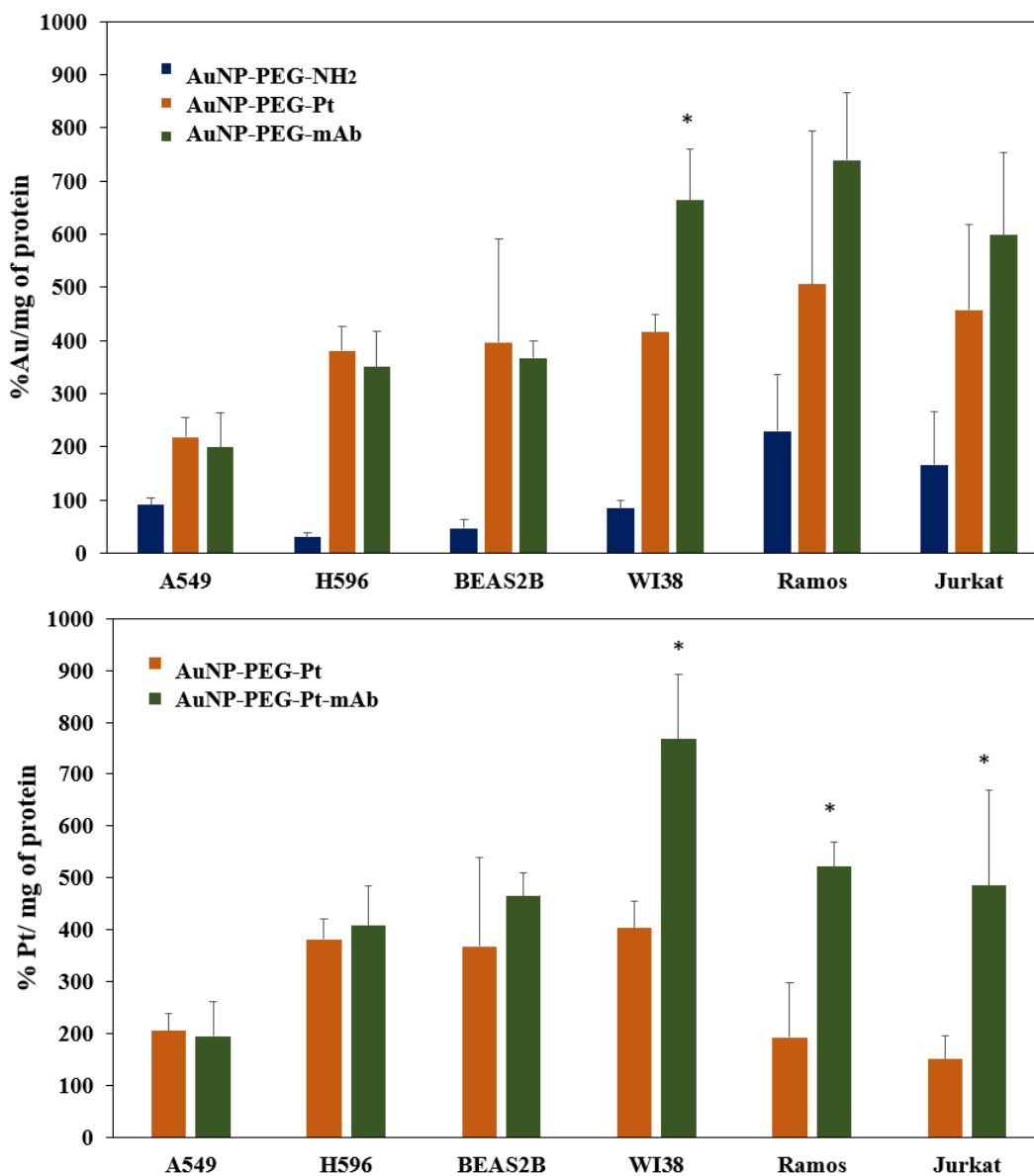


**Figure 20:** Uptake of AuNP-PEG-NH<sub>2</sub>, AuNP-PEG-Pt and AuNP-PEG-Pt-mAb by different cell lines. Top panel shows the Au uptake while the bottom panel shows Pt uptake. Au and Pt contents were measured using ICP-MS and normalized with protein content of the cell lines. \* p < 0.05 for AuNP-PEG-Pt vs AuNP-PEG-Pt-mAb.

**Conclusions:**

In this project we have successfully demonstrated the synthesis and characterization of a biologically compatible polymer (PEG) coated AuNP containing Pt(IV) complex and a mAb against CD22 were successfully prepared and characterized. The reproducibility of the formulation was demonstrated. Expression of CD22 on NSCLC and normal cell lines was determined and the results corroborate with the finds of Tuscano et al. However, uptake of the formulation AuNP-PEG-Pt-mAb does not correlate well with CD22 status.

## Chapter 4

### **Tetracycline-Containing MCM-41 Mesoporous Silica Nanoparticles for the Treatment of *Escherichia Coli***

#### **Abstract**

##### **Introduction:**

Tetracycline (TC) is a well-known broad spectrum antibiotic, which is effective against many Gram positive and Gram negative bacteria. However, its use has been limited due to the resistance developed by bacteria toward TC. There are several mechanisms through which TC resistance can be mediated. Removal of TC from the cytoplasm through efflux pumps, enzymatic degradation of TC, ribosomal mutations leading inactivation of TC function are some of them. Using nanoparticle formulations was shown to help overcome the resistance problem effectively. Mesoporous silica nanomaterials (MSNs) are widely studied for drug delivery applications; Mobile crystalline material 41 (MCM-41), a type of MSN, has a mesoporous structure with pores forming channels in a hexagonal fashion. Here, we prepared MCM-41 TC formulations and tested their efficacy in *E. coli*.

**Methods:**

TC containing MSNs of two sizes were prepared and characterized. *In vitro* drug release was studied. The efficacy of the nanoparticles was tested in *E. coli* at two different concentrations (0.5 µg/mL and 1 µg/mL TC). Further uptake of the nanoparticles by *E. coli* was studied using TEM.

**Results:**

TC containing MSCM-41 nanoparticles of sizes  $41 \pm 4$  and  $406 \pm 55$  nm were prepared. TC content in the TC-MCM-41 nanoparticles was 18.7% and 17.7% w/w, respectively. Release of TC from TC-MCM-41 nanoparticles was then measured in phosphate-buffered saline (PBS) and LB broth medium, pH 7.2, at 37 °C over a period of 5 h. Most antibiotic was released from both over this observation period; however, the majority of TC was released over the first hour. Efficacy of the TC-MCM-41 nanoparticles was then shown to be superior to free TC against *Escherichia coli* (*E. coli*) in culture over a 24 h period, while blank nanoparticles had no effect. The nanoparticles were taken up by *E. coli* within 1 h of treatment.

## Introduction:

Since their discovery in the 1920s, antibiotic agents are the first choice of drugs to combat any infectious diseases. Penicillin, the first known antibiotic<sup>179</sup> is followed by discovery of several other antibiotics later on. Tetracycline (TC) is a broad spectrum antibiotic which has been used for more than 60 years, and is on the World Health Organization's list of most important medications needed in the basic health system.<sup>180</sup> TC is effective against various Gram positive and Gram negative bacteria. TC was the most widely used antibiotic in the United States during 1950s and 1960s.<sup>181</sup> Doxycycline, minocycline, chlortetracycline, oxytetracycline are some examples of other antibiotics in the class of tetracyclines.

TC acts by preventing the association of aminoacyl- tRNA with the bacterial ribosome and thereby inhibiting the protein synthesis.<sup>182</sup> To obstruct the protein synthesis, TC has to cross the cellular membrane to bind to the ribosome.<sup>183</sup> TC enters the cell membrane through the porin channels in gram negative bacteria; while in gram positive bacteria, entry of TC is energy dependent.<sup>184</sup>

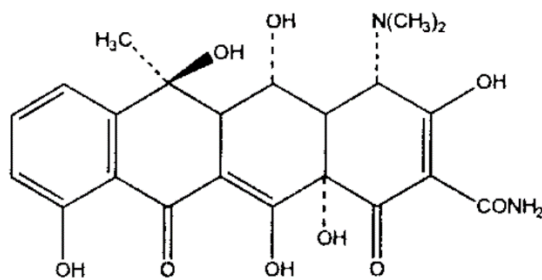


**Figure 21:** Structure of tetracycline.<sup>182</sup>

Antibiotic resistance poses a serious limitation to the use of TC. According to the statistics reported by center for disease control (CDC), nearly 2 million Americans are being infected by antibiotic resistant bacteria every year and nearly 23,000 people die each year because of these infections.<sup>185</sup> Evolution of multi-drug resistant bacteria is making it even harder to fight the problem. Resistance

can be innate or acquired. Innate resistance is specific for particular bacteria while acquired resistance can be through several mechanisms like acquisition of mutant genes, reduced cellular uptake of the antibiotics, defective binding of the antibiotic to the target, or combination of all.<sup>186</sup> For example, in case of TC, altering the porin proteins can affect the intake of TC and is one of reasons of TC resistance in gram negative bacteria.<sup>182,183,187</sup> The other mechanisms include genes which produce enzymes that promote inactivation of TC.<sup>188</sup> A prominent mechanism of TC resistance is by pumping the drug out through efflux pumps. There are nearly 28 efflux pumps identified so far in gram negative and gram positive bacteria.<sup>183</sup> Tet A is the most frequently noticed efflux pump variant in gram negative bacteria. TC is usually exchanged for a H<sup>+</sup> gradient or ATP efflux pump systems.<sup>189</sup> However, the effect of efflux pumps is different on different classes of TC. It was reported that the minimum inhibitory concentration (MIC) of TC in a *TetA* expressing bacteria was higher for TC while the MIC was significantly lower for doxycycline, minocycline and other generations of TC.<sup>182</sup> On a whole, combating antibiotic resistance has evolved as a serious life threatening challenge.

Developing new and novel antibiotic agents is one of the strategies to fight resistant bacteria. Omadacycline is one such new class of TC antibiotic currently being investigated in clinical trials is shown to be effective against several drug resistant pathogens.<sup>190</sup> In addition to developing new antibiotic agents, it is also important to have effective delivery systems. Having an efficient delivery system can help overcome certain obstacles in acquired antibiotic resistance like the efflux pumps, enzymatic degradation of the antibiotic, and specific targeting.<sup>191,192</sup> Nanoparticle drug delivery systems can be a promising solution in overcoming the bacterial resistance. Using nanoparticle delivery systems will help in delivering larger dose of antibiotic to the infected site.

Nanoparticles can also be used for targeted delivery of antibiotics to the infected site either by ligand based targeting or passive targeting.<sup>193</sup> With passive targeting, the nanoparticles can undergo extravasation to the sites of inflammation and cross the cellular membranes of the bacteria.<sup>194</sup> The surface properties of the nanoparticles can be changed in order to make them more biocompatible, thereby avoiding phagocytosis by the immune cells.<sup>195,196</sup>

Several different types of nanocarriers have been explored for the delivery of antibiotics. For example, liposomes encapsulated with ampicillin was reported to increase the bioavailability of the antibiotic.<sup>197</sup> A better anti-biofilm activity against *Staphylococcus epidermidis* was observed when liposomal rifampicin was used.<sup>198</sup> Levofloxacin- and ciprofloxacin-loaded inhalable PLGA nanoparticles were shown to have high activity against *Escherichia coli* in biofilm cells and biofilm-derived planktonic cells by Cheow et al.<sup>199</sup> Metal nanoparticles act as potent antibacterial agents. Silver nanoparticles show enhanced antibacterial activity compared to their ionic form. They act by damaging the bacterial cell membrane.<sup>191</sup> Zinc oxide nanoparticles were also shown to act against drug-resistant strains like *Campylobacter jejuni* and *Streptococcus agalactiae*.<sup>200</sup> Titanium oxide nanoparticles and magnesium oxide nanoparticles, gold and silver nanoparticles were also reported to have antibacterial activity.<sup>200</sup> Vancomycin when loaded on AuNP had significant enhancement in its antibacterial activity compared to the free drug.<sup>80</sup> Recently, Zhao et al. prepared bimetallic nanoparticles (Au-Pt) and demonstrated their antibacterial activity against *E. coli*, *P. aeruginosa* and *K. pneumoniae* and *S. choleraesuis*.<sup>201</sup>

TC, which was once used widely for its applications, is nearly not being used today because of the drug resistance developed in bacteria towards it. Using a nanoparticle delivery system could be a promising strategy to deliver TC is an efficient way to kill bacteria. TC nanoparticles were shown to be useful in treating periodontal infections when loaded into calcium sulfate bone cement beads.<sup>202</sup> PLGA nanoparticles loaded with TC and simvastatin were shown to be effective at targeting bone for the treatment of osteoporosis.<sup>203</sup> TC nanoparticles synthesized using high-energy ultrasonic waves showed bactericidal activity against TC-sensitive and TC-resistant bacteria. Controlled release TC formulations that allow for appropriate concentrations of TC to be maintained over long periods of time were also reported. TC and lovastatin controlled release PLGA nanoparticle formulation was shown to enhance periodontal regeneration.<sup>204</sup>

MSNs are widely studied for drug delivery applications due to their unique properties like the mesoporous structure, chemical stability, tunable size and surface chemistry.<sup>205</sup> Having a mesoporous structure, enables larger surface area which helps is more drug loading on MSNs and its release. MSNs are being studied as drug delivery systems for various disease conditions. Meng et al. used MSNs loaded with doxorubicin (DOX), an anti-cancer agent and tested its efficacy in an *in vivo* model.<sup>206</sup> The MSN-Dox formulation reduced the tumor burden and side effects better than the free drug. MSNs functionalized with n-[(3-trimethoxysilyl) propyl] ethylenediamine and capped with a cationic polymer of  $\epsilon$ -poly-L-lysine (ePLL) were used to deliver Vancomycin to gram-negative bacteria, showed an extended spectrum of activity against *E. coli*, *Salmonella typhimurium* and *Erwinia carotovora*.<sup>207</sup> Lysozyme-coated MSN had been shown to reduce the minimum inhibitory concentration to 5 times compare to free lysozyme.<sup>208</sup>

Mobile Crystalline Material-41 (MCM-41), a type of MSN, was first reported by Beck et al.<sup>209</sup> in 1992, is the most widely investigated mesoporous material for biomedical applications. MCM-41 has a mesoporous structure with pores forming channels in a hexagonal fashion. Its tunable intrinsic properties like pore size, particle size and large surface area make it an ideal host for various molecules.<sup>210</sup> Therapeutic formulations of various compounds like anti-inflammatory agents (i.e., naproxen),<sup>211</sup> antibiotics (i.e., vancomycin)<sup>212</sup> and anticancer agents (i.e., carboplatin)<sup>213</sup> have been developed using MCM-41 formulations and MCM-41 contributes to controlled drug release.<sup>214,215</sup> A MCM-41 was previously shown to be effective in adsorbing TC from aqueous solutions to avoid environmental pollution.<sup>216</sup> TC-loaded 100 nm MCM-41 spheres (12.7% w/w TC loading) were previously prepared and release of TC studied.<sup>217</sup> Hashemikia et al.<sup>218</sup> reported adsorption and controlled release of TC in SBA-15 type MSNs (42.3% w/w TC loading).

To explore the use of MCM-41 mesoporous silica nanoparticles as a delivery system for TC, we prepared two different sized TC-containing MCM-41 type MSNs ( $41 \pm 4$  nm and  $406 \pm 55$  nm) and investigated their *in vitro* release profiles in a biological relevant buffer. We then tested their efficacy against *Escherichia coli* (*E. coli*) in culture.

### **Materials and methods:**

Tetraethoxysilane (TEOS), hexadecyltrimethylammonium bromide (CTAB), sodium hydroxide and TC were purchased from Sigma-Aldrich (St. Louis, MO, USA). Anhydrous ethanol was

obtained from Pharmco-AAPER (Belmont, NC, USA). Phosphate buffered saline (0.0067 M; pH 7.0–7.2) was purchased from HyClone laboratories (Logan, UT, USA).

### **Synthesis of TC-containing MCM-41 nanoparticles (TC-MCM-41 MSNs):**

MCM-41A MSNs were prepared following previously published procedures with slight modifications.<sup>112,213,219</sup> NaOH (7 mL, 0.04 M) was added to H<sub>2</sub>O (480 mL) and the solution was heated to 60 °C. Then, CTAB (2.0 g) was added, followed by TEOS (11.3 mL, 50.6 mmol), while stirring. The mixture was stirred for another 10 min at 60 C, before filtered using aspiration and the precipitate washed three times with Milli-Q water (20 mL) followed by two additional rinses with absolute ethanol (20 mL). Later, a portion of the moist product (1.0 g) was added to absolute ethanol (150 mL) followed by concentrated HCl (0.5 mL) while stirring at r.t. for 2 h. The resulting white precipitate was vacuum filtered and washed with Milli-Q water (50 mL) followed by ethanol (50 mL) and dried *in vacuo* to yield MCM-41A. MCM-41B was prepared as previously described.<sup>112</sup> Figure 22 shows a demonstration of the synthesis of MCM-41 MSNs.<sup>220</sup>

Then, MCM-41A or MCM-41B (20 mg) were added to a 1 mL solution containing TC (10 mg/mL, 20.8 mM) in Milli-Q water. The suspension was stirred vigorously for 24 h at r.t. and then centrifuged at 1300 × g for 20 min. The resulting pellet was washed three times with H<sub>2</sub>O and dried *in vacuo* for 24 h. The supernatants from each step were collected and UV-vis spectra obtained. The dried MSNs were imaged using (TEM; Zeiss EM 910 transmission electron microscope; Zeiss, Jena, Germany).

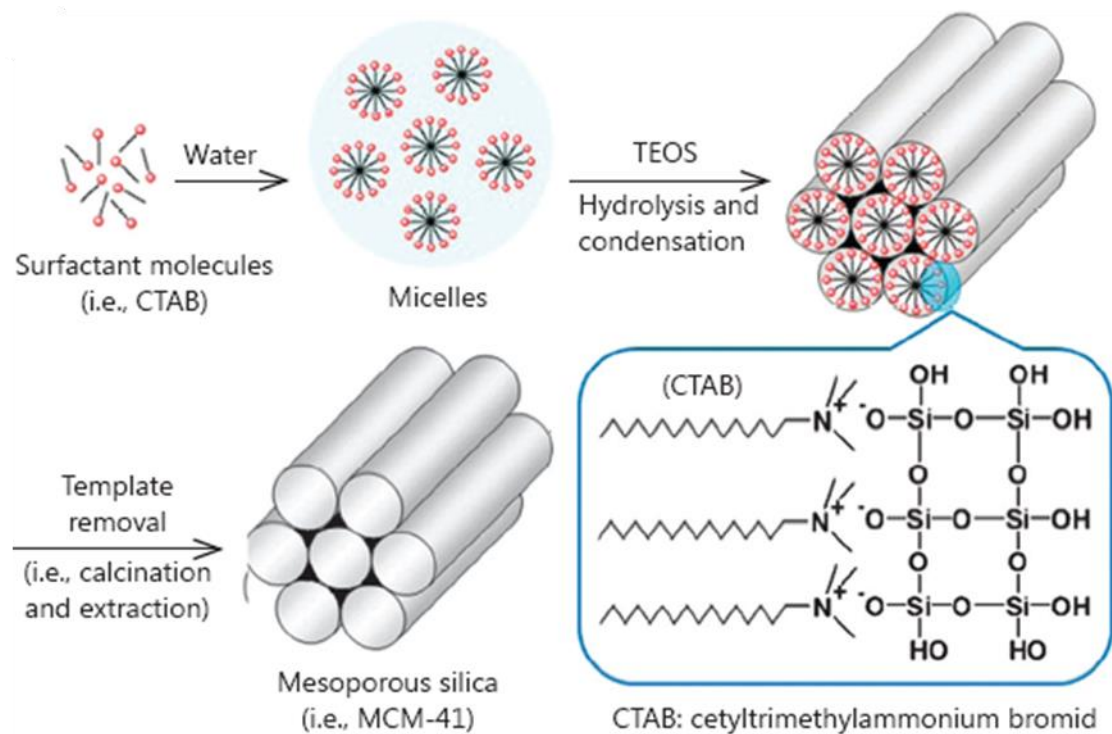


**Figure 22:** Schematic representation of MCM-41 nanoparticle synthesis and structure.<sup>220</sup>

### UV-Vis spectroscopy:

For estimating the drug adsorption by the nanoparticles, UV-vis spectroscopy (Cary 60 UV-vis spectrophotometer; Agilent Technologies, Santa Clara, CA, USA) was used. A 10 mg/mL solution of TC in Milli-Q water was prepared and the UV-vis absorption spectra measured at 0 and 24 h. Supernatants from all washes during the preparation of TC-containing MCM-41 nanoparticles were collected and UV-vis spectra recorded. The spectra of TC at 24 h was compared with that of the supernatants to calculate the drug adsorbed on the nanoparticles after 24 h. Percent drug incorporated was determined from the following formula:

$$\text{Drug Incorporated (\%)} = \left[ \frac{\text{Drug incorporated (mg)}}{\text{Drug - containing MSNs}} \right] \times 100$$

### ***In vitro* release studies:**

All release studies were carried out in PBS, pH (7–7.2), at 37 °C. TC- MCM-41A or TC-MCM-41B was weighed and suspensions of 1 mg/mL in PBS were prepared. The suspensions were then stirred vigorously at 37 °C, and release measured at 0, 0.5, 1, 3 and 5 h from the different suspensions. Samples were removed at their respective time points and centrifuged at 1000 g for 10 min at r.t. Supernatant was collected and the UV-vis spectra obtained. The amount of drug (mg) released was calculated by comparing the absorbance at 275 nm to the absorbance of a 10 mg/mL solution of TC in PBS. Percent drug released was calculated from both TC-MCM-41A and TC-MCM-41B using the following formula:

$$\text{Drug release (\%)} = \left[ \frac{\text{Drug released (mg)}}{\text{Drug loaded on MSNs (at } t = 0, \text{ mg)}} \right] \times 100$$

The release profile of TC-MCM-41 A was also studied in culture broth. Samples were prepared and drug release was measured by UV-Vis spectroscopy following the same procedure as above in a manner similar to above by replacing PBS with Lennox L broth (LB broth; Research Products International Corp. Mt Prospect, IL, USA). The obtained data was fit to an exponential regression using Microsoft Excel Solver.

### **Antibacterial activity of TC-MCM-41A and TC-MCM-41B against *E. coli*:**

The antibacterial activity of prepared TC-MCM-41A and TC-MCM-41B was further tested using *E. coli*, which was cultured in round-bottom culture tubes at 37 °C in a shaker at 250 rpm, with a

tube volume to culture volume ratio of 1.75:1. Lennox L broth (LB broth; Research Products International Corp. Mt Prospect, IL, USA) was used as growth medium.

The antibacterial activity was tested at two different concentrations of TC (1) 0.5 µg/mL and (2) 1.0 µg/mL. *E. coli* was pre-cultured in 4 mL medium at conditions mentioned above. From this 800 µL of *E. coli* was taken and inoculated into 250 mL of culture medium. This was further split into different culture tubes and received one of the following treatments. Group 1: (a) blank (no treatment); (b) 0.5 µg/mL TC alone; (c) MCM-41A; (d) MCM-41B; (e) TC-MCM-41A (0.5 µg/mL TC); and (f) TC-MCM-41B (0.5 µg/mL TC). Group 2: (a) blank (no treatment); (b) 1.0 µg/mL TC alone; (c) MCM-41A; (d) MCM-41B; (e) TC-MCM-41A (1.0 µg/mL TC) and (f) TC-MCM-41B (1.0 µg/mL TC) and (g) 10 µg/mL TC (positive control). In each group, the concentration of free TC was the same as the concentration of TC in MCM-41A and MCM-41B, and concentrations of MCM-41A and MCM-41B corresponded to concentrations of TC-MCM-41A and TC-MCM-41B, respectively.

The growth of *E. coli* in all treatment groups was then monitored in terms of change in turbidity at 0, 1, 2, 3, 4, 5, 12, 24, 30, 36, 48, 60 and 72 h by measuring UV-Vis spectra. Absorbance at 600 nm was used to compare the growth inhibition among various treatments [33]. %Survival was calculated using the following equation:

$$\text{Survival (\%)} = \left[ \frac{\text{Absorbance of treatment group (600 nm)}}{\text{Absorbance of no treatment group (600 nm)}} \right] \times 100$$

### **Uptake of TC-MCM-41A nanoparticles by *E. Coli*:**

The uptake of TC-MCM-41A nanoparticles by *E. Coli* was demonstrated using TEM. For this study, 2.5 mL of *E. coli* stock was taken and inoculated in 40 mL of culture medium. This was further split into four (1-4) culture tubes and incubated in a shaker at 37 °C in a shaker at 250 rpm for 4 h. The four tubes received either no treatment or 1 µg/mL TC (TC-MCM-41A) for 0, 0.5 and 1 h. After their respective time points, the tubes were removed from shaker, and cell pellet was collected by centrifuging at 1000 × g at 4°C. The pellet was then resuspended in PBS and spotted on a Formvar-coated copper grid for TEM imaging.

### **Results and discussion:**

The goal of this project is to formulate a nanocarrier delivery system for TC a very well-known antibiotic. The use of TC has been limited in recent times due to the resistance acquired by bacteria.<sup>182,221</sup> Bacterial resistance against antibiotics has emerged as an alarming problem worldwide. Using a delivery system that can help enhance the efficacy of antibiotics TC can be promising in this scenario. Several studies were published showing the use of a nanocarrier for antibiotic drug delivery to improve the drug efficacy.<sup>191-193,200,222</sup> Here, we used MSNs as a delivery vehicle for TC. MCM-41 nanoparticles of two sizes (MCM-41A and MCM-41B) were synthesized following published procedures. TC was loaded by exposing 20 mg of either MCM-41A or MCM-41B to a solution containing 10 mg/mL of TC hydrochloride in Milli-Q water. and the mixture was stirred vigorously for 24 h at room temperature. The TC-loaded nanoparticles (TC-MCM-41A and TC-MCM-41B) were characterized using transmission electron microscopy. Particle size was measured from TEM images using ImageJ software (1.47, National Institute of

Health, Bethesda, MD, USA). TC-CM-41A had a particle size of  $41 \pm 4$  nm (Figure 23A) and TC-MCM-41B has a particle size of  $406 \pm 55$  nm (Figure 23B). UV-Vis spectra of TC in Milli-Q water (10 mg/mL; control) were collected at 0 and 24 h (Figure 24). A slight downward shift in the TC spectrum was observed after 24 h, most likely due to the instability of TC in aqueous solution.

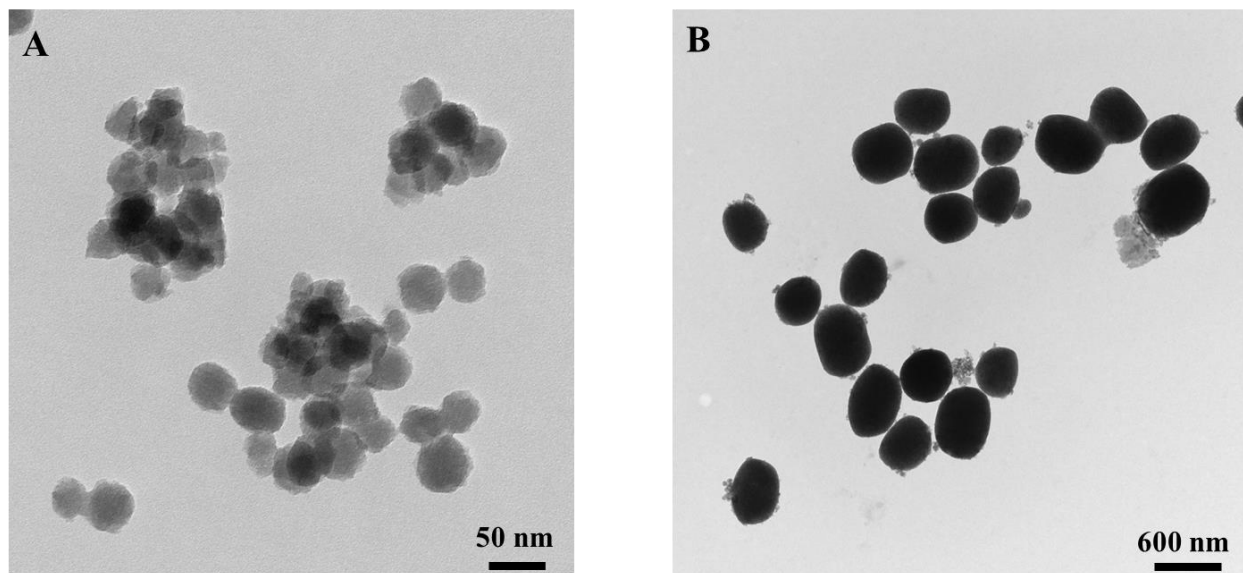


**Figure 23:** TEM images of tetracycline-containing MCM-41 nanoparticles. (A) MCM-41A ( $41 \pm 4$  nm) and (B) MCM-41B ( $406 \pm 55$  nm).

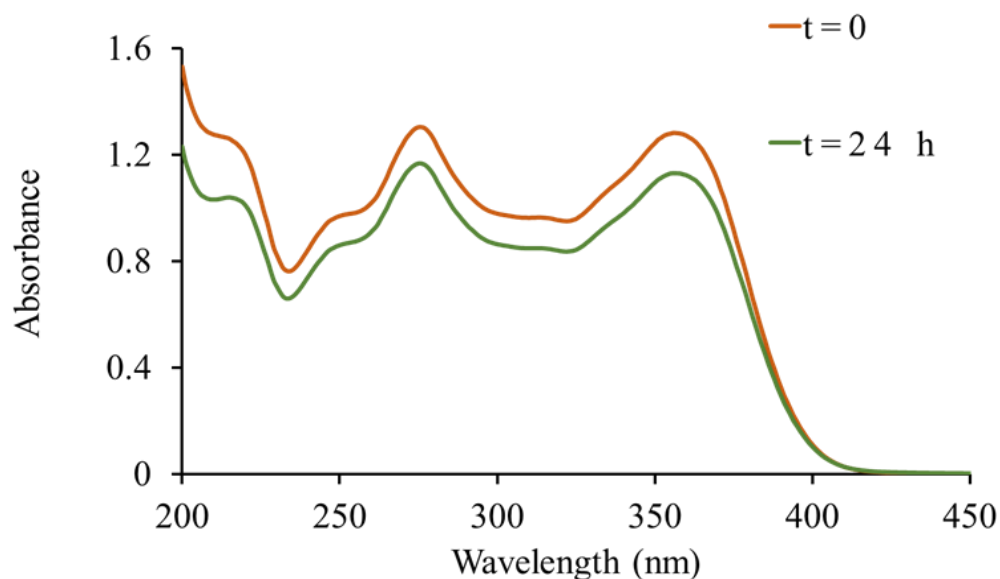


**Figure 24:** UV-vis spectra of tetracycline at 0 and 24 h. A slight downward shift in the spectra was observed at 24 h.

After loading the MSNs with TC, the supernatants from all washes were collected and the UV-vis spectra obtained (Figure 25). Percent loading of TC was calculated by comparing the absorption at  $\lambda = 275$  nm of the supernatants to that of the 24 h TC control. The weight percent of TC in TC-MCM-41A and TC-MCM-41B formulations were 18.7% and 17.7% w/w, respectively. Thus, drug loading is similar to that achieved by Lin et al. (12.7% w/w TC) using 100 nm MCM-41 MSNs.<sup>223</sup> When impregnated with lanthanum (La), MCM-41 was shown to adsorb TC more efficiently from aqueous samples in environmental studies; TC loading increased from approximately 3% to 20%.<sup>217</sup> When using SBA-15 to load drug, TC content was 42.3% w/w.<sup>218</sup> Variations in loading are most likely due to differences in physicochemical properties of the

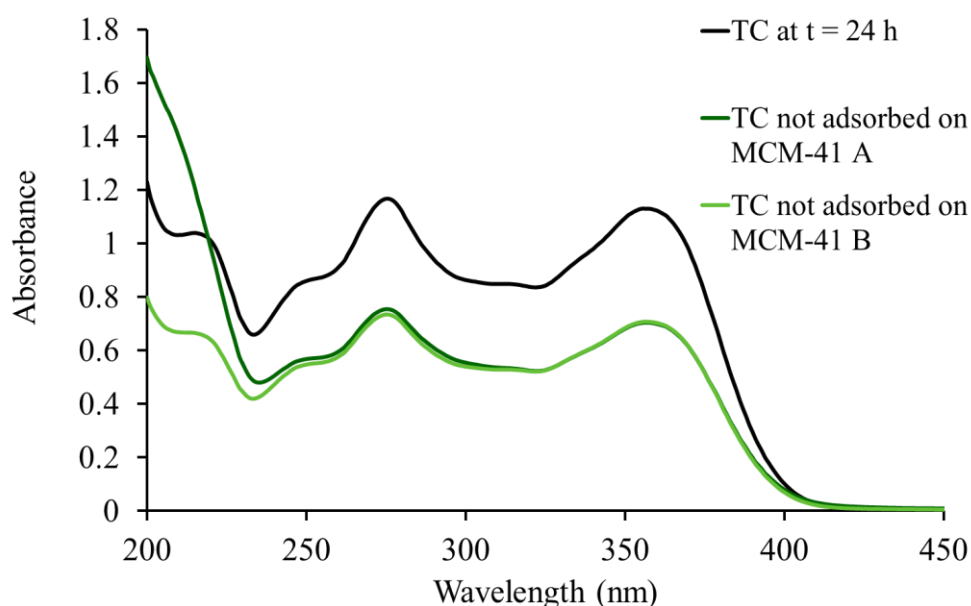


**Figure 25:** Adsorption of tetracycline (TC) by MCM-41A and MCM-41B. UV-vis spectra of TC control at 24 h and TC not adsorbed by MCM-41A (Green) and MCM-41B (Yellow). Percent drug adsorption was measured by comparing absorbance at 275 nm.

materials; however, how these differences affect biocompatibility of the nanoparticle need be considered.

The *in vitro* release of TC in phosphate buffered saline (PBS; pH 7–7.2) at 37 °C was then measured using UV-vis spectroscopy. Release was determined at 0, 0.5, 1, 3 and 5 h for both TC-MCM-41A and TC-MCM-41B (Figure 26). A burst release was observed in both formulations at  $t = 0$  and most drug was released by the end of the 5 h observation period (86% and 94% for TC-MCM-41A and TC-MCM-41B, respectively), although most TC was released over the first hour.

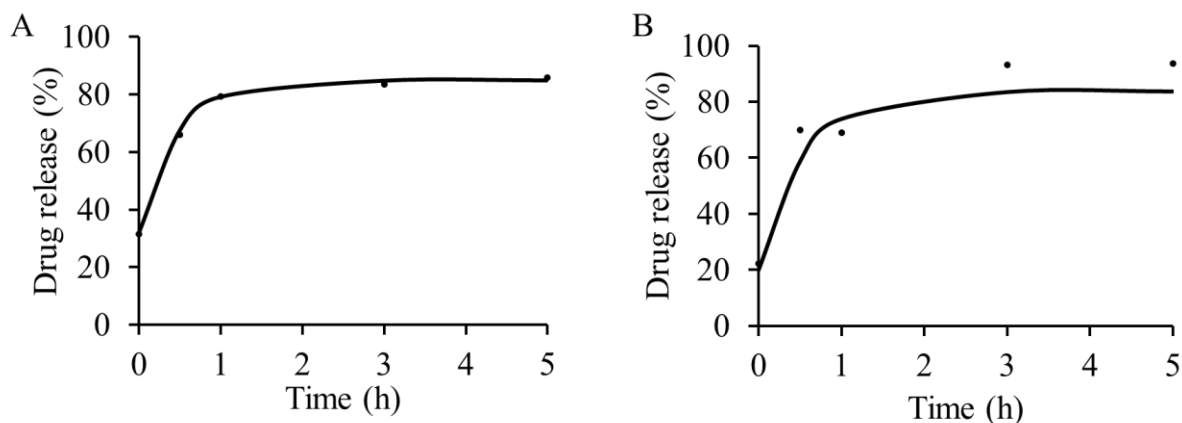


**Figure 26:** *In vitro* release of tetracycline from (A) TC-MCM-41A and (B) TC-MCM-41B, determined using UV-Vis spectroscopy. Most drug was released by 1 h. All studies were carried out in PBS, pH 7-7.2, at 37 °C.

The drug release from our formulations in PBS is faster, compared to the formulation by Lin et al. in simulated biological fluid (SBF; pH 7.4) at 37 °C; after five days 41.9% TC was released by the 100 nm MCM-41 in SBF.<sup>223</sup> It is known that differences in pore size can affect drug release from MSNs, and this could be a contributing factor here.<sup>224</sup> Drug release rate can also be controlled by functionalization of MSNs. For example, release of vancomycin from CdS capped MCM-41 type MSNs was shown to be extended for up to 3 days.<sup>212</sup> A controlled release of captopril using MCM-41 showed enhanced release profile upon silylation.<sup>225</sup> Amine functionalized SBA-15 type MSNs

release of TC was shown to be extended up to 48 h.<sup>218</sup> Thus, drug release could potentially be extended from our materials by surface functionalization.

Further, the release profile of TC- MCM-41A is studied in LB broth medium (Figure 27) to see if the burst release pattern in solvent dependent. The release of TC in LB broth is similar to that PBS.

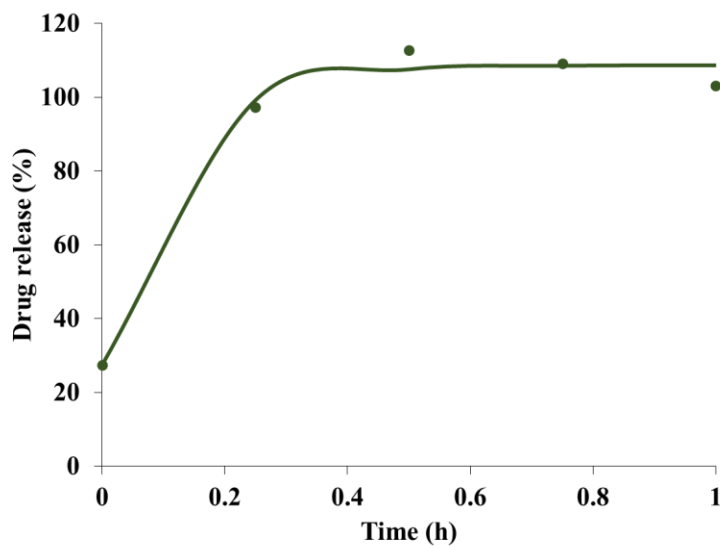


**Figure 27:** *In vitro* release of TC from (A) TC-MCM-41A determined using UV-vis spectroscopy in LB broth medium. Most drug was released by 1h.

#### **Antibacterial activity against *E. coli*:**

The antibacterial activity of prepared TC-MCM-41A and TC-MCM-41B was tested against *E. coli*, and compared with that of free TC and blank MCM-41A and MCM-41B, Figure 27. Two groups with different TC concentrations, 0.5 g/mL (Group 1, Figure 28A) and 1.0 g/mL (Group 2, Figure 28B), were investigated. In each group, the concentration of free TC was the same as the concentration of TC in TC-MCM-41A and TC-MCM-41B, and concentrations of MCM-41A and MCM-41B corresponded to concentrations of TC-MCM-41A and TC-MCM-41B, respectively. As illustrated in Figure 28, MCM-41A and MCM-41B did not show any effect on *E. coli* growth in either group. Within 4 h after treatment, free TC and TC-MCM-41A and TC-MCM-41B showed

similar inhibition of *E. coli* growth. However, after 4 h and up to 18 h for Group 1 and up to 24 h for Group 2, TC-MCM-41A and TC-MCM-41B both exhibited greater inhibition on bacteria growth than free TC. Percent survival of *E. coli* treated with 10 g/mL free TC decreased to 3% in 4 h and did not increase with time (data not shown). After 24 h, the *E. coli* with no treatment stopped growing as nutrients were exhausted. Slow release of TC could preserve the efficacy of TC, as not all antibiotic is in the medium at  $t = 0$ . The concentrations of TC used, 0.5  $\mu\text{g/mL}$  and 1  $\mu\text{g/mL}$  are below the minimum inhibitory concentrations of TC in *E. coli* (2-4  $\mu\text{g/mL}$ ). Both the formulations, at the concentration of 1  $\mu\text{g/mL}$  TC, inhibited bacterial growth more efficiently than the free drug. Though most of the drug is being released in the LB broth within the first 1 h (Figure 26), the drug's activity lasted up to 24 h (Figure 27B). This can be because the nanoparticles are immediately taken up by *E. coli* and TC is preserved from degradation because of being loaded on to MSNs.

In order to test the uptake of MSNs by *E. coli*, TEM imaging was done after treating the bacteria (*E. coli*) with TC-MCM41-A (1  $\mu\text{g/mL}$ ) for up to 1 h. After 1 h treatment, the nanoparticles have crossed the cell wall and entered the bacteria (Figure 29). As most of the drug is released within 1 h in LB broth, this uptake of nanoparticles by *E. coli* within 1 h of treatment can be the reason for the enhanced antimicrobial activity of TC containing MSNs compared to free TC (Figure 29B). It is possible that once inside the cell, TC is being protected by MSNs from being sent out by the

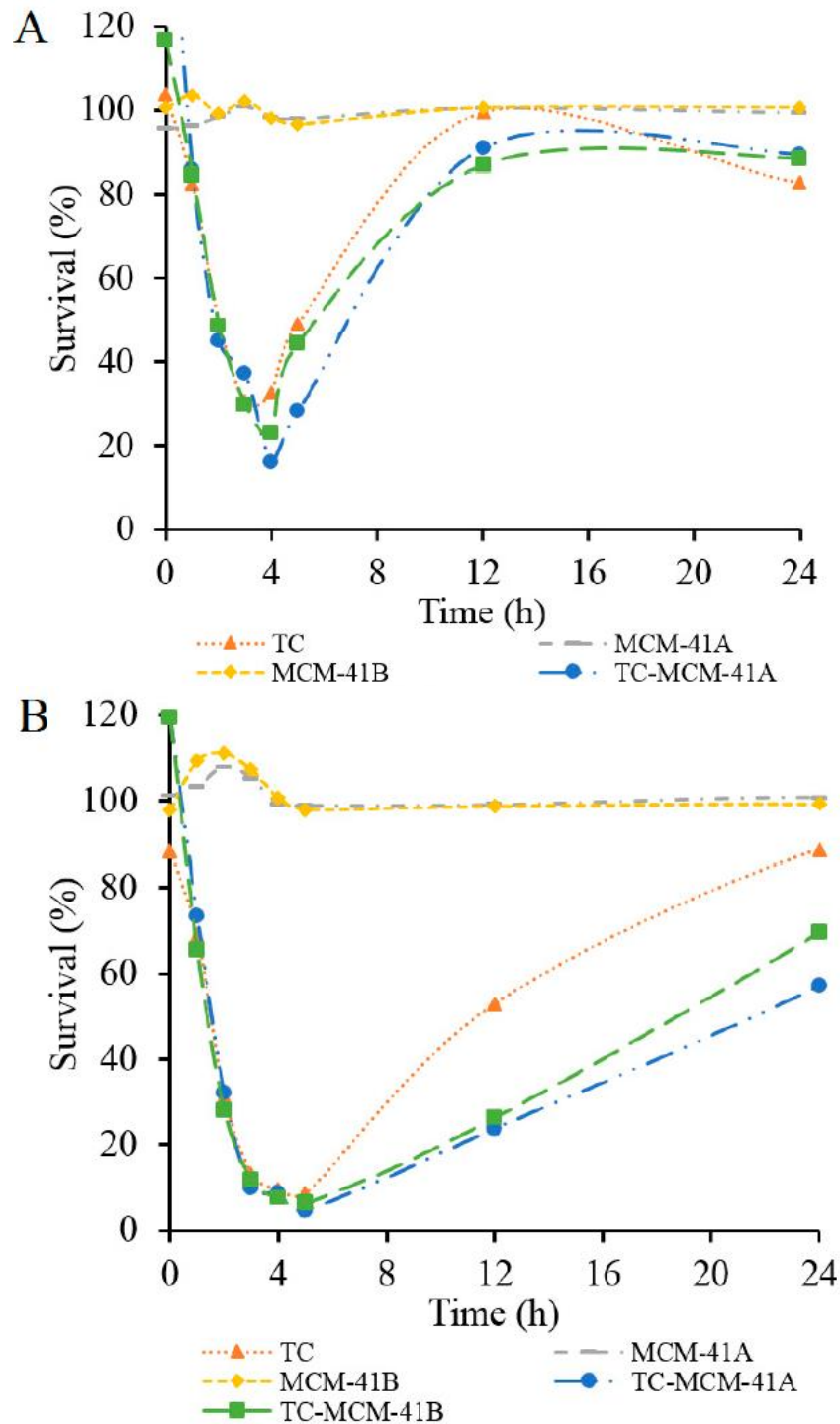


**Figure 28:** Survival (%) of *E. coli* treated by TC, MCM-41A, and TC-MCM-41B, determined using UV-vis spectroscopy. (A) TC concentration: 0.5 µg/mL and (B) TC concentration: 1.0 µg/mL. In each group, the concentration of free TC was the same as the concentration of TC in TC-MCM-41A and TC-MCM-41B, and concentrations of MCM-41A and MCM-41B corresponded to concentrations of TC-MCM-41A and TC-MCM-41B, respectively.

efflux pumps, which is usually the case with free TC. However, further studies are required to understand the actual mechanism of action of TC containing MSNs in improving TC efficacy.

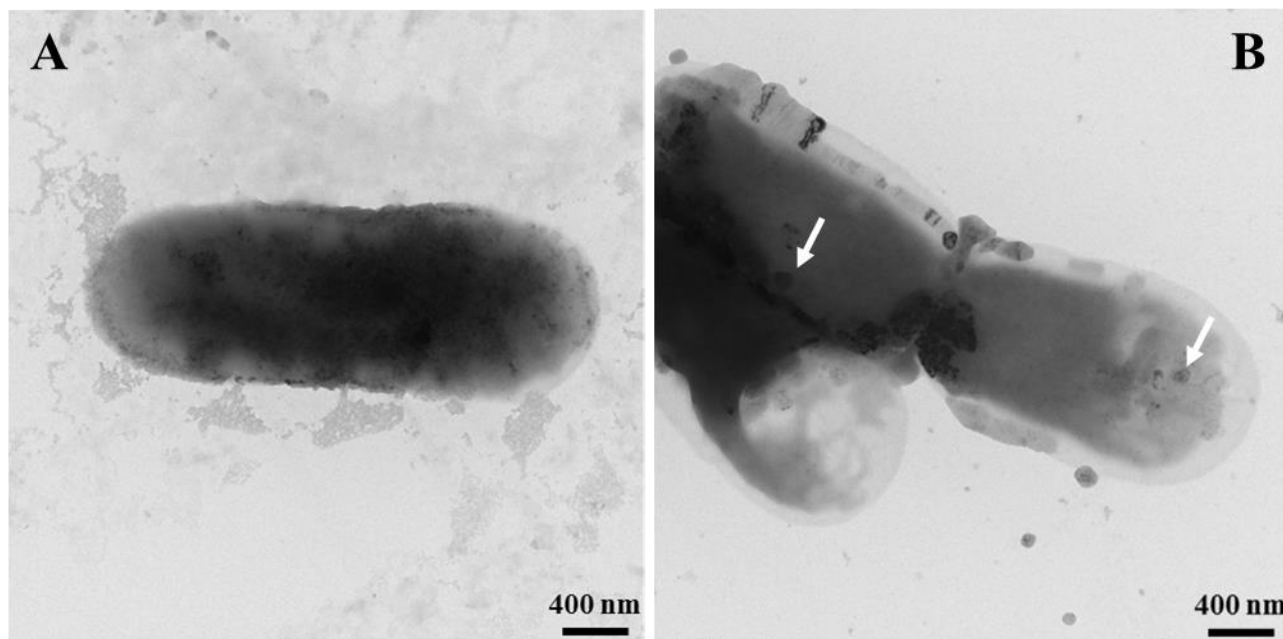


**Figure 29:** Uptake of TC from TC-MCM-41A by *E. coli* determined using TEM. A) 0 h after treatment B) 1 h after treatment with TC-MCM41-A ( $1\mu\text{g/mL}$ ). Arrows indicate TC-MCM41-A nanoparticles.

### Conclusions:

MCM-41 nanoparticles loaded with TC (TC-MCM-41A and TC-MCM-41B) were prepared in two different sizes ( $41 \pm 4$  nm and  $406 \pm 55$  nm, respectively); drug adsorption measured using UV-vis spectroscopy was 18.6% and 17.7% w/w TC, respectively. *In vitro* release studies were performed in PBS, pH 7.2, at  $37^\circ\text{C}$  and the efficacies of TC-MCM-41A and TC-MCM-41B were shown to be superior to free TC *in vivo*, while blank nanoparticles had no effect. Further the uptake of TC-MCM-41A MSNs by *E. coli* was demonstrated.

## CHAPTER 5

### SUMMARY AND FUTURE PERSPECTIVES

Inorganic nanomaterials exhibit various unique properties like tunable size and surface chemistry, plasmonic surface resonance, and ease of functionality. Research is currently being conducted around the globe to determine ways to efficiently use inorganic nanoparticles for therapy and diagnosis. The main objective of this project was to explore the use of various inorganic materials in biomedical sciences. We first studied the efficacy of  $^{166}\text{HoIG}$  loaded electrospun PAN nanofibrous mats (radiotherapeutic bandages) in an *in vivo* model of squamous cell carcinoma of skin. The radiotherapeutic bandage significantly reduced the tumor volume in mice compared to the non-radioactive bandage and no treatment. The dose used (~30 Gy) was less than that clinically used in humans. Histopathological evaluations showed slight epidermal thickening and ulceration but no damage to other surrounding organs was observed. This proof-of-concept study showed that the radiotherapeutic bandage is effective in significantly reducing tumor volume in just one dose. In the future, the efficacy of the bandage in complete eradication of the tumor can be tested using a higher dose or by using multiple doses at regular intervals. Furthermore, the formulation can be improved by incorporating radiosensitizers, which can reduce the radiation dose needed to treat the tumors. Then, investigational new drug (IND) studies can be conducted, which are required for the device to enter clinical trials. In the future, other formulations using  $^{166}\text{Ho}$  as the radioactive nuclide will be formulated for use in cancer radionuclide therapy.

In the second study, gold nanoparticles (AuNP) were used to develop a targeted platinum (Pt) drug delivery formulation for the treatment of non-small cell lung cancer. We demonstrated the preparation of PEGylated gold nanoparticles and the attachment of a Pt(IV) complex and an antibody. PEGylation not only improves the dispersion of nanoparticles, but also makes it more biocompatible by extending drug bioavailability. The CD22 status on lung cancer and normal lung cell lines was also demonstrated. Although the uptake of AuNP-PEG-Pt-mAb did not correlate well with CD22 expression in the cell lines tested, replacing the targeting agent with a different moiety (e.g., HER2 targeting for breast cancer) may be appropriate. However, increasing the Pt(IV) content of the nanoparticle should also be investigated.

In the third study, mesoporous silica nanoparticles (MSNs) were used for the delivery of tetracycline (TC). MCM-41 type MSNs were used in this study. The mesoporous structure of these nanoparticles increases surface area and, thus, enhances drug loading, and MSNs have tunable surface chemistry. Here, two different sizes of MCM-41 MSNs were synthesized and loaded with TC (~18 % w/w TC loading). The TC-MCM-41 nanoparticles of both sizes showed a similar trend in inhibiting the *E. coli* growth compared to free TC and blank MSNs. The nanoparticles were shown to be up taken by the bacterial cell within 1 h of the treatment. The trend observed in reduction of bacterial survival can be further studied. This formulation can be further improved by making it a controlled release TC formulation, through surface functionalization and by altering parameters such as pore size. Furthermore, we wish to test TC-MCM-41 MSN against TC-sensitive and -resistant pairs of bacteria to determine if this phenomenon is due to reduced efflux of TC. This can help us determine if using MSNs can help overcome the resistance developed due to efflux pumps in bacteria. In the future, more antibiotic formulations can be synthesized using the MC41-MSNs and be tested for efficacy in bacterial strains.

Overall, the promise of various inorganic nanomaterials in healthcare is great. All formulations studied in this work have the potential to emerge as powerful tools for therapy of various challenging diseases. Further study of these may lead to improved patient outcomes.

## References:

1. Murthy, S.K. Nanoparticles in modern medicine: state of the art and future challenges. *Int J Nanomedicine* 2, 129-141 (2007).
2. Salata, O. Applications of nanoparticles in biology and medicine. *J Nanobiotechnology* 2, 3 (2004).
3. Lin, W. Introduction: Nanoparticles in Medicine. *Chem Rev* 115, 10407-10409 (2015).
4. Lipinski, C. Poor aqueous solubility-an industry wide problem in drug discovery. *Am Pharm Rev* 5, 82-85 (2002).
5. Lipper, R. E Pluribus product. 55-60. *Modern Drug Disc* (1999).
6. Rodriguez-Aller, M., Guillarme, D., Veuthey, J.-L. & Gurny, R. Strategies for formulating and delivering poorly water-soluble drugs. *Journal of Drug Delivery Science and Technology* 30, 342-351 (2015).
7. Vo, C.L.-N., Park, C. & Lee, B.-J. Current trends and future perspectives of solid dispersions containing poorly water-soluble drugs. *European Journal of Pharmaceutics and Biopharmaceutics* 85, 799-813 (2013).
8. Yu, B.G., Okano, T., Kataoka, K. & Kwon, G. Polymeric micelles for drug delivery: solubilization and haemolytic activity of amphotericin B. *Journal of Controlled Release* 53, 131-136 (1998).
9. Junyaprasert, V.B. & Morakul, B. Nanocrystals for enhancement of oral bioavailability of poorly water-soluble drugs. *Asian Journal of Pharmaceutical Sciences* 10, 13-23 (2015).
10. FDA. Orange Book: Approved Drug Products with Therapeutic Equivalence Evaluations. Vol. 2016 (Food and Drug Administration Division of Freedom of Information, Rockville, MD).

11. Karve, S., *et al.* Revival of the abandoned therapeutic wortmannin by nanoparticle drug delivery. *Proc Natl Acad Sci U S A* 109, 8230-8235 (2012).
12. Mishra, P., Nayak, B. & Dey, R.K. PEGylation in anti-cancer therapy: An overview. *Asian Journal of Pharmaceutical Sciences* 11, 337-348 (2016).
13. Caliceti, P. & Veronese, F.M. Pharmacokinetic and biodistribution properties of poly(ethylene glycol)–protein conjugates. *Advanced Drug Delivery Reviews* 55, 1261-1277 (2003).
14. Bailon, P. & Berthold, W. Polyethylene glycol-conjugated pharmaceutical proteins. *Pharmaceutical Science & Technology Today* 1, 352-356 (1998).
15. Delgado, C., Francis, G.E. & Fisher, D. The uses and properties of PEG-linked proteins. *Crit Rev Ther Drug Carrier Syst* 9, 249-304 (1992).
16. Anselmo, A.C. & Mitragotri, S. Nanoparticles in the clinic. *Bioengineering & Translational Medicine* 1, 10-29 (2016).
17. Bobo, D., Robinson, K.J., Islam, J., Thurecht, K.J. & Corrie, S.R. Nanoparticle-Based Medicines: A Review of FDA-Approved Materials and Clinical Trials to Date. *Pharmaceutical Research* 33, 2373-2387 (2016).
18. Krown, S.E., Northfelt, D.W., Osoba, D. & Stewart, J.S. Use of liposomal anthracyclines in Kaposi's sarcoma. *Seminars in Oncology* 31, Supplement 13, 36-52 (2004).
19. Bourges, J.L., *et al.* Ocular drug delivery targeting the retina and retinal pigment epithelium using polylactide nanoparticles. *Invest Ophthalmol Vis Sci* 44, 3562-3569 (2003).
20. Wong, C., *et al.* Multistage nanoparticle delivery system for deep penetration into tumor tissue. *Proc Natl Acad Sci U S A* 108, 2426-2431 (2011).

21. Thamake, S.I., Raut, S.L., Gryczynski, Z., Ranjan, A.P. & Vishwanatha, J.K. Alendronate coated poly-lactic-co-glycolic acid (PLGA) nanoparticles for active targeting of metastatic breast cancer. *Biomaterials* 33, 7164-7173 (2012).
22. Hersh, D.S., *et al.* Evolving Drug Delivery Strategies to Overcome the Blood Brain Barrier. *Curr Pharm Des* 22, 1177-1193 (2016).
23. Cheng, Y., *et al.* Blood-brain barrier permeable gold nanoparticles: an efficient delivery platform for enhanced malignant glioma therapy and imaging. *Small* 10, 5137-5150 (2014).
24. Kong, S.D., *et al.* Magnetic targeting of nanoparticles across the intact blood-brain barrier. *J Control Release* 164, 49-57 (2012).
25. Sharma, S., *et al.* Vitamin B6 Tethered Endosomal pH Responsive Lipid Nanoparticles for Triggered Intracellular Release of Doxorubicin. *ACS Appl Mater Interfaces* (2016).
26. Benyettou, F., *et al.* Mesoporous gamma-Iron Oxide Nanoparticles for Magnetically Triggered Release of Doxorubicin and Hyperthermia Treatment. *Chemistry* (2016).
27. Rocca, J.D., *et al.* Polysilsesquioxane nanoparticles for triggered release of cisplatin and effective cancer chemoradiotherapy. *Nanomedicine* 11, 31-38 (2015).
28. Duncan, R. Polymer therapeutics: top 10 selling pharmaceuticals—what next? *Journal of Controlled release* 190, 371-380 (2014).
29. Berges, R. Eligard®: pharmacokinetics, effect on testosterone and PSA levels and tolerability. *European Urology Supplements* 4, 20-25 (2005).
30. Gabizon, A., *et al.* Prolonged circulation time and enhanced accumulation in malignant exudates of doxorubicin encapsulated in polyethylene-glycol coated liposomes. *Cancer research* 54, 987-992 (1994).

31. James, N., *et al.* Liposomal doxorubicin (Doxil): an effective new treatment for Kaposi's sarcoma in AIDS. *Clinical oncology* 6, 294-296 (1994).
32. Bui, H.T., Chung, O.H., Dela Cruz, J. & Park, J.S. Fabrication and characterization of electrospun curcumin-loaded polycaprolactone-polyethylene glycol nanofibers for enhanced wound healing. *Macromolecular Research* 22, 1288-1296 (2014).
33. Katti, D.S., Robinson, K.W., Ko, F.K. & Laurencin, C.T. Bioresorbable nanofiber-based systems for wound healing and drug delivery: optimization of fabrication parameters. *J Biomed Mater Res B Appl Biomater* 70, 286-296 (2004).
34. Shahi, R.G., *et al.* Novel bioactive tetracycline-containing electrospun polymer fibers as a potential antibacterial dental implant coating. *Odontology* (2016).
35. Zhang, Z., *et al.* Time-programmed DCA and oxaliplatin release by multilayered nanofiber mats in prevention of local cancer recurrence following surgery. *Journal of Controlled Release* 235, 125-133 (2016).
36. Hofmann-Antenbrink, M., Grainger, D.W. & Hofmann, H. Nanoparticles in medicine: Current challenges facing inorganic nanoparticle toxicity assessments and standardizations. *Nanomedicine: Nanotechnology, Biology and Medicine* 11, 1689-1694 (2015).
37. Giner-Casares, J.J., Henriksen-Lacey, M., Coronado-Puchau, M. & Liz-Marzán, L.M. Inorganic nanoparticles for biomedicine: where materials scientists meet medical research. *Materials Today* 19, 19-28 (2016).
38. Michalet, X., *et al.* Quantum dots for live cells, *in vivo* imaging, and diagnostics. *Science* 307, 538-544 (2005).

39. Bhattacharyya, S., Kudgus, R.A., Bhattacharya, R. & Mukherjee, P. Inorganic nanoparticles in cancer therapy. *Pharm Res* 28, 237-259 (2011).
40. Wang, M. & Thanou, M. Targeting nanoparticles to cancer. *Pharmacol Res* 62, 90-99 (2010).
41. Kresge, C., Leonowicz, M., Roth, W., Vartuli, J. & Beck, J. Ordered mesoporous molecular sieves synthesized by a liquid-crystal template mechanism. *nature* 359, 710-712 (1992).
42. Kwon, S., *et al.* Silica-based mesoporous nanoparticles for controlled drug delivery. *Journal of tissue engineering* 4, 2041731413503357 (2013).
43. Trewyn, B.G., Slowing, I.I., Giri, S., Chen, H.-T. & Lin, V.S.-Y. Synthesis and functionalization of a mesoporous silica nanoparticle based on the sol-gel process and applications in controlled release. *Accounts of Chemical Research* 40, 846-853 (2007).
44. Klichko, Y., *et al.* Mesostructured silica for optical functionality, nanomachines, and drug delivery. *Journal of the American Ceramic Society* 92(2009).
45. Fan, J., *et al.* Targeted anticancer prodrug with mesoporous silica nanoparticles as vehicles. *Nanotechnology* 22, 455102 (2011).
46. Thiesen, B. & Jordan, A. Clinical applications of magnetic nanoparticles for hyperthermia. *Int J Hyperthermia* 24, 467-474 (2008).
47. society, A.c. Cancer facts and figures 2016. (ACS, 2016).
48. Pombo Garcia, K., *et al.* Zwitterionic-coated "stealth" nanoparticles for biomedical applications: recent advances in countering biomolecular corona formation and uptake by the mononuclear phagocyte system. *Small* 10, 2516-2529 (2014).

49. Mahalingam, D., *et al.* Phase I study of intravenously administered ATI-1123, a liposomal docetaxel formulation in patients with advanced solid tumors. *Cancer Chemother Pharmacol* 74, 1241-1250 (2014).
50. Wicki, A., Witzigmann, D., Balasubramanian, V. & Huwyler, J. Nanomedicine in cancer therapy: Challenges, opportunities, and clinical applications. *Journal of Controlled Release* 200, 138-157 (2015).
51. Mamot, C., *et al.* Tolerability, safety, pharmacokinetics, and efficacy of doxorubicin-loaded anti-EGFR immunoliposomes in advanced solid tumours: a phase 1 dose-escalation study. *Lancet Oncol* 13, 1234-1241 (2012).
52. Senanayake, T.H., *et al.* Encapsulation of poorly soluble drugs in polymer-drug conjugates: effect of dual-drug nanoformulations on cancer therapy. *Pharm Res* 31, 1605-1615 (2014).
53. Sawant, R.R. & Torchilin, V.P. Challenges in development of targeted liposomal therapeutics. *AAPS J* 14, 303-315 (2012).
54. Xiang, G., Wu, J., Lu, Y., Liu, Z. & Lee, R.J. Synthesis and evaluation of a novel ligand for folate-mediated targeting liposomes. *International Journal of Pharmaceutics* 356, 29-36 (2008).
55. Malhi, S.S., *et al.* Intracellular delivery of redox cycler-doxorubicin to the mitochondria of cancer cell by folate receptor targeted mitocancerotropic liposomes. *International Journal of Pharmaceutics* 432, 63-74 (2012).
56. Zhai, G., *et al.* A transferrin receptor-targeted liposomal formulation for docetaxel. *J Nanosci Nanotechnol* 10, 5129-5136 (2010).

57. Wicki, A., *et al.* Targeting tumor-associated endothelial cells: anti-VEGFR2 immunoliposomes mediate tumor vessel disruption and inhibit tumor growth. *Clin Cancer Res* 18, 454-464 (2012).
58. Torres, M.M., Jain, T.K., Labhasetwar, V. & Leslie-Pelecky, D. Magnetic studies of iron oxide nanoparticles coated with oleic acid and Pluronic $\bar{U}$  block copolymer. *Journal of Applied Physics* 97, 10Q905 (2005).
59. Xu, H., *et al.* Antibody conjugated magnetic iron oxide nanoparticles for cancer cell separation in fresh whole blood. *Biomaterials* 32, 9758-9765 (2011).
60. Patra, C.R., *et al.* Targeted delivery of gemcitabine to pancreatic adenocarcinoma using cetuximab as a targeting agent. *Cancer Res* 68, 1970-1978 (2008).
61. Hirsch, L.R., *et al.* Nanoshell-mediated near-infrared thermal therapy of tumors under magnetic resonance guidance. *Proc Natl Acad Sci U S A* 100, 13549-13554 (2003).
62. Xu, C., Tung, G.A. & Sun, S. Size and Concentration Effect of Gold Nanoparticles on X-ray Attenuation As Measured on Computed Tomography. *Chem Mater* 20, 4167-4169 (2008).
63. McQuaid, H.N., *et al.* Imaging and radiation effects of gold nanoparticles in tumour cells. *Sci Rep* 6, 19442 (2016).
64. Popovtzer, R., *et al.* Targeted gold nanoparticles enable molecular CT imaging of cancer. *Nano Lett* 8, 4593-4596 (2008).
65. Libutti, S., *et al.* Results of a completed phase I clinical trial of CYT-6091: A pegylated colloidal gold-TNF nanomedicine. in *ASCO annual meeting proceedings*, Vol. 27 3586 (2009).

66. Di Pasqua, A.J., *et al.* Preparation of Neutron-Activatable Holmium Nanoparticles for the Treatment of Ovarian Cancer Metastases. *small* 8, 997-1000 (2012).
67. Pottier, A., Borghi, E. & Levy, L. New use of metals as nanosized radioenhancers. *Anticancer Res* 34, 443-453 (2014).
68. Gill, P. Nanocarriers, nanovaccines, and nanobacteria as nanobiotechnological concerns in modern vaccines. *Scientia Iranica* 20, 1003-1013 (2013).
69. Zaman, M., Good, M.F. & Toth, I. Nanovaccines and their mode of action. *Methods* 60, 226-231 (2013).
70. Moon, J.J., *et al.* Antigen-displaying lipid-enveloped PLGA nanoparticles as delivery agents for a Plasmodium vivax malaria vaccine. *PLoS One* 7, e31472 (2012).
71. Harper, D.M., Vierthaler, S.L. & Santee, J.A. Review of Gardasil. *J Vaccines Vaccin* 1(2010).
72. Kim, S.Y., *et al.* Oral immunization with Helicobacter pylori-loaded poly(D, L-lactide-co-glycolide) nanoparticles. *Helicobacter* 4, 33-39 (1999).
73. Minigo, G., *et al.* Poly-L-lysine-coated nanoparticles: a potent delivery system to enhance DNA vaccine efficacy. *Vaccine* 25, 1316-1327 (2007).
74. Bosetti, M., Mass, A., Tobin, E. & Cannas, M. Silver coated materials for external fixation devices: *in vitro* biocompatibility and genotoxicity. *Biomaterials* 23(2002).
75. Brayner, R., *et al.* Toxicological impact studies based on Escherichia coli bacteria in ultrafine ZnO nanoparticles colloidal medium. *Nano Lett* 6(2006).
76. Goodman, C., McCusker, C., Yilmaz, T. & Rotello, V. Toxicity of gold nanoparticles functionalized with cationic and anionic side chains. *Bioconjug Chem* 15(2004).

77. Zhao, Y., *et al.* Small molecule-capped gold nanoparticles as potent antibacterial agents that target Gram-negative bacteria. *J Am Chem Soc* 132, 12349-12356 (2010).
78. Li, X., *et al.* Functional gold nanoparticles as potent antimicrobial agents against multi-drug-resistant bacteria. *ACS nano* 8, 10682-10686 (2014).
79. Hetrick, E.M., Shin, J.H., Paul, H.S. & Schoenfisch, M.H. Anti-biofilm efficacy of nitric oxide-releasing silica nanoparticles. *Biomaterials* 30, 2782-2789 (2009).
80. Gu, H., Ho, P., Tong, E., Wang, L. & Xu, B. Presenting vancomycin on nanoparticles to enhance antimicrobial activities. *Nano letters* 3, 1261-1263 (2003).
81. Park, H., *et al.* Inactivation of *Pseudomonas aeruginosa* PA01 biofilms by hyperthermia using superparamagnetic nanoparticles. *Journal of microbiological methods* 84, 41-45 (2011).
82. Lellouche, J., Friedman, A., Lellouche, J.-P., Gedanken, A. & Banin, E. Improved antibacterial and antibiofilm activity of magnesium fluoride nanoparticles obtained by water-based ultrasound chemistry. *Nanomedicine: Nanotechnology, Biology and Medicine* 8, 702-711 (2012).
83. Ismail, R.A., Sulaiman, G.M., Abdulrahman, S.A. & Marzoog, T.R. Antibacterial activity of magnetic iron oxide nanoparticles synthesized by laser ablation in liquid. *Materials Science and Engineering: C* 53, 286-297 (2015).
84. Ren, G., *et al.* Characterisation of copper oxide nanoparticles for antimicrobial applications. *International journal of antimicrobial agents* 33, 587-590 (2009).
85. Muppidi, K., Wang, J., Betageri, G. & Pumerantz, A.S. PEGylated liposome encapsulation increases the lung tissue concentration of vancomycin. *Antimicrob Agents Chemother* 55, 4537-4542 (2011).

86. Swenson, C.E., Stewart, K., Hammett, J., Fitzsimmons, W. & Ginsberg, R. Pharmacokinetics and *in vivo* activity of liposome-encapsulated gentamicin. *Antimicrobial agents and chemotherapy* 34, 235-240 (1990).
87. Garg, M., Asthana, A., Agashe, H.B., Agrawal, G.P. & Jain, N.K. Stavudine-loaded mannosylated liposomes: in-vitro anti-HIV-I activity, tissue distribution and pharmacokinetics. *J Pharm Pharmacol* 58, 605-616 (2006).
88. Kaur, C.D., Nahar, M. & Jain, N.K. Lymphatic targeting of zidovudine using surface-engineered liposomes. *Journal of drug targeting* 16, 798-805 (2008).
89. Dutta, T., *et al.* Poly (propyleneimine) dendrimer based nanocontainers for targeting of efavirenz to human monocytes/macrophages *in vitro*. *J Drug Target* 15, 89-98 (2007).
90. Zhao, X., *et al.* A rapid bioassay for single bacterial cell quantitation using bioconjugated nanoparticles. *Proceedings of the National Academy of Sciences of the United States of America* 101, 15027-15032 (2004).
91. Ramirez, C.C., Federman, D.G. & Kirsner, R.S. Skin cancer as an occupational disease: the effect of ultraviolet and other forms of radiation. *International journal of dermatology* 44, 95-100 (2005).
92. Dubas, L.E. & Ingraffea, A. Nonmelanoma skin cancer. *Facial plastic surgery clinics of North America* 21, 43-53 (2013).
93. Karia, P.S., Han, J. & Schmults, C.D. Cutaneous squamous cell carcinoma: estimated incidence of disease, nodal metastasis, and deaths from disease in the United States, 2012. *Journal of the American Academy of Dermatology* 68, 957-966 (2013).

94. Bonerandi, J.J., *et al.* Guidelines for the diagnosis and treatment of cutaneous squamous cell carcinoma and precursor lesions. *J Eur Acad Dermatol Venereol* 25 Suppl 5, 1-51 (2011).
95. Belkin, D. & Carucci, J.A. Mohs surgery for squamous cell carcinoma. *Dermatologic clinics* 29, 161-174, vii (2011).
96. Viola, K.V., *et al.* Mohs micrographic surgery and surgical excision for nonmelanoma skin cancer treatment in the Medicare population. *Archives of dermatology* 148, 473-477 (2012).
97. Cranmer, L.D., Engelhardt, C. & Morgan, S.S. Treatment of unresectable and metastatic cutaneous squamous cell carcinoma. *Oncologist* 15, 1320-1328 (2010).
98. Jennings, L. & Schmults, C.D. Management of high-risk cutaneous squamous cell carcinoma. *J Clin Aesthet Dermatol* 3, 39-48 (2010).
99. Lovett, R.D., Perez, C.A., Shapiro, S.J. & Garcia, D.M. External irradiation of epithelial skin cancer. *Int J Radiat Oncol Biol Phys* 19, 235-242 (1990).
100. Bhatnagar, A. Nonmelanoma skin cancer treated with electronic brachytherapy: results at 1 year. *Brachytherapy* 12, 134-140 (2013).
101. society, A.c. The Science Behind Radiation Therapy. Vol. 2016 (ed. ACS) (2014).
102. NCCN. NCCN clinical practice guidelines in oncology (NCCN guidelines), Squamous cell skin cancer. Vol. 2015 (NCCN, 2015).
103. society, R. Medical Isotopes : General Concepts. Vol. 2016.
104. Lee, J.D., *et al.* Radionuclide therapy of skin cancers and Bowen's disease using a specially designed skin patch. *Journal of nuclear medicine : official publication, Society of Nuclear Medicine* 38, 697-702 (1997).

105. Munaweera, I., Koneru, B., Shi, Y., Di Pasqua, A.J. & Balkus Jr, K.J. Chemoradiotherapeutic wrinkled mesoporous silica nanoparticles for use in cancer therapy. *APL Materials* 2, 113315 (2014).
106. Vasita, R. & Katti, D.S. Nanofibers and their applications in tissue engineering. *Int J Nanomedicine* 1, 15-30 (2006).
107. Zeleny, J. The electrical discharge from liquid points, and a hydrostatic method of measuring the electric intensity at their surfaces. *Physical Review* 3, 69 (1914).
108. Shin, Y., Hohman, M., Brenner, M. & Rutledge, G. Electrospinning: A whipping fluid jet generates submicron polymer fibers. *Applied physics letters* 78, 1149-1151 (2001).
109. Frenot, A. & Chronakis, I.S. Polymer nanofibers assembled by electrospinning. *Current opinion in colloid & interface science* 8, 64-75 (2003).
110. Li, W.J., Laurencin, C.T., Caterson, E.J., Tuan, R.S. & Ko, F.K. Electrospun nanofibrous structure: a novel scaffold for tissue engineering. *Journal of biomedical materials research* 60, 613-621 (2002).
111. Fridrikh, S.V., Yu, J.H., Brenner, M.P. & Rutledge, G.C. Controlling the fiber diameter during electrospinning. *Phys Rev Lett* 90, 144502 (2003).
112. Di Pasqua, A.J., *et al.* Neutron-activatable holmium-containing mesoporous silica nanoparticles as a potential radionuclide therapeutic agent for ovarian cancer. *Journal of nuclear medicine : official publication, Society of Nuclear Medicine* 54, 111-116 (2013).
113. Hail, N., Jr., Youssef, E.M. & Lotan, R. Evidence supporting a role for mitochondrial respiration in apoptosis induction by the synthetic retinoid CD437. *Cancer Res* 61, 6698-6702 (2001).

114. Song, W.S., *et al.* Tumor volume increase during preoperative chemotherapy as a novel predictor of local recurrence in extremity osteosarcoma. *Ann Surg Oncol* 18, 1710-1716 (2011).
115. Johnson, L., *et al.* Beta-particle dosimetry in radiation synovectomy. *European journal of nuclear medicine* 22, 977-988 (1995).
116. Mowlavi, A.A., Afzalifar, A., Afzalifar, N. & Kashani, E. Depth dose calculation of Holmium-166 for different shape source by VARSKIN3 code. *Iranian Journal of Nuclear Medicine* 18, 32-36 (2010).
117. Jeong, J.M., *et al.* Preparation of (188) Re-labeled paper for treating skin cancer. *Appl Radiat Isot* 58, 551-555 (2003).
118. A. Boschi, L.U., M. Pasquali, A. Duatti, A. Taibi, G. Pupillo, and J. Esposito. 188W/188Re Generator System and Its Therapeutic Applications. *Journal of chemistry* 2014, 14 pages (2014).
119. society, A.c. Cancer facts and figures. Vol. 2016 (American cancer society, Atlanta GA, 2016).
120. Society, A.C. Chemotherapy for non-small cell lung cancer. Vol. 2015 (2015).
121. Spiro, S.G. & Porter, J.C. Lung cancer—where are we today? Current advances in staging and nonsurgical treatment. *American journal of respiratory and critical care medicine* 166, 1166-1196 (2002).
122. institute, N.c. NCI supported clinical trials. Vol. 2016 (2016).
123. Masters, G.A., *et al.* Systemic therapy for stage IV non–small-cell lung cancer: American Society of Clinical Oncology clinical practice guideline update. *Journal of Clinical Oncology*, JCO. 2015.2062. 1342 (2015).

124. Clinicaltrials.gov. A Phase III Study of MPDL3280A (Anti-PD-L1 Antibody) in Combination With Carboplatin + Paclitaxel With or Without Bevacizumab in Patients With Stage IV Non-squamous Non-small Cell Lung Cancer [IMpower 150]. Vol. 2016 (2016).
125. Rosenberg, B. & Vancamp, L. Platinum compounds: a new class of potent antitumour agents. *Nature* 222, 385-386 (1969).
126. Jamieson, E.R. & Lippard, S.J. Structure, recognition, and processing of cisplatin-DNA adducts. *Chemical reviews* 99, 2467-2498 (1999).
127. Johnstone, T.C., Park, G.Y. & Lippard, S.J. Understanding and improving platinum anticancer drugs—phenanthriplatin. *Anticancer research* 34, 471-476 (2014).
128. Wang, D. & Lippard, S.J. Cellular processing of platinum anticancer drugs. *Nature reviews Drug discovery* 4, 307-320 (2005).
129. Gately, D. & Howell, S. Cellular accumulation of the anticancer agent cisplatin: a review. *British journal of cancer* 67, 1171 (1993).
130. Von Hoff, D., *et al.* Toxic effects of cis-dichlorodiammineplatinum (II) in man. *Cancer treatment reports* 63, 1527 (1979).
131. Oberoi, H.S., Nukolova, N.V., Kabanov, A.V. & Bronich, T.K. Nanocarriers for delivery of platinum anticancer drugs. *Advanced drug delivery reviews* 65, 1667-1685 (2013).
132. Rose, W.C., Crosswell, A.R., Schurig, J.E. & Casazza, A.M. Preclinical antitumor activity of orally administered platinum (IV) complexes. *Cancer chemotherapy and pharmacology* 32, 197-203 (1993).

133. Pendyala, L., Cowens, J.W., Chheda, G.B., Dutta, S.P. & Creaven, P.J. Identification of cis-dichloro-bis-isopropylamine platinum (II) as a major metabolite of iproplatin in humans. *Cancer research* 48, 3533-3536 (1988).
134. Sinisi, M., Intini, F.P. & Natile, G. Dependence of the reduction products of platinum (IV) prodrugs upon the configuration of the substrate, bulk of the carrier ligands, and nature of the reducing agent. *Inorganic chemistry* 51, 9694-9704 (2012).
135. Weaver, E.L. & Bose, R.N. Platinum (II) catalysis and radical intervention in reductions of platinum (IV) antitumor drugs by ascorbic acid. *Journal of inorganic biochemistry* 95, 231-239 (2003).
136. Nakai, T., Ando, M., Okamoto, Y., Ueda, K. & Kojima, N. Modulation of oxidative DNA damage and DNA-crosslink formation induced by cis-diammine-tetrachloro-platinum (IV) in the presence of endogenous reductants. *Journal of inorganic biochemistry* 105, 1-5 (2011).
137. Volckova, E., Dudones, L.P. & Bose, R.N. HPLC determination of binding of cisplatin to DNA in the presence of biological thiols: implications of dominant platinum-thiol binding to its anticancer action. *Pharmaceutical research* 19, 124-131 (2002).
138. Volckova, E., Weaver, E. & Bose, R.N. Insight into the reactive form of the anticancer agent iproplatin. *European journal of medicinal chemistry* 43, 1081-1084 (2008).
139. Hall, M.D., Dolman, R.C. & Hambley, T.W. Platinum (IV) anticancer complexes. *Metal ions in biological systems* 42, 297-322 (2004).
140. Casper, E.S., Smart, T.C., Hakes, T.B., Ochoa, M., Jr. & Kaufman, R.J. Clinical trial of iproplatin (cis-dichloro-trans-dihydroxy-bis-isopropylamine platinum IV, CHIP) in patients with advanced breast cancer. *Invest New Drugs* 6, 87-91 (1988).

141. Sternberg, C.N., *et al.* Phase III trial of satraplatin, an oral platinum plus prednisone vs. prednisone alone in patients with hormone-refractory prostate cancer. *Oncology* 68, 2-9 (2005).
142. Wexselblatt, E. & Gibson, D. What do we know about the reduction of Pt(IV) pro-drugs? *Journal of Inorganic Biochemistry* 117, 220-229 (2012).
143. Shi, Y., Liu, S.A., Kerwood, D.J., Goodisman, J. & Dabrowiak, J.C. Pt(IV) complexes as prodrugs for cisplatin. *J Inorg Biochem* 107, 6-14 (2012).
144. Yi Shi, B.K., Warren Redfearn, Michael L. Miller, Lara Myers, Anthony J. Di Pasqua. Platinum(IV) cisplatin derivative trans, cis, cis-bis(heptanoato)amine(cyclohexylamine)dichloridoplatinum(IV) has an enhanced therapeutic index compared to cisplatin for the treatment of non-small cell lung cancer. *Inorganica Chimica Acta* 432, 215–219 (2014).
145. Presnov, M.A., Konovalova, A.L., Kozlov, A.M., Brovtsyn, V.K. & Romanova, L.F. The antitumor activity of oxoplatinum. *Neoplasma* 32, 73-83 (1985).
146. Dhar, S., Gu, F.X., Langer, R., Farokhzad, O.C. & Lippard, S.J. Targeted delivery of cisplatin to prostate cancer cells by aptamer functionalized Pt(IV) prodrug-PLGA-PEG nanoparticles. *Proc Natl Acad Sci U S A* 105, 17356-17361 (2008).
147. Dhar, S., Daniel, W.L., Giljohann, D.A., Mirkin, C.A. & Lippard, S.J. Polyvalent oligonucleotide gold nanoparticle conjugates as delivery vehicles for platinum(IV) warheads. *J Am Chem Soc* 131, 14652-14653 (2009).
148. Shi, Y., Goodisman, J. & Dabrowiak, J.C. Cyclodextrin capped gold nanoparticles as a delivery vehicle for a prodrug of cisplatin. *Inorganic chemistry* 52, 9418-9426 (2013).

149. McWhinney, S.R., Goldberg, R.M. & McLeod, H.L. Platinum neurotoxicity pharmacogenetics. *Mol Cancer Ther* 8, 10-16 (2009).
150. Koshkina, N.V., *et al.* Paclitaxel liposome aerosol treatment induces inhibition of pulmonary metastases in murine renal carcinoma model. *Clinical cancer research* 7, 3258-3262 (2001).
151. Karra, N., *et al.* Antibody conjugated PLGA nanoparticles for targeted delivery of paclitaxel palmitate: efficacy and biofate in a lung cancer mouse model. *Small* 9, 4221-4236 (2013).
152. Wheate, N.J., Walker, S., Craig, G.E. & Oun, R. The status of platinum anticancer drugs in the clinic and in clinical trials. *Dalton transactions* 39, 8113-8127 (2010).
153. Seymour, L.W., *et al.* Phase II studies of polymer-doxorubicin (PK1, FCE28068) in the treatment of breast, lung and colorectal cancer. *Int J Oncol* 34, 1629-1636 (2009).
154. Munaweera, I., *et al.* Chemoradiotherapeutic magnetic nanoparticles for targeted treatment of nonsmall cell lung cancer. *Molecular pharmaceutics* 12, 3588-3596 (2015).
155. Sadhukha, T., Wiedmann, T.S. & Panyam, J. Inhalable magnetic nanoparticles for targeted hyperthermia in lung cancer therapy. *Biomaterials* 34, 5163-5171 (2013).
156. Akhter, S., Ahmad, M.Z., Ahmad, F.J., Storm, G. & Kok, R.J. Gold nanoparticles in theranostic oncology: current state-of-the-art. *Expert Opin Drug Deliv* 9, 1225-1243 (2012).
157. Arruebo, M., Valladares, M. & González-Fernández, Á. Antibody-conjugated nanoparticles for biomedical applications. *Journal of Nanomaterials* 2009, 37 (2009).
158. Hirsch, L., Jackson, J., Lee, A., Halas, N. & West, J. A whole blood immunoassay using gold nanoshells. *Analytical Chemistry* 75, 2377-2381 (2003).

159. Butterworth, K.T., *et al.* Preclinical evaluation of gold-DTDTPA nanoparticles as theranostic agents in prostate cancer radiotherapy. *Nanomedicine* 11, 2035-2047 (2016).
160. Chan, B.A. & Hughes, B.G. Targeted therapy for non-small cell lung cancer: current standards and the promise of the future. *Transl Lung Cancer Res* 4, 36-54 (2015).
161. Dacic, S. & Nikiforova, M.N. Present and future molecular testing of lung carcinoma. *Adv Anat Pathol* 21, 94-99 (2014).
162. Savas, P., Hughes, B. & Solomon, B. Targeted therapy in lung cancer: IPASS and beyond, keeping abreast of the explosion of targeted therapies for lung cancer. *J Thorac Dis* 5 Suppl 5, S579-592 (2013).
163. Arteaga, C.L. The epidermal growth factor receptor: from mutant oncogene in nonhuman cancers to therapeutic target in human neoplasia. *J Clin Oncol* 19, 32S-40S (2001).
164. Alameer, M., Ganju, V. & Watkins, D.N. Novel therapeutic targets in non-small cell lung cancer. *Curr Opin Pharmacol* 13, 394-401 (2013).
165. Fukuoka, M., *et al.* Multi-institutional randomized phase II trial of gefitinib for previously treated patients with advanced non-small-cell lung cancer. *Journal of Clinical Oncology* 21, 2237-2246 (2003).
166. Perez-Soler, R. The role of erlotinib (Tarceva, OSI 774) in the treatment of non-small cell lung cancer. *Clinical cancer research* 10, 4238s-4240s (2004).
167. Sandler, A. Bevacizumab in non small cell lung cancer. *Clin Cancer Res* 13, s4613-4616 (2007).
168. Kwak, E.L., *et al.* Anaplastic lymphoma kinase inhibition in non-small-cell lung cancer. *New England Journal of Medicine* 363, 1693-1703 (2010).

169. Doebele, R.C., *et al.* Mechanisms of resistance to crizotinib in patients with ALK gene rearranged non-small cell lung cancer. *Clinical cancer research* 18, 1472-1482 (2012).
170. Soda, M., *et al.* Identification of the transforming EML4-ALK fusion gene in non-small-cell lung cancer. *Nature* 448, 561-566 (2007).
171. Poe, J.C. & Tedder, T.F. CD22 and Siglec-G in B cell function and tolerance. *Trends Immunol* 33, 413-420 (2012).
172. Tuscano, J.M., *et al.* CD22 antigen is broadly expressed on lung cancer cells and is a target for antibody-based therapy. *Cancer Res* 72, 5556-5565 (2012).
173. Pop, L.M., *et al.* A reevaluation of CD22 expression in human lung cancer. *Cancer research* 74, 263-271 (2014).
174. Anthony J. Di Pasqua, R.E.M.I., Yan-Li Ship, James C. Dabrowiak , Tewodros Asefa. Preparation of antibody-conjugated gold nanoparticles. *Materials Letters* 63 1876-1879 (2009).
175. El-Sayed, I.H., Huang, X. & El-Sayed, M.A. Surface plasmon resonance scattering and absorption of anti-EGFR antibody conjugated gold nanoparticles in cancer diagnostics: applications in oral cancer. *Nano Lett* 5, 829-834 (2005).
176. Dobrovolskaia, M.A., *et al.* Interaction of colloidal gold nanoparticles with human blood: effects on particle size and analysis of plasma protein binding profiles. *Nanomedicine: Nanotechnology, Biology and Medicine* 5, 106-117 (2009).
177. Du, S., *et al.* Aggregation and adhesion of gold nanoparticles in phosphate buffered saline. *Journal of nanoparticle research* 14, 1-14 (2012).
178. Mishra, P., Nayak, B. & Dey, R. PEGylation in anti-cancer therapy: An overview. *asian journal of pharmaceutical sciences* 11, 337-348 (2016).

179. Fleming, A. On the antibacterial action of cultures of a penicillium, with special reference to their use in the isolation of B. influenzae. *British journal of experimental pathology* 10, 226 (1929).
180. WorldHealthOrganization. WHO Model Lists of Essential Medicines. Vol. 2015 (2015).
181. Nelson, M.L. & Levy, S.B. The history of the tetracyclines. *Annals of the New York Academy of Sciences* 1241, 17-32 (2011).
182. Chopra, I. & Roberts, M. Tetracycline antibiotics: mode of action, applications, molecular biology, and epidemiology of bacterial resistance. *Microbiol Mol Biol Rev* 65, 232-260 ; second page, table of contents (2001).
183. Schnappinger, D. & Hillen, W. Tetracyclines: antibiotic action, uptake, and resistance mechanisms. *Archives of microbiology* 165, 359-369 (1996).
184. Speer, B.S., Shoemaker, N.B. & Salyers, A.A. Bacterial resistance to tetracycline: mechanisms, transfer, and clinical significance. *Clinical microbiology reviews* 5, 387-399 (1992).
185. prevention, C.f.d.c.a. About Antimicrobial Resistance. Vol. 2016 (2015).
186. Lin, J., et al. *Mechanisms of antibiotic resistance*, (Frontiers Media SA, 2015).
187. Nguyen, F., et al. Tetracycline antibiotics and resistance mechanisms. *Biol Chem* 395, 559-575 (2014).
188. Speer, B.S. & Salyers, A.A. Characterization of a novel tetracycline resistance that functions only in aerobically grown Escherichia coli. *J Bacteriol* 170, 1423-1429 (1988).
189. Paulsen, I.T., Brown, M.H. & Skurray, R.A. Proton-dependent multidrug efflux systems. *Microbiological reviews* 60, 575-608 (1996).

190. Macone, A., *et al.* The *In Vitro* and *In Vivo* Antibacterial Activities of Omadacycline, a Novel Aminomethylcycline. *Antimicrobial agents and chemotherapy*, AAC. 01242-01213 (2013).
191. Rudramurthy, G.R., Swamy, M.K., Sinniah, U.R. & Ghasemzadeh, A. Nanoparticles: Alternatives Against Drug-Resistant Pathogenic Microbes. *Molecules* 21(2016).
192. Salouti, M. & Ahangari, A. Nanoparticle based Drug Delivery Systems for Treatment of Infectious Diseases. *Application of Nanotechnology in Drug Delivery. USA: InTech*, 155-192 (2014).
193. Gao, W., Thamphiwatana, S., Angsantikul, P. & Zhang, L. Nanoparticle approaches against bacterial infections. *Wiley Interdisciplinary Reviews: Nanomedicine and Nanobiotechnology* 6, 532-547 (2014).
194. Lee, W.L. & Liles, W.C. Endothelial activation, dysfunction and permeability during severe infections. *Current opinion in hematology* 18, 191-196 (2011).
195. Laverman, P., *et al.* Microscopic localization of PEG-liposomes in a rat model of focal infection. *Journal of controlled release* 75, 347-355 (2001).
196. Utrecht, T. Sterically stabilized liposomes labeled with indium-111 to image focal infection. *Journal of nuclear medicine : official publication, Society of Nuclear Medicine* 36, 1639-1644 (1995).
197. Bakker-Woudenberg, I.A., Lokerse, A., Roerdink, F., Regts, D. & Michel, M. Free Versus Liposome-Entrapped Ampicillin in Treatment of Infection Due to *Listeria monocytogenes* in Normal and Atbymic (Nude) Mice. *Journal of Infectious Diseases* 151, 917-924 (1985).

198. Moghadas-Sharif, N., Fazly Bazzaz, B.S., Khameneh, B. & Malaekheh-Nikouei, B. The effect of nanoliposomal formulations on Staphylococcus epidermidis biofilm. *Drug Dev Ind Pharm* 41, 445-450 (2015).
199. Cheow, W.S., Chang, M.W. & Hadinoto, K. Antibacterial efficacy of inhalable levofloxacin-loaded polymeric nanoparticles against *E. coli* biofilm cells: the effect of antibiotic release profile. *Pharm Res* 27, 1597-1609 (2010).
200. Dizaj, S.M., Lotfipour, F., Barzegar-Jalali, M., Zarrintan, M.H. & Adibkia, K. Antimicrobial activity of the metals and metal oxide nanoparticles. *Materials Science and Engineering: C* 44, 278-284 (2014).
201. Zhao, Y., Ye, C., Liu, W., Chen, R. & Jiang, X. Tuning the composition of AuPt bimetallic nanoparticles for antibacterial application. *Angewandte Chemie International Edition* 53, 8127-8131 (2014).
202. Reddy, N.S., *et al.* Tetracycline nanoparticles loaded calcium sulfate composite beads for periodontal management. *Biochimica et Biophysica Acta (BBA)-General Subjects* 1840, 2080-2090 (2014).
203. Wang, H., *et al.* Tetracycline-grafted PLGA nanoparticles as bone-targeting drug delivery system. *International journal of nanomedicine* 10, 5671 (2015).
204. Lee, B.S., *et al.* Controlled-release of tetracycline and lovastatin by poly(D,L-lactide-co-glycolide acid)-chitosan nanoparticles enhances periodontal regeneration in dogs. *Int J Nanomedicine* 11, 285-297 (2016).
205. I. I. Slowing, B.G.T., S. Giri and V. S.-Y. Lin. Mesoporous Silica Nanoparticles for Drug Delivery and Biosensing Applications. *Advanced Functional Materials* 17, 1225–1236 (2007).

206. Meng, H., *et al.* Use of size and a copolymer design feature to improve the biodistribution and the enhanced permeability and retention effect of doxorubicin-loaded mesoporous silica nanoparticles in a murine xenograft tumor model. *ACS Nano* 5, 4131-4144 (2011).
207. Mas, N., *et al.* Enhanced efficacy and broadening of antibacterial action of drugs via the use of capped mesoporous nanoparticles. *Chemistry* 19, 11167-11171 (2013).
208. Li, L.I. & Wang, H. Enzyme-Coated Mesoporous Silica Nanoparticles as Efficient Antibacterial Agents *In Vivo*. *Advanced healthcare materials* 2, 1351-1360 (2013).
209. J. S. Beck , J.C.V., W. J. Roth , M. E. Leonowicz , C. T. Kresge , K. D. Schmitt , C. T. W. Chu , D. H. Olson , E. W. Sheppard ,. A new family of mesoporous molecular sieves prepared with liquid crystal templates. *J. Am. Chem. Soc.* 114, 10834–10843 (1992).
210. Vallet-Regi, M., Balas, F. & Arcos, D. Mesoporous materials for drug delivery. *Angewandte Chemie* 46, 7548-7558 (2007).
211. Halamova, D.Z., V. NSAID naproxen in mesoporous matrix MCM-41: drug uptake and release properties. *Journal of inclusion phenomena and macrocyclic chemistry* 72, 15-23 (2012).
212. Lai, C.Y., *et al.* A mesoporous silica nanosphere-based carrier system with chemically removable CdS nanoparticle caps for stimuli-responsive controlled release of neurotransmitters and drug molecules. *Journal of the American Chemical Society* 125, 4451-4459 (2003).
213. Di Pasqua, A.J., Wallner, S., Kerwood, D.J. & Dabrowiak, J.C. Adsorption of the Pt(II) anticancer drug carboplatin by mesoporous silica. *Chemistry & biodiversity* 6, 1343-1349 (2009).

214. Fengyu Qu, G.Z., Shiyong Huang, Shougui Li, , Jinyu Sun, Daliang Zhang, Shilun Qiu. Controlled release of Captopril by regulating the pore size and morphology of ordered mesoporous silica. *Microporous and Mesoporous Materials* 92, 1-9 (2006).
215. Kwon, S., *et al.* Silica-based mesoporous nanoparticles for controlled drug delivery. *Journal of tissue engineering* 4, 2041731413503357 (2013).
216. Liu, M., *et al.* MCM-41 impregnated with A zeolite precursor: Synthesis, characterization and tetracycline antibiotics removal from aqueous solution. *Chemical engineering journal* 223, 678-687 (2013).
217. Vu, B.K., Snisarenko, O., Lee, H.S. & Shin, E.W. Adsorption of tetracycline on La-impregnated MCM-41 materials. *Environmental technology* 31, 233-241 (2010).
218. Hashemikia, S., Hemmatinejad, N., Ahmadi, E. & Montazer, M. Optimization of tetracycline hydrochloride adsorption on amino modified SBA-15 using response surface methodology. *Journal of colloid and interface science* 443, 105-114 (2015).
219. Di Pasqua, A.J., *et al.* Cytotoxicity of mesoporous silica nanomaterials. *Journal of inorganic biochemistry* 102, 1416-1423 (2008).
220. Yang, P., Gai, S. & Lin, J. Functionalized mesoporous silica materials for controlled drug delivery. *Chem Soc Rev* 41, 3679-3698 (2012).
221. Griffin, M.O., Fricovsky, E., Ceballos, G. & Villarreal, F. Tetracyclines: a pleiotropic family of compounds with promising therapeutic properties. Review of the literature. *American journal of physiology. Cell physiology* 299, C539-548 (2010).
222. Capeletti, L.B., *et al.* Tailored silica-antibiotic nanoparticles: overcoming bacterial resistance with low cytotoxicity. *Langmuir : the ACS journal of surfaces and colloids* 30, 7456-7464 (2014).

223. Lin, C.X., Qiao, S.Z., Yu, C.Z., Ismadji, S. & Lu, G.Q. Periodic mesoporous silica and organosilica with controlled morphologies as carriers for drug release. *Microporous and Mesoporous Materials* 117, 213-219 (2009).
224. Horcajada, P., Ramila, A., Perez-Pariente, J. & Vallet-Regi, M. Influence of pore size of MCM-41 matrices on drug delivery rate. *Microporous and Mesoporous Materials* 68, 105-109 (2004).
225. Qu, F., Zhu, G., Huang, S., Li, S. & Qiu, S. Effective controlled release of captopril by silylation of mesoporous MCM-41. *Chemphyschem : a European journal of chemical physics and physical chemistry* 7, 400-406 (2006).



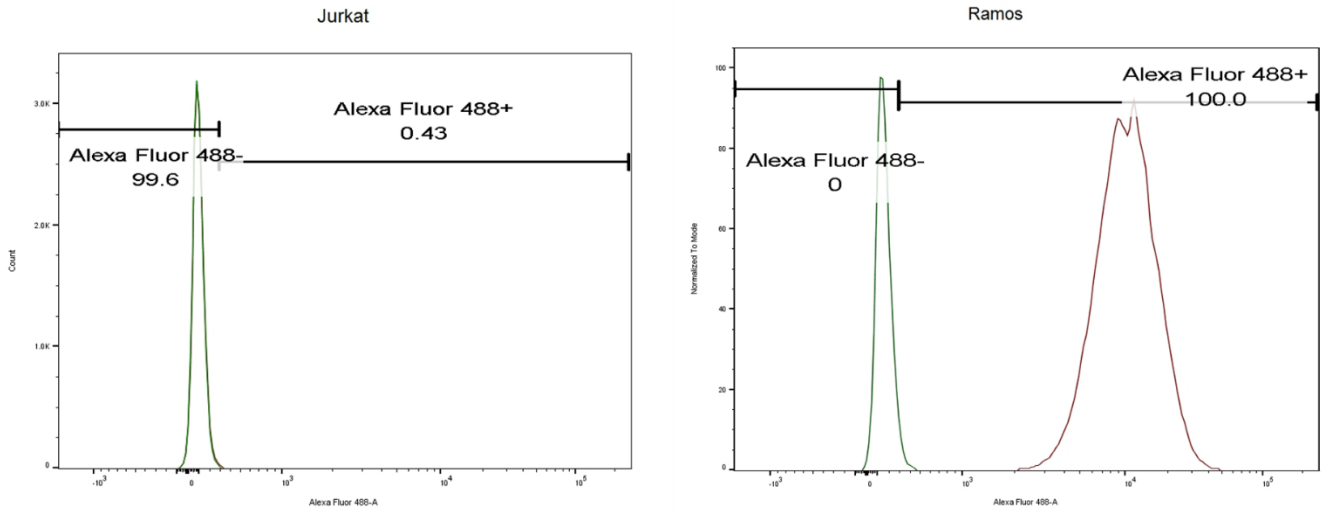


**Figure A2:** Image showing the peak shift in fluorescence intensity in Ramos (CD22 +; right panel) and no peak shift observed in Jurkat (CD22 -; left panel). This indicates the mAb used is specific for CD22.

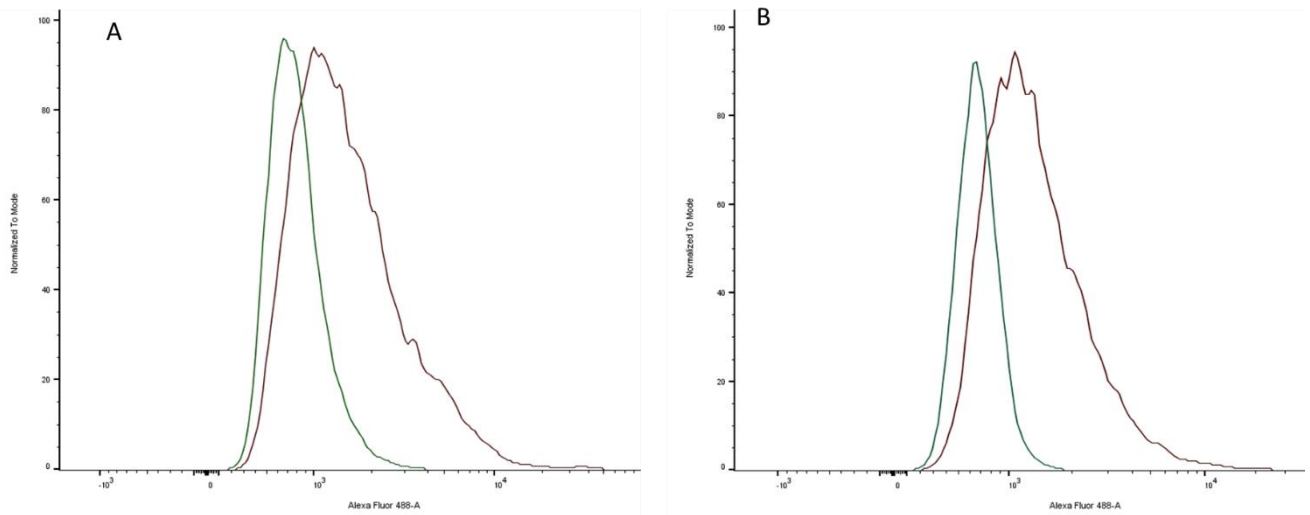


**Figure A3:** Image showing the peak shift in fluorescence intensity in A549 cells. Two morphologically different subsets of cells were observed in A549 when analyzing using flow. A) peak shift in subset 1 B) peak shift in subset 2. Green line is the negative control of the respective cell line, where the cells are treated with only secondary antibody.

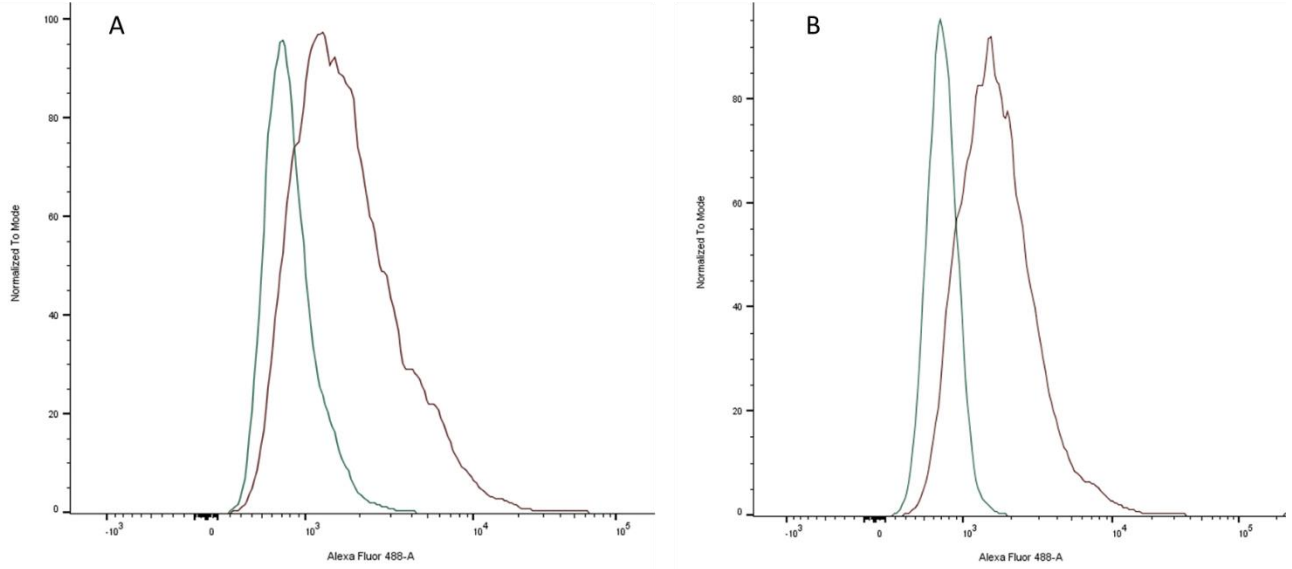


**Figure A4:** Image showing the peak shift in fluorescence intensity in A549 cells. In order to confirm if having two subsets of cells is due to cross contamination of cells, A549 cells from a different batch were also analyzed using flow. Similar distinction of cells was observed. A) peak shift in subset 1 B) peak shift in subset 2. Green line is the negative control of the respective cell line, where the cells are treated with only secondary antibody.

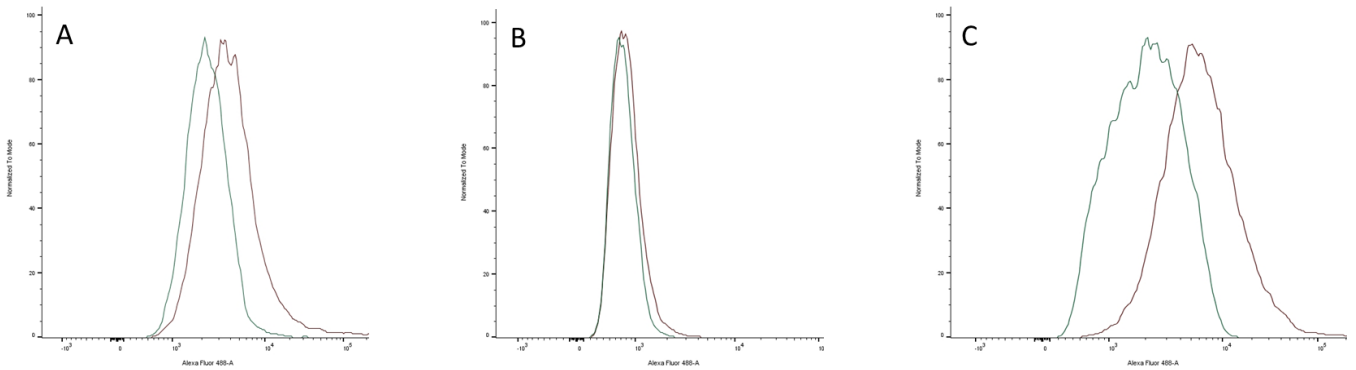


**Figure A5:** Image showing the peak shift in fluorescence intensity in A) H596 B) BEAS-2B and C) WI-38 cells. Green line is the negative control of the respective cell line, where the cells are treated with only secondary antibody.